



Universiteit
Leiden

The Netherlands

The cochlea depicted: radiological evaluation of cochlear morphology and the implanted cochlea

Jagt, M.A. van der

Citation

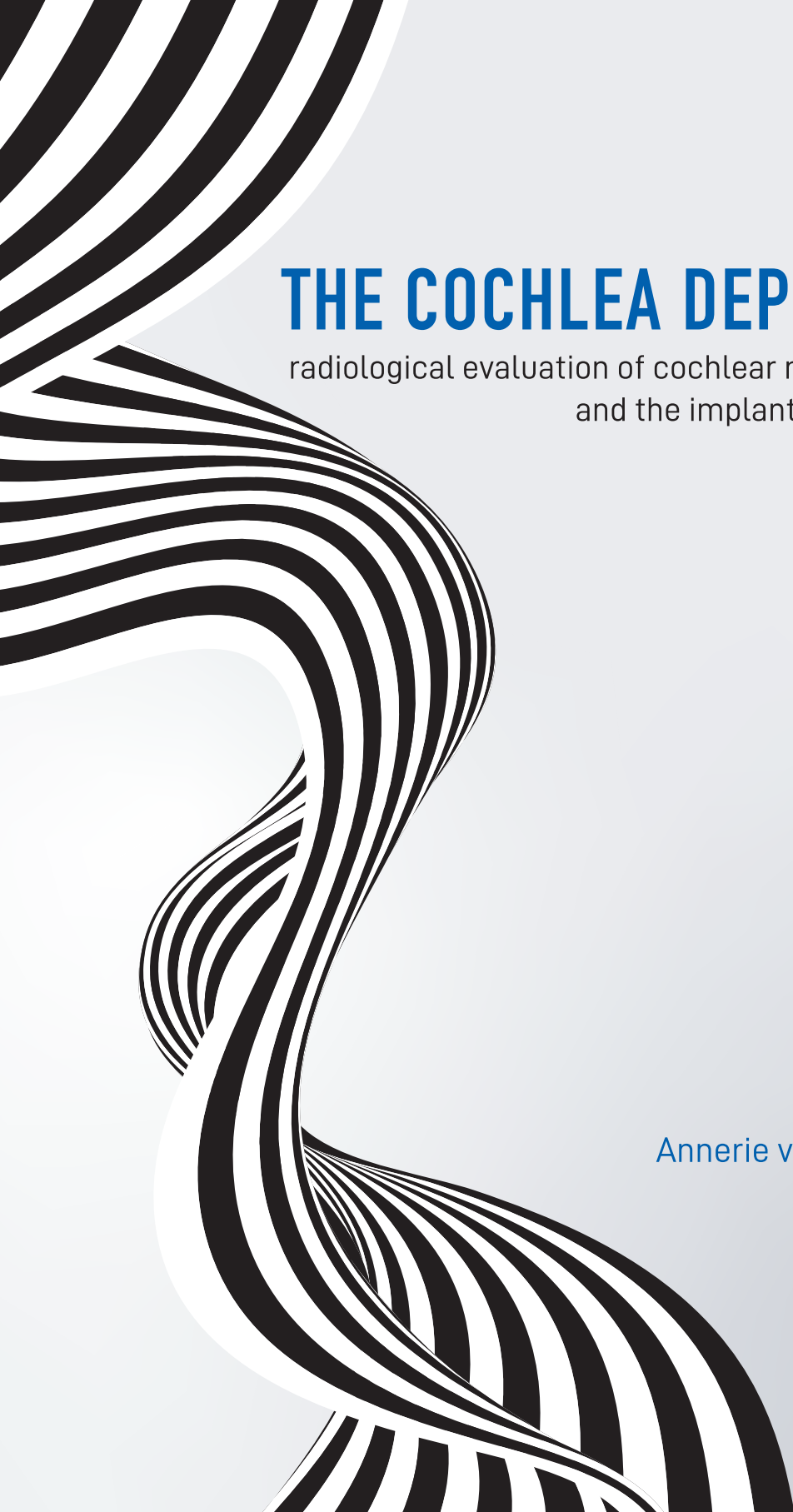
Jagt, M. A. van der. (2021, November 2). *The cochlea depicted: radiological evaluation of cochlear morphology and the implanted cochlea*. Retrieved from <https://hdl.handle.net/1887/3238993>

Version: Publisher's Version

License: [Licence agreement concerning inclusion of doctoral thesis in the Institutional Repository of the University of Leiden](#)

Downloaded from: <https://hdl.handle.net/1887/3238993>

Note: To cite this publication please use the final published version (if applicable).



THE COCHLEA DEPICTED

radiological evaluation of cochlear morphology
and the implanted cochlea

Annerie van der Jagt

The Cochlea Depicted

Radiological Evaluation of Cochlear Morphology and the Implanted Cochlea

Maria Anna van der Jagt

ISBN 978 94 6423 392 6

All rights reserved. No part of this publication may be reproduced, stored in a retrieval system or transmitted, in any form or by any means, electronic, mechanical, photocopying, recording or otherwise, without prior permission of the author or the copyright-owning journals for previous published chapters.

Cover: Wendy Schoneveld || wenz ID

Printing: ProefschriftMaken || www.proefschriftmaken.nl

This research was funded by:
Advanced Bionics Corporation

This thesis was financially supported by:
Advanced Bionics, Cochlear, Med-EL, Chipsoft, Daleco Pharma, EmiD audiologische
apparatuur, Engineers, Makker Hoortoestellen, Oticon Medical, ALK, Viatris, Sonova
Nederland BV

The Cochlea Depicted

Radiological Evaluation of Cochlear Morphology and the Implanted Cochlea

Proefschrift

ter verkrijging van de graad van doctor
aan de Universiteit Leiden, op gezag van
rector magnificus prof.dr.ir. H. Bijl,
volgens besluit van het college voor promoties
te verdedigen op
dinsdag 2 november klokke 15:00 uur

Door

Maria Anna van der Jagt
Geboren te Leiden in 1985

Promotor
Copromotoren

Prof. dr. ir. J.H.M. Frijns
Dr. ir. J.J. Briaire
Dr. B.M. Verbist

Leden promotiecommissie

Prof. dr. P.P.B. van Benthem
Prof. Dr. E.A.M. Mylanus (Radboud UMC)
Prof. Dr. I. Dhooge (UZ Gent)
Dr. L.J.C. Rotteveel
Dr. F.A. Pameijer (UMC Utrecht)

Voor mijn ouders

Contents

Chapter 1	General Introduction	9
Chapter 2	Visualization of Human Inner Ear Anatomy with High Resolution Magnetic Resonance Imaging at 7 Tesla: initial clinical assessment	23
Chapter 3	Variations in cochlear duct shape revealed on clinical CT images with an automatic tracing method	39
Chapter 4	Comparison of the HiFocus Mid-Scala and HiFocus 1J electrode array; angular insertion depths and speech perception outcomes	59
Chapter 5	Improved cochlear implant position detection with spatially synchronized pre- and post-operative midmodiolar cross-section CT and MR images	81
Chapter 6	Prolonged insertion time reduces translocation rate of the HiFocus Mid-Scala electrode array in cochlear implantation	97
Chapter 7	Discussion and implications for future developments	115
Chapter 8	Nederlandse Samenvatting	129
	Appendices	135
	Abbreviations	136
	List of Publications	137
	Acknowledgements	139
	Curriculum Vitae	141





Chapter 1

Introduction

Introduction

Hearing loss and rehabilitation

Hearing loss affects a large part of the world's population; it is the fourth most common cause of disabilities worldwide¹. The World Health Organization (WHO) reported that, currently, 466 million people, including 34 million children, experience disabling hearing loss². This number will likely grow rapidly in the next decades, due to increases in life span and cumulative noise exposure. Apart from the primary effect of impaired communication, hearing loss also impacts an individual's psychosocial, health, and economic status³. Hearing loss can arise from many genetic or acquired defects, and its severity and progression vary widely among patients. A large part of the affected population has age-related hearing loss (i.e., presbycusis), which is mostly due to degeneration of the sensory hair cells of the organ of Corti in the cochlea. However, this process is often accelerated by the damaging effects of noise exposure, ototoxic drugs, or increased hair cell susceptibility, due to genetic disposition. This can lead to profound, sensorineural hearing loss, which is not always treatable with conventional hearing aids. Hearing loss is typically categorized as conductive or sensorineural. Conductive hearing loss is a limitation in the transmission of sound from the outer world towards the inner ear, due to pathology in the outer or middle ear. Normally, sound pressure alterations are transmitted from the eardrum, through the ossicular chain in the middle ear, towards the oval window. The oval window communicates with the perilymph fluid in the vestibule and the scala vestibuli of the cochlea. Thus, sound pressures cause movements in the perilymph, which bend the stereocilia of the sensory hair cells, and this bending elicits a neural signal. In contrast, sensorineural hearing loss is caused by functional impairments in the sensory hair cells, the neural components of the cochlea, or the auditory nerve. Most conductive hearing loss and most light or moderate sensorineural hearing loss can be treated by fitting the patient with conventional hearing aids, implanting a bone conduction device in the skull, or surgically restoring the ossicles. However, these interventions cannot sufficiently restore hearing in individuals with severe-to-profound sensorineural hearing loss. In these individuals, cochlear implantation became the standard of care.

Cochlear implantation

A cochlear implant device bypasses the middle ear and the damaged structures of the cochlea and directly stimulates the nerve fibres of the auditory nerve. The cochlear implant comprises an electrode array that is surgically placed within the cochlea, preferably in the scala tympani (Figure 1). The device consists of an external microphone that captures environmental sounds and a speech processor that filters and converts the sounds into a digital code. The digitized signal is sent to a headpiece, which transmits the signal to a subcutaneous receiver embedded in the skull. The receiver responds to these signals by sending electrical stimuli through an internal wire to the individual contacts in an electrode



array. The electrode array is inserted into scala tympani of the cochlea. The electrode contacts sense frequency-specific signals. The frequency-specific electrode arrangement reflects the tonotopical organization of the cochlea. Thus, high frequency sounds are transmitted to the base of the cochlea, and lower frequency sounds are transmitted to the apical part of the cochlea.

The most common surgical procedure for a cochlear implantation consists of a canal wall up mastoidectomy and posterior tympanotomy, which provide access to the round window. Subsequently, the electrode array can be introduced into the cochlea, either through a(n) (extended) round window approach or a cochleostomy.



Figure 1: Illustration of a cochlear implant device (right ear) with the external and internal components. The external components include the microphone, speech processor and headpiece. The internal components consist of the internal receiver, internal wire and electrode array inside the cochlea. Image courtesy of Prof. Völter, head of Hearing competence centre Ruhr-University Bochum, Germany.

William F. House is considered the founder of cochlear implantation⁴. Early in his career, in 1958, one of his patients showed him a newspaper report that described an experiment performed by Djournio and Eyries in France. They had placed an electrode directly on part of an exposed auditory nerve⁵. With this electrode, a patient with hearing loss could experience sound; however, speech recognition was not yet achieved. Eventually, Dr. House became thoroughly involved in developing a cochlear implant. He developed the first implant, with a single electrode that could be placed into the cochlea, and it could stimulate the neural components by producing a periodic pitch. Since then, many researchers, clinicians,

and engineers all over the world have become involved in developing cochlear implants. An early trial by House et al. tested a single-channel functioning cochlear implant, which showed some basic functions in 13 patients⁶. These patients could not understand speech through their implants; however, it significantly improved environmental sound recognition and enhanced their lip-reading capacities. Additionally, that trial demonstrated the safety of the procedure, which led to FDA approval. Subsequently, the Australian, Graham Clarke, developed a cochlear implant with multiple channels. This configuration allowed frequency place coding that mimicked the tonotopical organization of the cochlea⁷. The development of multi-channel cochlear implants represented a large leap towards a device that could provide speech understanding⁸. Currently, thousands of patients per year receive cochlear implants worldwide, and speech perception scores are gradually approaching the level of normal hearing.

Imaging in cochlear implantation

Imaging plays a central role in several aspects of cochlear implantation. Depictions of the inner ear provide insight into the possible underlying causes of hearing loss and the variety of temporal bone anatomy. Previous studies have revealed that the human cochlea is extensively varied in shape, size, and coiling pattern⁹⁻¹¹. This variability may have implications for cochlear implantation, in terms of surgical aspects, the choice of electrode array, and potentially, speech perception outcomes. In our institution, both computed tomography (CT) and magnetic resonance imaging (MRI) are performed in the preoperative work-up for cochlear implant candidates. These modalities have complementing capacities. However, it should be noted that this approach varies among cochlear implant centres worldwide.

Preoperative assessments provide insight into whether the cochlea is normally developed, with an average of 2.6 cochlear turns¹¹, and whether the cochlear duct is patent. In addition, retrocochlear pathology can be assessed and it provides a map of temporal bone anatomy. This information supports surgical planning and allows the surgeon to anticipate potential surgical difficulties¹². For instance, a high jugular bulb can limit access to the round window niche, or an overhanging tympanic tegmen increases the risk of causing a cerebrospinal leak when drilling for the mastoidectomy. In some cases, preoperative imaging of the inner ear plays a crucial role in selecting the ‘best’ ear for implantation. CT is superior to MRI for delineating osseous components, and it is commonly used for preoperative evaluations of the temporal bone^{13,14}. When cochlear implantation was first launched, the clinical value of MRI had not been standardized for cochlear implant candidacy¹². Later, it was shown that fibrosis could be detected on T1- and T2-weighted MRI images of an obliterated cochlea¹². However, despite this acknowledged added value, MRIs required thick slices and long acquisition times, which impaired accurate evaluations and made MRIs unsuitable for clinical applications. Subsequently, clinically applicable 1.5 Tesla (T) and 3T MRIs were introduced, with new pulse sequences and multi-channel phased array coils, which made it possible



to achieve a high signal-to-noise ratio (SNR), within a limited scan duration¹⁵. In addition, the administration of intravenous gadolinium further increased the ability to detect small lesions¹⁶. Currently, the entire pathway, from the outer ear canal to the auditory cortex, can be depicted in high detail with high resolution MRI. MRI scans are superior to CT scans in depicting soft tissues; thus, MRIs are mainly deployed to evaluate the entire auditory nerve tract, from the cochlea to the brainstem.

Currently, 1.5 or 3T MRI scanners are used in clinical practice. However, scanners with higher field strengths might potentially increase the SNR. A better SNR allows analysis with a reduced voxel size, which provides a more refined delineation of the anatomical structures. However, in strong magnetic fields, image quality can be degraded, due to image artefacts caused by interactions between the patient and the radiofrequency field¹⁷. Furthermore, ultra-high magnetic field imaging increases the tissue temperature and causes unpleasant side effects, like dizziness and nausea, which impede its clinical use¹⁸. Brink et al. conducted a study to determine whether artefact issues in inner ear imaging might be overcome with dielectric ear pads¹⁹. The pads were filled with barium titanate, and they enhanced the B_1^+ field signal and improved the quality of imaging in the inner ear region. Additionally, they investigated subjective experiences and discomfort. Based on those results, the pads were deemed to be safe¹⁸. These pads facilitated further explorations that aimed to determine the potential of 7T imaging in the inner ear (Chapter 2).

In many centres, after implantation, part of the standard work-up is to assess the intracochlear position of the cochlear implant electrode array, typically with conventional X-ray or CT imaging. With conventional X-ray, patients are exposed to a limited radiation dose. However, a multi-section CT (MSCT) scan provides more detail in visualizing the temporal bone structures and the position of the electrode array after implantation²⁰. MRI is avoided in evaluating the implanted cochlea, due to the risk of displacing or demagnetizing the subcutaneous receiver, which could require removal of the magnet. Nevertheless, for other indications that require MRI-based evaluations of the head region in patients with cochlear implants, some manufactures are developing MRI-compatible electrode designs, and a few designs have met safety requirements²¹.

Postoperative images provide feedback on the surgical procedure; for example, imaging is performed to ensure the (entire) electrode array is correctly placed in the targeted scala tympani. In addition, imaging provides a means to check for signs of kinking in the wire or a fold at the tip. Although rare, sometimes imaging reveals that the electrode array is situated in an undesirable position, like in the internal auditory canal or in the middle ear²². In more detail, the insertion depth of the electrode array and proximity of the individual electrode contacts to the modiolus can be evaluated. These postoperative findings may have clinical

implications; thus, increasingly, researchers are investigating the postoperative position of electrode arrays for potential influences on speech perception outcomes.

Intra-cochlear position

Variability in speech perception with a cochlear implant is thought to be partly due to differences in the intra-cochlear position of the electrode array and the presence and degree of insertion trauma. Current imaging techniques provide an accurate depiction of the intra-cochlear position of the electrode array for evaluations of surgical- and design-related effects on speech perception. Various studies have investigated the insertion depth of the electrode array, described as either a linear or angular depth, and its relationship to speech understanding. Based on some theories, it was postulated that a deeper insertion might provide better speech understanding, because this placement could facilitate stimulation of the lower frequencies in the more apical region of the cochlea^{23,24}. Opposing theories postulated a negative impact on speech perception outcomes, because (1) the gradually decreasing size of the cochlear duct presents a higher risk of insertion trauma and loss of residual hearing²⁵, (2) a deep insertion might limit stimulation of the high frequency regions in the basal part of the cochlea, or (3) the spiral ganglion cells are more closely organized in the apical region, which might lead to pitch confusion²⁶. However, a recent systematic review that addressed this topic did not find evidence to support any of these hypotheses²⁷. A potential explanation for this lack of evidence might be the heterogeneity of the studied populations. Frequently, studies are not comparable, in terms of inclusion criteria, baseline characteristics and evaluation methods. Fair comparisons between studies are limited, when the results are not consistently stratified for well-recognized patient-related factors that can influence speech recognition. These factors include: age at implantation; some aetiologies of deafness, such as meningitis; the presence or absence of residual hearing; the duration of deafness; and the preoperative level of speech recognition²⁸⁻³¹. In addition, presumably, intelligence, brain plasticity, and motivation for rehabilitation might explain some of the variability in performance among patients with cochlear implants, but these influences are difficult to objectify.

Another frequently investigated radiological feature is the distance between the electrode contacts and the inner cochlear wall. This distance can be measured, due to the SNR improvements achieved with the advent of high resolution MSCT imaging³². The distance between an electrode contact and the inner cochlear wall influences the pattern of stimulation at the neural fibres in the modiolus. Cochlear implants generally aim to stimulate as many neural fibres as possible, while limiting stimulating overlapping regions by adjacent electrode contacts. Various electrode designs were proposed to achieve the ultimate stimulation by achieving different horizontal intra-scalar positions, either resting on the lateral wall or hugging the modiolus, combined with different speech coding strategies. However, in addition to implant design, it is important to be aware of the large



variety of cochlear morphologies, which also impact the electrode position, in terms of the insertion depth and proximity to the modiolus⁹. Postoperative imaging techniques allow an evaluation of the specific cochlear implant design, the individual morphological characteristics, and their potential influences on speech perception. To date, no study has demonstrated superiority for any of the specific electrode designs. However, comparison of electrode designs is difficult due to selection bias and, in case of multicentre studies, data heterogeneity due to differences in clinical approach. Nevertheless, a recent study comparing a straight and precurved cochlear implant design from one manufacturer showed superior speech perception outcomes in the group of 85 patients who received a precurved electrode array³³.

Improvements in the abilities of cochlear implants to enhance speech perception have led to more flexibility in patient selection criteria; thus, patients with residual hearing are also considered candidates for cochlear implants^{34,35}. These extended selection criteria have prompted improvements in cochlear implantation techniques. Companies began to investigate electrode array designs that reduced the risk of insertion trauma to preserve residual hearing and to maintain the integrity of intra-cochlear anatomy as much as possible. Thus, it is possible to consider a combination of electric and acoustic stimulation (EAS) for patients with residual hearing³⁶. With the EAS approach, a cochlear implant stimulates the basal neurons and a conventional hearing aid rehabilitates the lower frequency range. This combination has improved hearing capabilities, compared to a conventional hearing aid or a cochlear implant alone³⁷. The ambition of preserving residual hearing has also led to the development of so-called soft-surgery techniques. These techniques were first described in 1993, and they aimed to limit intra-cochlear damage caused by the electrode array insertion³⁸.

Insertion trauma

When the cochlear implant is inserted, the electrode array is targeted to the scala tympani (Figure 2), one of the three fluid-filled compartments of the cochlea. The rationale behind this positioning lies first in accessibility; i.e., the scala tympani can be reached through the round window; and second, proximity, because the electrode array can be placed close to the targeted spiral ganglion cells. From previous studies, we know that the central axons of the spiral ganglion cells are less susceptible to degeneration than the more peripheral parts of the neural fibres³⁹; thus, the central axons are favoured for stimulation. In some unfortunate cases, the electrode array becomes translocated; that is, it traverses from the scala tympani into the scala vestibuli, by penetrating the basilar membrane, the osseous spiral lamina, or both. In those cases, the peripheral neural components deteriorate, and the electrode contacts are positioned further away from the targeted spiral ganglion cells and their central axons. Furthermore, translocation may lead to extensive fibrosis or even ossification, which limits the electrical stimulation of neural fibres, impairs residual hearing, and reduces the

probability of an optimal re-implantation in the future, which is necessary in a large part of the younger population, due to the expected lifespan of the implant. Apart from an implant translocation, other, more subtle, traumas can occur after the electrode array is introduced into the cochlea. For example, a leak of perilymph fluid can reduce the intra-scalar pressure; or the cells may mount a response to the foreign body, which can cause damage from toxins, fibrosis, and/or ossification⁴⁰. Unfortunately, these subtle changes cannot be detected with current clinical imaging techniques.

Several imaging techniques are used in in-vivo studies to determine the intra-cochlear position of the electrode array, including cone beam CT, flat-panel CT, conventional X-rays, or MSCT. However, depending on the type of scanner employed, it can be challenging to obtain an accurate determination of the position of the individual electrode contacts, due to blooming artefacts that emanate from the implant's metal components. A blooming artefact can blur anatomical structures, such as the osseous spiral lamina, and the basilar membrane. Several solutions have been proposed to overcome this problem. For instance, anatomic structures can be reconstructed with registration techniques, based on one or multiple templates from micro-CT data^{41,42}. Another option is to overlay a preoperative scan of the patient⁴³. However, because cochlear morphology is known to be highly variable among patients, it must be kept in mind that general templates might not be useful, due to the potential for inaccurate alignments.

Insertion trauma is not an uncommon event. A systematic review by Hoskinson et al. reported an overall insertion trauma rate of 17.6%⁴⁴. That rate was based on data from both in-vivo and ex-vivo studies; thus, in addition to array translocations into the scala vestibuli, the trauma rate included elevations and disruptions of the basilar membrane, which were detected on histological images. To evaluate the probability of translocation for cochlear implant electrode arrays, we must identify relevant risk factors. Risk factors might be associated with the surgical approach or technique, the morphological characteristics of the cochlea, or the design of the cochlear implant electrode array. Moreover, the impact of a scalar translocation must be further clarified. A few studies have shown the benefit of positioning the array completely in the scala tympani^{42,45,46}.



Figure 2: Histological mid-modiolus cross-sectional image of a cochlea. The electrode array is targeted to the scala tympani (*); translocation can occur into the scala vestibuli (°) or the scala media (•). The scala media is the location of the actual hearing organ, the Organ of Corti. Image courtesy of F. Linthicum, House Ear Institute, USA

Aims and outline of this thesis

The aims of this thesis were:

- (1) to gain insight into cochlear morphology by investigating the inner ear with high-resolution 7T MRI and by measuring variations in the shape of the cochlear duct by analysing clinical CT images with an automatic tracing method;
- (2) to evaluate the intra-cochlear positions of cochlear implant electrode arrays on postoperative CT images, with a special emphasis on insertion trauma, and to correlate these findings with speech intelligibility and surgical techniques.

Chapter 2 describes an investigation into the applicability of using clinical 7T MRI for visualizing the inner ear. It also describes a comparison of 7T and 3T MRI qualities for visualizing anatomic inner ear structures. This investigation required the development of a high-resolution imaging protocol, which included improvements in contrast homogeneity and transmitting efficiency in the region of the inner ear. In Chapter 3, we present an automatic method for tracing the first and second turns of the cochlea in high detail on preoperative CT scans. This method is expected to provide insight into the large variations in cochlear morphology, which could have potential implications for cochlear implantation. In Chapter 4, two cochlear implant electrode designs, the straight HiFocus 1J and the pre-curved HiFocus MS, are compared, in terms of the angular insertion depth, the frequency mismatch, and speech perception outcomes. Chapter 5 describes a study that aimed to facilitate the detection of insertion traumas. In that study, spatially synchronized, pre- and postoperative mid-modiolus, cross-sectional CT and MR images were assessed for their value in detecting the intra-cochlear positions of individual electrode contacts in cochlear implants. Chapter 6 describes the application of this evaluation method. In that study, we evaluated the effects of insertion speed and surgical approach on the risk of insertion trauma in a population that received cochlear implants equipped with the HiFocus MS electrode array. Chapter 7 describes the conclusions from Chapters 2-6, a general discussion, and implications for future developments.



References

1. Vos T, Allen C, Arora M, et al. Global, regional, and national incidence, prevalence, and years lived with disability for 310 diseases and injuries, 1990–2015: a systematic analysis for the Global Burden of Disease Study 2015. *Lancet*. 2016;388(10053):1545-1602. doi:10.1016/S0140-6736(16)31678-6
2. *World Health Organization*.
3. Cunningham LL, Tucci DL. Hearing loss in adults. *N Engl J Med*. 2017;377(25):2465-2473. doi:10.1056/NEJMra1616601
4. Eisenberg LS. The contributions of William F. House to the field of implantable auditory devices. *Hear Res*. 2015;322:52-56. doi:10.1016/j.heares.2014.08.003
5. Eisen MD. Djourno, eyries, and the first implanted electrical neural stimulator to restore hearing. *Otol Neurotol*. 2003;24(3):500-506. doi:10.1097/00129492-200305000-00025
6. Bilger RC, Black FO, Hopkinson NT ME. Implanted auditory prosthesis: an evaluation of subjects presently fitted with cochlear implants. *Trans Sect Otorhinolaryngol Am Acab Ophthalmol Otolaryngol*. 1977;84(4):677-682.
7. Chouard CH. The early days of the multi channel cochlear implant: Efforts and achievement in France. *Hear Res*. 2015;322:47-51. doi:10.1016/j.heares.2014.11.007
8. Clark GM. The multi-channel cochlear implant: Multi-disciplinary development of electrical stimulation of the cochlea and the resulting clinical benefit. *Hear Res*. 2015;322:4-13. doi:10.1016/j.heares.2014.08.002
9. van der Marel KS, Briaire JJ, Wolterbeek R, Snel-Bongers J, Verbist BM, Frijns JHM. Diversity in Cochlear Morphology and Its Influence on Cochlear Implant Electrode Position. *Ear Hear*. November 2013:1-12. doi:10.1097/01.aud.0000436256.06395.63
10. Rask-Andersen H, Liu W, Erixon E, et al. Human cochlea: anatomical characteristics and their relevance for cochlear implantation. *Anat Rec (Hoboken)*. 2012;295(11):1791-1811. doi:10.1002/ar.22599
11. Erixon E, Högstorp H, Wadin K, Rask-Andersen H. Variational anatomy of the human cochlea: implications for cochlear implantation. *Otol Neurotol*. 2009;30(1):14-22. doi:10.1097/MAO.0b013e31818a08e8
12. Harnsberger HR, Dart DJ, Parkin JL, Smoker WR, Osborn AG. Cochlear implant candidates: Assessment with CT and MR imaging. *Radiology*. 1987;164(1):53-57. doi:10.1148/radiology.164.1.3108956
13. Phelps PD, Proops DW. Imaging for cochlear implants. *J Laryngol Otol*. 1999;113(SUPPL. 24):21-23. doi:10.1017/S0022215100146043
14. Verbist BM. Imaging of sensorineural hearing loss: a pattern-based approach to diseases of the inner ear and cerebellopontine angle. *Insights Imaging*. 2012;3(2):139-153. <http://www.pubmedcentral.nih.gov/articlerender.fcgi?artid=3314739&tool=pmcentrez&rendertype=abstract>. Accessed October 11, 2012.
15. Naganawa S, Nakashima T. Cutting edge of inner ear MRI. *Acta Otolaryngol Suppl*. 2009;(560):15-21. doi:10.1080/00016480902729819

16. Counter S a, Bjelke B, Borg E, Klason T, Chen Z, Duan ML. Magnetic resonance imaging of the membranous labyrinth during in vivo gadolinium (Gd-DTPA-BMA) uptake in the normal and lesioned cochlea. *Neuroreport*. 2000;11(18):3979-3983. <http://www.ncbi.nlm.nih.gov/pubmed/11192613>.
17. Sled JG, Pike GB. Standing-wave and RF penetration artifacts caused by elliptic geometry: an electrodynamic analysis of MRI. *Ieee Trans Med Imaging*. 1998;17(4):653-662.
18. Versluis MJ, Teeuwisse WM, Kan HE, van Buchem M a, Webb AG, van Osch MJ. Subject tolerance of 7 T MRI examinations. *J Magn Reson Imaging*. 2013;38:722-725. doi:10.1002/jmri.23904
19. Brink WM, van der Jagt AMA, Versluis MJ, Verbist BM, Webb AG. High Permittivity Dielectric Pads Improve High Spatial Resolution Magnetic Resonance Imaging of the Inner Ear at 7 T. *Invest Radiol*. 2014;00(00):1-7.
20. Verbist BM, Joemai RMS, Teeuwisse WM, Veldkamp WJH, Geleijns J, Frijns JHM. Evaluation of 4 multisection CT systems in postoperative imaging of a cochlear implant: a human cadaver and phantom study. *AJNR Am J Neuroradiol*. 2008;29(7):1382-1388. doi:10.3174/ajnr.A1108
21. Cass ND, Honce JM, O'Dell AL, Gubbels SP. First MRI with New Cochlear Implant with Rotatable Internal Magnet System and Proposal for Standardization of Reporting Magnet-Related Artifact Size. *Otol Neurotol*. 2019;40(7):883-891. doi:10.1097/MAO.0000000000002269
22. Mehanna AM, Gamaleldin OA, Fathalla MF. The misplaced cochlear implant electrode array. *Int J Pediatr Otorhinolaryngol*. 2019;117(October 2018):96-104. doi:10.1016/j.ijporl.2018.11.027
23. Başkent D, Shannon R V. Interactions between cochlear implant electrode insertion depth and frequency-place mapping. *J Acoust Soc Am*. 2005;117(3):1405.
24. O'Connell BP, Cakir A, Hunter JB, et al. Electrode Location and Angular Insertion Depth Are Predictors of Audiologic Outcomes in Cochlear Implantation. *Otol Neurotol*. 2016;37(8):1016-1023. doi:10.1097/MAO.0000000000001125
25. Biedron S, Prescher A, Ilgner J, Westhofen M. The internal dimensions of the cochlear scalae with special reference to cochlear electrode insertion trauma. *Otol Neurotol*. 2010;31(5):731-737. doi:10.1097/MAO.0b013e3181d27b5e
26. Gani M, Valentini G, Sigrist A, Kós M-I, Boëx C. Implications of deep electrode insertion on cochlear implant fitting. *J Assoc Res Otolaryngol*. 2007;8(1):69-83. doi:10.1007/s10162-006-0065-4
27. Heutink F, De Rijk SR, Verbist BM, Huinck WJ, Mylanus EAM. Angular Electrode Insertion Depth and Speech Perception in Adults with a Cochlear Implant: A Systematic Review. *Otol Neurotol*. 2019;40(7):900-910. doi:10.1097/MAO.0000000000002298
28. Holden LK, Firszt JB, Reeder RM, Uchanski RM, Dwyer NY, Holden TA. Factors affecting outcomes in cochlear implant recipients implanted with a perimodiolar electrode array located in scala tympani. *Otol Neurotol*. 2016;37(10):1662-1668. doi:10.1097/MAO.0000000000001241
29. Blamey P, Arndt P. Factors affecting auditory performance of postlinguistically deaf adults using cochlear implants. *Audiol Neurootol*. 1996;1:293-306.
30. Rubinstein JT, Parkinson WS, Tyler RS, Gantz BJ. Residual speech recognition and cochlear implant performance effects of implantation criteria. *Am J Otol*. 1999;20:445-452.
31. Dijk JE, van Olphen AF, Langereis MC, Mens LHM, Brokx JPL, Smoorenburg GF. Predictors of cochlear implant performance. *Audiology*. 1999;38:109-116.



32. Van Der Beek FB, Briaire JJ, Van Der Marel KS, Verbist BM, Frijns JHM. Intracochlear position of cochlear implants determined using CT scanning versus fitting levels: Higher threshold levels at basal turn. *Audiol Neurotol*. 2016;21(1):54-67. doi:10.1159/000442513
33. Heutink F, Verbist BM, van der Woude, W-J, et al. Factors Influencing Speech Perception in Adults With a Cochlear Implant. *Ear Hear*. 2021; Publish Ahead of Print:1-12. doi:10.1097/aud.0000000000000988
34. Snel-Bongers J, Netten AP, Boermans PPBM, Rotteveel LJC, Briaire JJ, Frijns JHM. Evidence-based inclusion criteria for cochlear implantation in patients with postlingual deafness. *Ear Hear*. 2018;39(5):1008-1014. doi:10.1097/AUD.0000000000000568
35. van der Straaten TFK, Briaire JJ, Vickers D, Boermans PPBM, Frijns JHM. Selection Criteria for Cochlear Implantation in the United Kingdom and Flanders: Toward a Less Restrictive Standard. *Ear Hear*. 2020;42(1):68-75. doi:10.1097/AUD.0000000000000901
36. von Ilberg C, Kiefer J, Tillein J et al. Electric-Acoustic Stimulation of the Auditory System. *ORL J Otorhinolaryngol Relat Spec*. 1999;(61):334-340.
37. Gstoettner WK, van de Heyning P, O'Connor AF, et al. Electric acoustic stimulation of the auditory system: results of a multi-centre investigation. *Acta Otolaryngol*. 2008;128(9):968-975.
38. E. Lehnhardt. Intracochlear placement of cochlear implant electrodes in soft surgery technique. *HNO*. 1993;41(7):356-359.
39. Hinojosa R, Marion M. Histopathology of Profound Sensorineural Deafness. *Ann N Y Acad Sci*. 1983;405(1):459-484. doi:10.1111/j.1749-6632.1983.tb31662.x
40. Carlson ML, Driscoll CLW, Gifford RH, et al. Implications of minimizing trauma during conventional cochlear implantation. *Otol Neurotol*. 2011;32(6):962-968. doi:10.1097/MAO.0b013e3182204526
41. Skinner MW, Holden T a., Whiting BR, et al. In Vivo Estimates of the Position of Advanced Bionics Electrode Arrays in the Human Cochlea. *Ann Otol Rhinol Laryngol*. 2007;116(4):2-24. doi:10.1177/000348940711600401
42. Finley CC, Skinner MW. Role of electrode placement as a contributor to variability in cochlear implant outcomes. *Otol Neurotol*. 2008;29(7):920-928.
43. Schuman T a, Noble JH, Wright CG, Wanna GB, Dawant B, Labadie RF. Anatomic verification of a novel method for precise intrascalar localization of cochlear implant electrodes in adult temporal bones using clinically available computed tomography. *Laryngoscope*. 2010;120(11):2277-2283. doi:10.1002/lary.21104
44. Hoskison E, Mitchell S, Coulson C, Hoskison E, Mitchell S, Coulson C. Systematic review : Radiological and histological evidence of cochlear implant insertion trauma in adult patients Systematic review : Radiological and histological evidence of cochlear implant insertion trauma in adult patients. 2017;0100(June). doi:10.1080/14670100.2017.1330735
45. Shepherd RK, Hatsushika S, Clark GM. Electrical stimulation of the auditory nerve: the effect of electrode position on neural excitation. *Hear Res*. 1993;66(1):108-120.
46. Aschendorff A, Kubalek R, Turowski B, et al. Quality control after cochlear implant surgery by means of rotational tomography. *Otol Neurotol*. 2005;26(1):34-37. <http://www.ncbi.nlm.nih.gov/pubmed/15699717>.





Chapter 2

Visualization of Human Inner Ear Anatomy with High Resolution Magnetic Resonance Imaging at 7 Tesla: initial clinical assessment

MA van der Jagt, WM Brink,
MJ Versluis, SCA Steens, JJ Briaire,
AG Webb, JHM Frijns, BM Verbist

*Published in American Journal
of Neuroradiology, 2014*

Abstract

Background and purpose: In many centers, MRI of the inner ear and auditory pathway performed on 1.5 or 3 Tesla systems is part of the preoperative work-up of cochlear implant (CI) candidates. We investigated the applicability of clinical inner ear imaging at 7 Tesla MRI and compared the visibility of inner ear structures and nerves within the internal auditory canal (IAC) with images acquired at 3 Tesla.

Methods: 13 patients with sensorineural hearing loss (SNHL) eligible for cochlear implantation underwent examinations on 3 and 7 Tesla scanners. Two experienced head and neck radiologists evaluated the 52 inner ear data sets. A total of 24 anatomical structures of the inner ear and 1 overall score for image quality were assessed using a 4-point-grading scale for degree of visibility.

Results: The visibility of 11 out of the 24 anatomical structures was rated higher on the 7 Tesla images. There was no significant difference in the visibility of 13 anatomical structures and overall quality rating. A higher incidence of artifacts was observed in the 7 Tesla images.

Conclusions: The gain in SNR at 7T yielded a more detailed visualization of many anatomical structures, especially delicate ones, despite the challenges accompanying MRI at high magnetic field.



Introduction

Patients with sensorineural hearing loss (SNHL) suffer from malfunction of the inner ear, cochlear nerve or central auditory pathway. Treatment consists of amplification of sound or, in case of severe to profound SNHL, direct electrical stimulation of the cochlear nerve by a cochlear implant. MRI of patients with SNHL focuses on the integrity of the auditory pathways from the cochlea to the auditory cortex in the brain. In particular, the fluid-filled spaces of the labyrinth and internal auditory canal (IAC) and the cerebellopontine angle (CPA) are of interest because the most commonly identified pathologies that cause SNHL are found in these regions.¹⁻⁵

One clear trend in the development of MRI systems has been the drive to higher magnetic field strengths.⁶ For clinical inner ear scanning, MRI scanners with a magnetic field strength of 1.5 or 3 Tesla are routinely used. The relatively recent introduction of commercial 7 Tesla scanners potentially enables increased SNR resulting in more detailed imaging of anatomical structures. Concerning inner ear imaging, the visualization of delicate and small-sized inner ear structures might benefit from such high resolution imaging. This may yield new opportunities for obtaining normative measurements and for evaluating pathological alterations within the inner ear or associated nerves. Such detailed anatomical description has gained particular interest for assessment of cochlear implant candidates, since it gives decisive information on implantation feasibility, possible surgical risks, and choice of implant device. As such it would aid in patient-specific preoperative planning of cochlear implantation and could provide valuable information for individualized assessment of insertion.

Transition from a conventional 3 Tesla scanner to a stronger 7 Tesla scanner is challenging, however, due to technical complexities accompanying higher magnetic field strength.⁶ One of these technical complexities is the increased inhomogeneity of the static (B_0) and radiofrequency (B_1) field, typically featuring areas of low B_1 close to the temporal lobes. The B_0 inhomogeneities are caused primarily by the susceptibility difference between inner ear fluids and the surrounding bone, and the B_1 inhomogeneities by the elliptical shape of the head. Both of these effects can result in loss of signal in the inner ear region as previously described by Takahara et al and Van Egmond et al.⁷⁻⁹ Additionally, the specific absorption rate, for which regulatory safety limits are defined, scales approximately quadratic with field strength, ultimately limiting the imaging speed at high fields in vivo. Recently, we introduced geometrically tailored dielectric pads to locally tailor the B_1 distribution. This improved contrast homogeneity and transmit efficiency in the region of the inner ear without increasing the specific absorption rate, which contributed to the development of a high resolution imaging protocol at 7 Tesla.¹⁰

The aim of this study was (1) to investigate the applicability of clinical inner ear imaging at 7 Tesla MRI and (2) to compare the visibility of inner ear structures and nerves within the internal auditory canal (IAC) with images acquired at 3 Tesla.

Materials and methods

Patients

This prospective study was approved by the hospital institutional review board (P07.096). Patients with SNHL, eligible for cochlear implantation and referred for 3 Tesla imaging between December 2012 and May 2013, were asked to participate in the study. Exclusion criteria were age under 18 years and contraindications for exposure to the magnetic field. Seventeen candidates for cochlear implantation were enrolled in the study; 9 females and 8 males between 27 and 78 years of age. Etiology and duration of hearing loss are described in Table 1. All patients underwent an MRI examination at 3 Tesla as part of the standard work-up for cochlear implantation. After obtaining written informed consent, sixteen patients underwent an examination at 7 Tesla; one patient was excluded due to intracranial foreign body of unknown composition. Three other patients were excluded after the scanning procedure due to the following reasons: scans of two patients were incomplete due to premature termination of the scanning procedure due to an unspecified technical defect and the scanning procedure of one patient had to be aborted due to claustrophobia. After the procedure patients were asked if they had suffered from dizziness, as this is a frequently reported but temporary side effect of scanning at 7 Tesla.

Table 1. Demographic details of studied patients (N=17)

		N
Sex		
	Male	8
	Female	9
Pathologic imaging reportings		
	Cochlea malformation	1*
	Hypoplasia acoustic nerve	1*
	Fenestral otosclerosis	1
	Labyrinthitis ossificans	1
	None	14
Etiology		
<i>Congenital</i>		
	Pendred syndrome	1
	of unknown origin	5
<i>Acquired</i>		
	Sudden deafness	2
	MIDD**	1
	Otosclerosis	2
	Rubella infection	2
<i>Unknown</i>		4
		Mean (years)
Duration of deafness		23.2

* Same patient



Imaging technique

All patients underwent examination on a Philips Achieva or Ingenia 3 Tesla system (Philips Healthcare, Best, The Netherlands) as part of the standard preoperative work-up. The following scan parameters were used for the T_2 -weighted TSE sequence: field-of-view 130 x 130 x 24 mm, 0.6 mm³ isotropic voxels, TR/TE/TSE factor = 2400ms/200ms/73 and 80 slices, resulting in an acquisition time of approximately 6 minutes. In addition, all patients were scanned on a Philips Achieva 7 Tesla system (Philips Healthcare, Best, The Netherlands) as described by Brink et al, using a quadrature transmit and 32 channel receive coil (Nova Medical, Wilmington, MA).¹⁰ To improve contrast homogeneity and transmit efficiency two gender-specific high permittivity pads, containing a suspension of barium titanate and deuterated water, were positioned next to both ears.¹⁰ High resolution T_2 -weighted images were acquired using the following parameters: field-of-view 180 x 180 x 24 mm, 0.3 mm³ isotropic voxels, TR/TE/TSE factor = 3000 ms/200 ms/69, tip angle/refocusing angle = 90°/135°, parallel imaging reduction factor = 2.5 x 1.5 and 160 slices. This resulted in an acquisition time of approximately 10 minutes.

Image analysis

The high resolution T_2 -weighted images acquired at both the 3 and 7 Tesla scanners were transferred to OsiriX DICOM viewer.¹¹ The images were anonymized and presented in randomized order. Evaluation was performed by two head and neck radiologists with 5 and 13 years of experience, respectively. A total of 24 anatomical structures of the inner ear were assessed using a 4-point-grading scale for degree of visibility for diagnostic evaluation: 1 = not assessable, 2 = poor, 3 = adequate, 4 = excellent. The structures selected were those most relevant for cochlear implantation. In addition, an overall score for diagnostic image quality was granted: 1 = not diagnostic, 2 = poor, 3 = adequate, 4 = excellent. Both ears were evaluated separately. Subsequently the scores of the two ears and two observers were averaged and normalized into a parameter between 0 and 1. An overview of the anatomical structures and their difference in rating is shown in Figure 4. The numbers I, II and III refer to the basal, mid and apical turn, respectively.

Statistical analysis

Statistical analysis was performed using SPSS (IBM Corp Released 2011. IBM Statistics for Windows, Version 20.0. Armonk, NY: IBM Corp). In order to study the influence of observed asymmetrical signal intensity between the right and left inner ear on the 7 Tesla images, a linear mixed model was performed. Statistical differences per anatomical structure between the 3 and 7 Tesla scanner were determined using a Wilcoxon signed rank test. The inter-rater variability was determined by the Kappa coefficient of Cohen. All tests were two-tailed and $P < 0.05$ was considered to indicate a statistically significant difference.

Results

Twenty six inner ears of 13 patients were available for image analysis. The occasionally observed asymmetrical signal intensity on some of the 7 Tesla images did not result in a significant different rating of the right and left inner ear ($p=0.215$). Therefore no distinction between inner ear sides was used for analysis. As 24 anatomical structures per inner ear were evaluated on T_2 -weighted images acquired on 3 and 7 Tesla scanners plus an additional score for overall image quality, this resulted in 2600 ratings applied by the two observers together. The ratings were averaged over ear and observer, leaving 650 ratings for statistical analysis. The visibility of 11 out of the 24 anatomical structures was rated higher on the 7 Tesla images. None of the anatomical structures were better depicted on the 3 Tesla images. There was no significant difference in the visibility of 13 anatomical structures and the overall diagnostic image quality rating. The inter-observer agreement was moderate with a κ -value of 0.55. None of the patients reported excessive or extended dizziness during or after the scan procedure.

Cochlea

Figure 1 shows the cochlea on an axial cross-section image, clearly illustrating the improved resolution of the 7 Tesla image contributing to a more detailed depiction of the inner ear anatomy. Evaluated cochlear structures include the scala vestibuli, scala tympani, scala media, osseous spiral lamina and interscalar septa. All structures were evaluated separately for each cochlear turn. Significant differences in favor of the 7 Tesla images were found for the scala tympani and vestibuli in the 2nd and 3rd turn, with a mean difference of 0.13 ($p = 0.023$) and 0.31 ($p = 0.023$) for the 2nd turn and 0.14 ($p = 0.002$) and 0.31 ($p = 0.002$) for the 3rd turn. The scala media in the first turn could be distinguished in 7 out of 52 ratings on the 7 Tesla images, but in none of the inner ears on the 3 Tesla images. Visualization of these distinguished scala medias were 6 times evaluated as 'poor' and one time as 'adequate'. The resulting score difference of 0.05 was not significant ($p = 0.066$). In the second turn, the scala media was visible in 21 inner ears on the 7 Tesla images, compared to none on the 3 Tesla images. The degree of visibility of these structures was rated 'poor' in 16 cases, 'adequate' in 3 cases and 'very good' in 2 cases. The score difference of 0.18 was significant for this turn ($p = 0.005$). In the second and third turn, the depiction of the osseous spiral lamina was better on the 7 Tesla images, resulting in a sharp delineation of the scala tympani and vestibule ($p = 0,006$ for the second turn and $p = 0.001$ for the third turn). The visibility of the interscalar septum between the second and third turn also significantly benefits from high resolution imaging at 7 Tesla ($p = 0.003$).

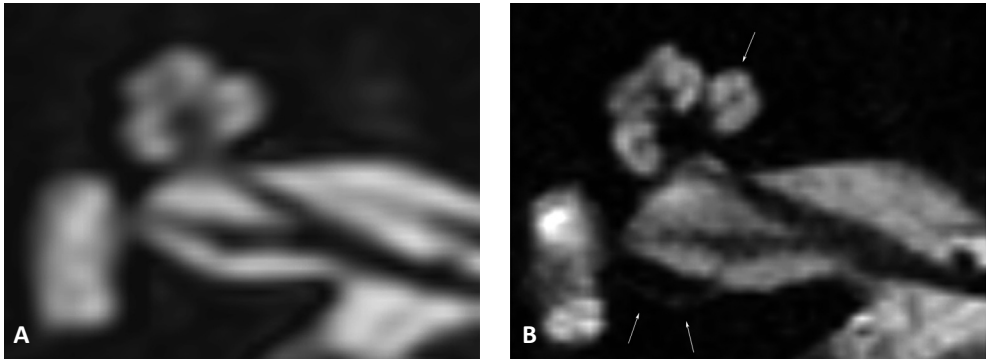


Figure 1: Axial cross-section of a right inner ear, rendered at 3 Tesla (A) and 7 Tesla (B); improved discrimination of the intra cochlear structures and compartments is shown. Also sharper delineation of the nerves in the internal auditory canal is demonstrated. The single arrow indicates the scala media at the first turn. The double arrows indicate the superior ampullary nerve.

Internal auditory canal

Statistical differences in visualization of the facial ($p = 0.259$), superior ($p = 0.131$) and inferior vestibular ($p = 0.242$) and cochlear nerve ($p = 0.151$) through the internal auditory canal could not be demonstrated. On the 3 Tesla images, the intermediate nerve was observed 5 out of 52 times, compared to 31 times on the 7 Tesla images. On the 7 Tesla images the visibility of the intermediate nerve was evaluated as ‘poor’ in 14 cases, ‘adequate’ in 8 cases and ‘excellent’ in 9 cases. This resulted in a significant difference of 0.32 ($p = 0.002$). An example of the clear depiction of an intermediate nerve is shown in Figure 2. Also a sharper delineation of the other neural structures is obtained. The superior ampullary nerve is indicated in Figure 1B by two white arrows. This small neural structure is not regularly visualized on 3 Tesla scans. In this study it was observed 10 out of 52 times on the 3 Tesla scans; 7 times ‘poor’ and 3 times ‘adequate’, compared to 28 times on the 7 Tesla scans; 11 times ‘poor’, 6 times ‘adequate’ and 11 times ‘excellent’. This resulted in a significant difference of 0.28 ($p = 0.009$).

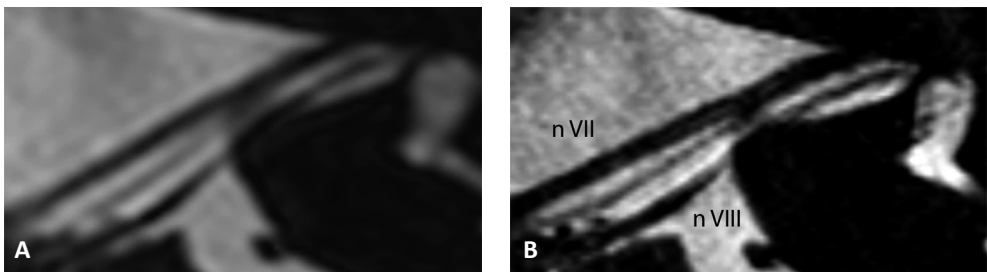


Figure 2: Axial cross-section along the course of the facial nerve of a left inner ear, rendered at 3 Tesla (A) and 7 Tesla (B). A sharp delineation of the neural structures and clear depiction of the intermediate nerve between n VII and n VIII is demonstrated at the 7 Tesla image.

The visualization of the falciform crest was significantly improved on the 7 Tesla images; it was identified in 47 out of 52 readings on the 7 Tesla images, compared to 41 readings on the 3 Tesla images. This led to a score difference of 0.25 ($p = 0.022$). Bill's bar was only occasionally observed at either magnetic field strength.

Cochlear and vestibular aqueducts

Visualization of the vestibular aqueduct (VA) and cochlear aqueduct (CA) did not differ significantly among the 3 and 7 Tesla images. A score difference of 0.16 ($p = 0.107$) of the VA and 0.01 ($p = 0.836$) of the CA were found.

Artifacts

A higher incidence of image artifacts was observed in the 7 Tesla images; 9 out of the 13 scans versus none of the 3 Tesla scans. These artifacts include motion artifacts likely due to the prolonged scan duration compared to 3T. Also off-resonance effects due to the increased B_0 inhomogeneities causing signal loss and stripe-like artifacts likely due to B_1 -inhomogeneities were observed. An example of their appearances is shown in Figure 3.

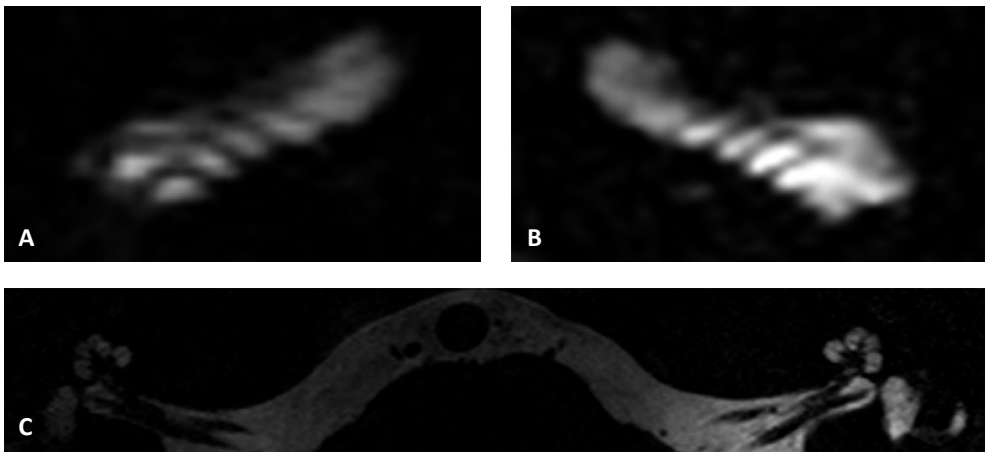


Figure 3: 7 Tesla images showing stripe like-artifacts at the level of the first turn of a right (A) and left (B) cochlea of 2 different patients, disturbing the quality of its representation and impeding the distinction of the scala vestibuli and tympani. Asymmetrical signal intensity was observed occasionally (C).

Overall image quality

Image quality can be expressed as either the mean of scores per magnetic field strength or the actual applied score for image quality. Firstly we calculated the sum of scores, separately for each magnetic field strength. Comparison of these values resulted in a significant difference of 0.11 per anatomical structure in favor of the 7 Tesla scanner ($p < 0.001$). Secondly, the score for overall image quality as rated directly was analyzed. This score for overall image quality was applied in the context of diagnostic value, meaning distortion of

the image quality by artifacts was taken into account. Comparing these scores did not show a significant difference between the two field strengths ($p = 0.631$).

An overview of all the described outcomes is presented in Figure 4.



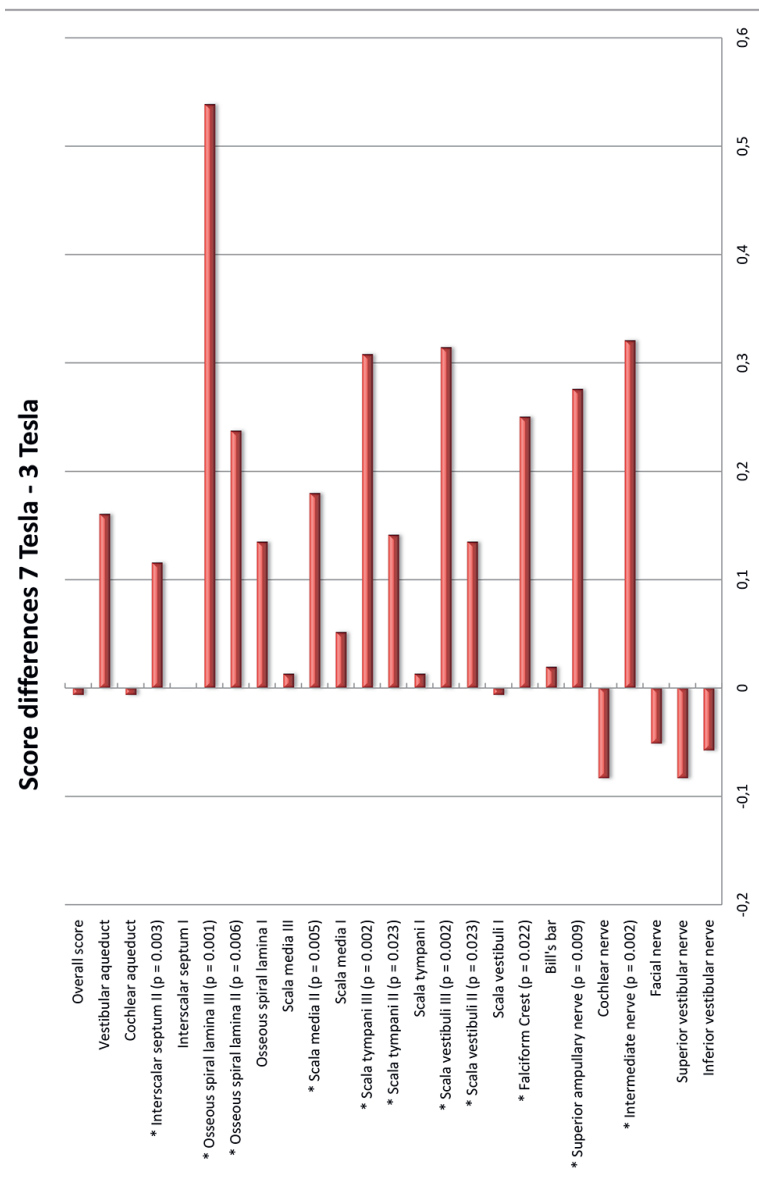


Figure 4: Mean differences in scoring of anatomical structures depicted at 3 and 7 Tesla images. The red bars on the right side of the 0-line indicate differences in favor of the 7 Tesla images. The bars on the left side indicate differences in favor of the 3 Tesla images. The structures showing significant differences are marked with an asterisk on the left and p-values are mentioned if significant.

Discussion

7 Tesla MR imaging of the inner ear was successfully performed in patients with profound SNHL eligible for cochlear implantation. Comparison with 3 Tesla images demonstrated improved visualization of a large number of anatomical structures of the inner ear and internal auditory canal with high resolution 7 Tesla imaging and emphasized the potential of clinical imaging at 7 Tesla.

Regarding the cochlear structures, the benefit of increased SNR was most pronounced for visualization of the microstructures of the 2nd and 3rd turn. The accurate distinction of the different turns and compartments is essential to accurately diagnose and localize pathologies and to support surgical planning. One specific development over the last years that has emphasized the role of radiological evaluation of cochlear implant candidates is the expanded criteria for cochlear implant recipients. A malformed cochlea is no longer an absolute contraindication for implantation, which is important as up to 20% of the patients with SNHL show some degree of inner ear malformation.¹² However, when a malformation is present, the surgical procedure carries a higher risk for complications such as cerebrospinal fluid gusher, and often a different surgical approach and electrode type need to be chosen to ensure a good outcome.¹³ These considerations require precise preoperative planning, and an increase in anatomical information as achieved with 7 Tesla could be beneficial in such patients. Another example where an increase in anatomical information could be extremely relevant includes patients with obliterated cochleas. This fibrotic or osseous obliteration of the cochlear lumen is usually caused by meningitis-induced labyrinthitis. When parts of the cochlea are not patent, a different surgical approach should be followed with, in some cases, the use of a split array electrode.¹⁴ This device was developed to maximize the coverage of spiral ganglion cells by inserting two separate arrays through different cochleostomies. To precisely guide this procedure, comprehensive details of the cochlea anatomy are required. For electro-acoustic stimulation (EAS), cochlear trauma needs to be minimized and preoperative delineation of the cochlear anatomy should be as accurate as possible. In addition, gain in detailed anatomical information of the cochlea enables further research on morphological characteristics, their influence on electrode position and its relation to CI recipients' performance.^{15,16}

At the location of the internal auditory canal, smaller nerve branches such as the superior ampullary nerve and the intermediate nerve were in general better depicted at 7 Tesla. The fact that larger neural structures did not benefit from the increased resolution at 7 Tesla can be explained by (1) motion artifacts, (2) off-resonance and stripe-like artifacts and (3) the scoring system. The internal auditory canal where these structures are housed was particularly vulnerable to patient-induced motion artifacts. It was observed that the neural structures in the internal auditory canal were more frequently affected than the cochlear



structures when motion of the head took place during the scan procedure. An explanation for this observation is not well defined yet, but one can realistically hypothesize a combination of the direction of the motion and the dimensions of the IAC that makes it more vulnerable. Scanner-related artifacts such as the stripe-like artifacts and off-resonance were only pronounced at higher field strength, as might be expected from the implicit larger absolute change in resonance frequency. Another contributing factor might have been the chosen 4-point grading scale. In the majority of cases, the visibility of nerves were rated 'excellent', based on delineation of the neural structures in both the 3 and 7 Tesla images. Consequently a distinction in visualization between the 2 scanners is hardly detectable and decisive for evaluation was the presence of artifacts. Yet, although not evaluated systematically one observer reported more confident assessment on cochlear nerve hypoplasia at 7 Tesla.

With respect to the clinical relevance, it is important to realize that many etiologies causing SNHL cannot be seen *in vivo* with current techniques. By increasing SNR and resolution, however, it is expected that more anatomical changes related to SNHL can be demonstrated. By showing the capability of 7 Tesla MRI to visualize anatomical structures such as the distinguished scalas of the 2nd and 3rd turn, scala media, intermediate nerve and superior vestibular nerve, a first step towards that expectation has been made. When etiologies are known, treatment and prognosis can be tailored more accurately. Improved image quality does however come with a number of drawbacks and limitations. An example of such a limitation is the prolonged scan duration. In our study scan duration was prolonged from 6 to 10 minutes. This prolongation together with the lack of communication possibilities for this specific patient population caused an increased susceptibility to subject-induced artifacts, and therefore the use of communicative visual signaling during scanning is recommended. Additionally, the likelihood of motion artifacts could be reduced by shortening scan duration through reduced FOV imaging techniques.¹⁷ Another important issue is the presence of possible side effects during 7 Tesla examinations. Previous research reports a slightly higher incidence of dizziness than at 3 Tesla, discomfort from the gradient noise and a metallic taste.^{18–20} Nevertheless, these side effects are widely accepted and in general 7 Tesla examinations are tolerated well. In our study population none of the patients mentioned excessive discomfort during the scan procedure.

Another limitation of our study is the difference in background of the observers. One observer normally evaluates MR images acquired at 3 Tesla, whereas the second observer normally evaluates MR images acquired at 1.5 Tesla only. This may have resulted in overvaluation of the 3 Tesla images by the second observer, thereby diminishing the difference between the 3 and 7 Tesla images and decreasing the a k-value.

Conclusion

We report progress toward the use of 7 Tesla MRI for inner ear scanning in a clinical setting. The gain in SNR resulted in a more detailed visualization of a large number of relevant anatomical structures despite the remaining difficulties accompanying high magnetic field imaging. The findings of this study are encouraging to continue research on technical adjustments to push the limits of 7 Tesla MRI to reach its full potential and make it suitable for clinical applications.



References

1. Verbist BM. Imaging of sensorineural hearing loss: a pattern-based approach to diseases of the inner ear and cerebellopontine angle. *Insights Imaging*. 2012;3(2):139–53.
2. Casselman JW. Diagnostic imaging in clinical neuro-otology. *Curr Opin Neurol*. 2002;15(1):23–30.
3. St Martin MB, Hirsch BE. Imaging of hearing loss. *Otolaryngol Clin North Am*. 2008;41(1):157–78.
4. Mohan S, Hoeffner E, Bigelow DC, Loevner L a. Applications of magnetic resonance imaging in adult temporal bone disorders. *Magn Reson Imaging Clin N Am*. 2012;20(3):545–72.
5. Davidson HC. Imaging evaluation of sensorineural hearing loss. *Semin Ultrasound CT MR*. 2001;22(3):229–49.
6. Robitaille P, Berliner L. *Ultra high-field magnetic resonance imaging*; 2006.
7. Sled JG, Pike GB. Standing-wave and RF penetration artifacts caused by elliptic geometry: an electrodynamic analysis of MRI. *IEEE Trans Med Imaging*. 1998;17(4):653–62.
8. Takahara T, Hoogduin H, Visser F, Naganawa S, Kwee T, Luijten P. Imaging of the Inner Ear at 7T : Initial Results. In: *Proceedings of the 18th Annual Meeting of ISMRM. Stockholm, Sweden; 2010:4448*. Vol 17.
9. Van Egmond SL, Visser F, Pameijer F a, Grolman W. Ex Vivo and In Vivo Imaging of the Inner Ear at 7 Tesla MRI. *Otol Neurotol*. 2014:1–5.
10. Brink WM, van der Jagt AMA, Versluis MJ, Verbist BM, Webb AG. High Permittivity Dielectric Pads Improve High Spatial Resolution Magnetic Resonance Imaging of the Inner Ear at 7 T. *Invest Radiol*. 2014;00(00):1–7.
11. Rosset A, Spadola L, Ratib O. OsiriX: an open-source software for navigating in multidimensional DICOM images. *J Digit Imaging*. 2004;17(3):205–16.
12. Sennaroglu L. Cochlear implantation in inner ear malformations--a review article. *Cochlear Implants Int*. 2010;11:4–41.
13. Sennaroglu L, Sarac S, Ergin T. Surgical results of cochlear implantation in malformed cochlea. *Otol Neurotol*. 2006;27:615–623.
14. Millar D a, Hillman T a, Shelton C. Implantation of the ossified cochlea: management with the split electrode array. *Laryngoscope*. 2005;115(12):2155–60.
15. Van der Marel KS, Briaire JJ, Wolterbeek R, Snel-Bongers J, Verbist BM, Frijns JHM. Diversity in Cochlear Morphology and Its Influence on Cochlear Implant Electrode Position. *Ear Hear*. 2013:1–12.
16. Holden LK, Finley CC, Firszt JB, et al. Factors affecting open-set word recognition in adults with cochlear implants. *Ear Hear*. 2013;34(3):342–60.
17. Wargo CJ, Moore J, Gore JC. A comparison and evaluation of reduced-FOV methods for multi-slice 7T human imaging. *Magn Reson Imaging*. 2013;31(8):1349–59.
18. Heilmaier C, Theysohn JM, Maderwald S, Kraff O, Ladd ME, Ladd SC. A large-scale study on subjective perception of discomfort during 7 and 1.5 T MRI examinations. *Bioelectromagnetics*. 2011;32:610–9.
19. Theysohn JM, Maderwald S, Kraff O, Moeninghoff C, Ladd ME, Ladd SC. Subjective acceptance of 7 Tesla MRI for human imaging. *MAGMA*. 2008;21:63–72.

20. Versluis MJ, Teeuwisse WM, Kan HE, van Buchem M a, Webb AG, van Osch MJ. Subject tolerance of 7 T MRI examinations. *J Magn Reson Imaging*. 2013;38:722–5.







Chapter 3

Variations in cochlear duct
shape revealed on clinical CT
images with an automatic
tracing method

MA van der Jagt, RK Kalkman,
JJ Briaire, BM Verbist, JHM Frijns

*Published in Nature Scientific
Reports, 2017*

Abstract

Cochlear size and morphology vary greatly and may influence the course of a cochlear implant electrode array during insertion and its final intra-cochlear position. Detailed insight into these variations is valuable for characterizing each cochlea and offers the opportunity to study possible correlations with surgical or speech perception outcomes. This study presents an automatic tracing method to assess individual cochlear duct shapes from clinical CT images.

On pre-operative CT scans of 479 inner ears the cochlear walls were discriminated by interpolating voxel intensities along radial and perpendicular lines within multiplanar reconstructions at 1 degree intervals from the round window.

In all 479 cochleas, the outer wall could be traced automatically up to 720 degrees. The inner wall and floor of the scala tympani in 192 cochleas. The shape of the cochlear walls were modelled using a logarithmic spiral function including an offset value. The vertical trajectories of the scala tympani exhibited a non-monotonous spiral slope with specific regions at risk for CI-related insertion trauma, and three slope categories could be distinguished.

This presented automatic tracing method allows the detailed description of cochlear morphology and can be used for both individual and large cohort evaluation of cochlear implant patients.

Introduction

The human cochlea exhibits considerable interindividual variability in size and morphology¹⁻⁵. This variation influences the final position of the electrode array after performing cochlear implant (CI) surgery and may be important for patient-specific surgical planning^{5,6}. Optimal placement of the electrode array to maximize speech recognition should be achievable in all individual cochleas; to accomplish this, increased insight into cochlear morphology is needed.

The human cochlea is a spiral-shaped cavity in the bony labyrinth with the scala tympani (ST) as the targeted compartment for insertion of a CI electrode array. Both the course and final position of the electrode array are influenced by several factors, including cochlear morphology. In relation to cochlear morphology, Van der Marel et al. showed that 12% of the variance in angular insertion depth can be explained by cochlear size alone⁵. Escudé et al. studied the effect of cochlear size on insertion depth and reported that a 2 mm larger diameter of the basal turn produces a 5.0 mm larger length of the lateral wall⁶. The diameter or circumference of the basal turn is often used as an indicator to describe the size of the cochlea. The diameter of the basal turn, measured from the center of the round window (RW) to the opposite outer cochlear wall, varies between 5.6 and 8.2 mm, and the circumference of the basal turn, often referred to as the cochlear duct length (CDL), varies in length between 20.3 and 24.3 mm². Dimensional variations of the second turn have been limited investigated, even rarely in vivo, but it is conceivable that variations at this level also play an important role in the surgical outcome after cochlear implantation, especially with somewhat longer electrode designs.

Other, less frequently described characteristics of the human cochlea relevant for cochlear implantation are its coiling pattern and vertical trajectory. The Archimedean and logarithmic spiral function are most often used to describe the coiled shape of the cochlea⁷. Previous studies from our group confirmed the applicability of the logarithmic function on the shape of the basal turn⁵. Erixon et al. found that each cochlea is individually shaped and reported a large variation in coiling characteristics, suggesting that the spiral functions do not fit all individual cochleas². Specifically, the shape and size of the basal turn of the cochlea is influenced by the coiling pattern; early coiling results in a smaller, more compressed cochlea with an earlier increase in the vertical trajectory. The vertical trajectory of the ST exhibits an undulating slope and likely plays a critical role in the occurrence of intra-cochlear trauma during CI surgery. Earlier ex vivo studies have demonstrated three high-risk areas for intra-cochlear trauma along this trajectory^{1,8}. First at the site of insertion, near the RW, and is related to the surgical procedure of insertion. The second one is located approximately 180-200 degrees from the RW, where the presence of a downward slope of the ST, in many cases, is likely to alter the course of the electrode array. This may expose the osseous spiral lamina (OSL) or basilar membrane (BM) to compression forces. A subsequent steep upward slope



will force the tip of the electrode array to press against the floor of the ST and bend upward⁸. These provoked changes in the course of the implant are considered to be associated with insertion trauma. As with size, height, and coiling pattern, large variation exists in the vertical trajectory, and three slope categories were identified based on the anatomical features of this vertical trajectory in micro-CT data in a series of temporal bones¹. We hypothesize that, if such a detailed account of the vertical trajectory can be obtained *in vivo*, it may be a valuable pre-operative indicator for estimating the risk of insertion trauma.

Here, we present a novel, automatic method for determining the cochlear walls and floor of the ST from multiplanar reconstructions (MPRs) of clinical CT images. The cochlear walls are traced from the RW up to a cochlear angle of 720 degrees, providing the unique opportunity of assessing cochlear morphology *in vivo* up to and including the second turn. The method will be shown to be applicable in a large population of CI candidates.

Materials and Methods

Patient population

We analyzed pre-operative CT scans of all patients consecutively implanted at Leiden University Medical Center in the Netherlands between January 2011 and December 2014. Patients with cochlear malformations (n = 14), obliteration of the cochlear lumen by fibrosis or ossification (n = 16), or fenestral and/or cochlear otosclerosis obscuring identification of the RW (n = 4) were excluded. Scans performed at external institutions or with inferior scan quality due to movement artefacts were excluded (n = 39). A total of 479 inner ear CT scans from 242 patients were included in the analysis. Table 1 summarizes the demographic characteristics of the patient population (n = 242).

Table 1. Demographic characteristics

Total population (N = 242 patients)		
Age at implantation	Mean, SD (years)	47, 24
Gender	Male : Female	111:131
Etiology of deafness		
<i>Congenital</i>	Hereditary	45
	Acquired	12
	Anatomical	3
	Unknown	50
<i>Acquired</i>	Meningitis	10
	Meniere's disease	8
	Trauma	2
	Otosclerosis	1
	Recurrent otitis	1
<i>Unknown</i>		110

All methods were carried out in accordance with relevant guidelines and regulations related to retro-spective research with existing data, as stated by our institutional Medical Ethical Committee.

Image reconstruction and analysis

At Leiden University Medical Center, CI candidates undergo a CT scan of both inner ears prior to implantation to gain insight into the etiology of deafness and feasibility of implantation as part of a standard work-up. The CT scans evaluated in this study were acquired using an Acquilion scanner (Toshiba Medical Systems, Otowara, Japan). MPRs were assembled from these scans and a 3D coordinate system was applied that enables general assessment of the inner ear anatomy (Verbist et al., 2010a). The basis of this coordinate system is formed by the cochlear view perpendicular to the basal turn. A three-dimensional cylindrical system is created by adding a z-axis through the center of the modiolus with its origin at the helicotrema. The RW is chosen as the zero degree angle of rotation.

Automatic tracing procedure

To automatically trace the cochlear walls in pre-operative MPRs, a custom algorithm was written using MATLAB and its image processing toolbox (version R2015a). The basic principle behind the automatic tracing algorithm is illustrated in Figure 1. Figure 1a shows an MPR slice with a coordinate system as defined in the consensus study by Verbist et al. (2010b). The edges of the RW are marked by red crosses (note that the edges were determined in a different MPR slice than the one depicted). The red line through the center of the RW and the modiolus of the cochlea indicates the $0^{\circ}/180^{\circ}$ cochlear angle line, and the blue line indicates the $90^{\circ}/270^{\circ}$ cochlear angle. The point where the red and blue lines intersect is the location of the modiolar axis. In this MPR, a radial line is plotted at an arbitrary cochlear angle of 25° (yellow line), along which the locations of the inner and outer walls were determined.

Figure 1b shows the corresponding midmodiolar cross-section at 25° , which is obtained by first calculating image profiles using the 'improfile' function in MATLAB, which interpolates the voxel intensities along the radial lines in each MPR slice (the lines were extended across the entire MPR slice and thus also included the opposite side of the modiolar axis, i.e. the radial line at 205°). Next, these image profiles were set as rows of pixels in a two-dimensional image, which was then up scaled using the 'imresize' function to generate the midmodiolar cross-section shown. In both the improfile and imresize functions bicubic interpolation was used and the pixel size was set equal to the voxel dimensions in the original MPR slices.

In Figure 1b, the modiolar axis is indicated by a black vertical line at the center of the image and two radial lines, set in consecutive MPR slices which are 0.5 mm apart, are again plotted in yellow. Figure 1c shows the image profiles calculated along the radial lines shown in Figure 1b; the top plot corresponds to the top yellow line in Figure 1b, and the bottom plot



corresponds to the bottom yellow line. In these image profiles, the minima and maxima closest to the inner and outer cochlear walls are indicated by black dots. The locations of the cochlear walls were determined in each image profile by assuming that the voxel intensity values at the boundaries are halfway between the nearest minimum and maximum intensity value; the location of the outer wall found in this manner is marked in each image profile with purple circles, while the inner wall is marked with a light blue circle.

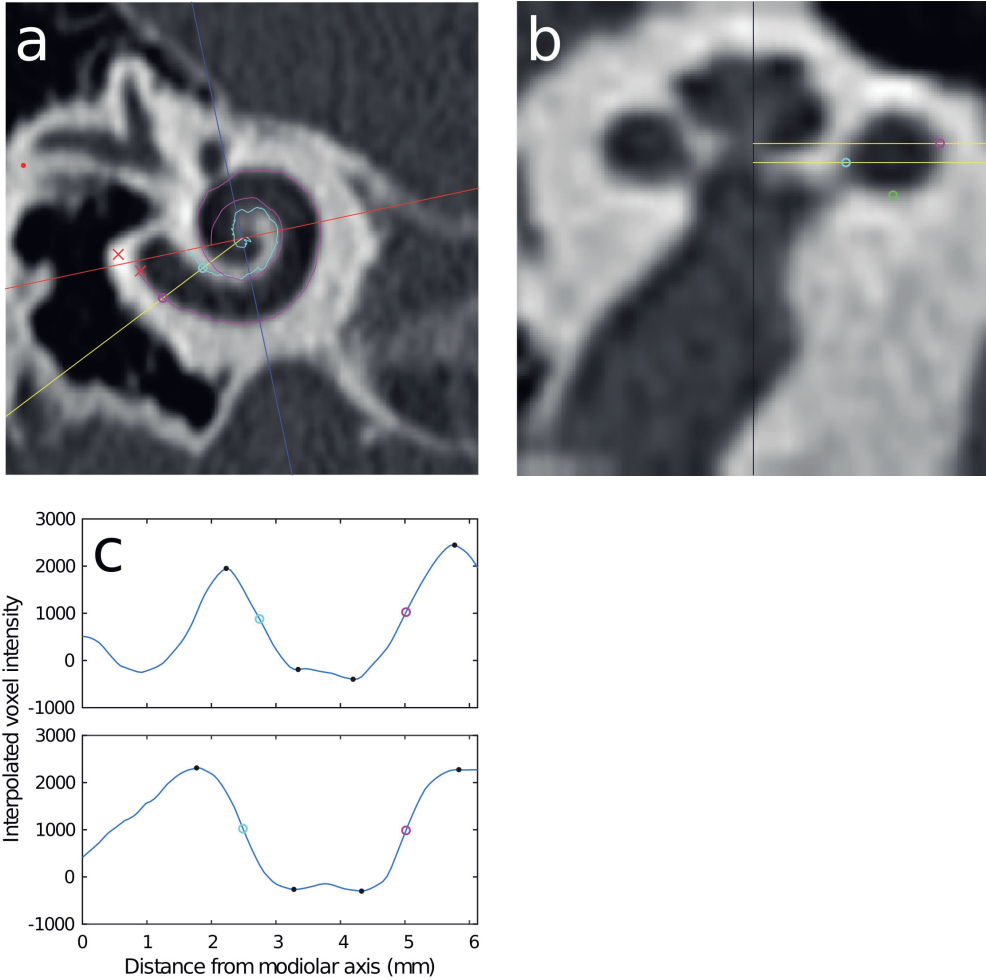


Figure 1: Illustration of the automatic tracing method. (a) MPR slice of a pre-operative cochlear CT scan. (b) Midmodiolar cross-section of the cochlea at the angle indicated by the yellow line in (a). (c) Interpolated voxel intensity along the yellow lines in (a) and (b); the top plot shows voxel intensities along the top yellow line in figure (b), while the bottom plot corresponds to the bottom yellow line shown in (b). The purple, light blue and green circles indicate the locations determined for the outer wall, inner wall, and floor of the scala tympani, respectively. The purple and light blue curves in the MPR of figure (a) are projections of the automatically traced outer and inner walls. The Black dots in figure (c) indicate minima and maxima.



These outer and inner wall points were determined for every MPR slice at 1 degree intervals, starting from the line through the center of the RW (0°) to a maximum angle of 720°. At each angle, the most laterally located outer wall point and the most medially located inner wall point were selected for the final traces of the outer and inner walls, respectively. In the example given in figure 1, the outer wall point in the top image profile of figure 1c was selected for the trace of the outer wall, and the inner wall point of the bottom image profile was selected for the inner wall trace; these selected points are also plotted as purple and light blue circles in figures 1a and 1b. The two-dimensional projections of the full traces of the outer and inner wall are respectively plotted as purple and light blue curves in figure 1a.

After the outer and inner walls were traced, the bottom walls were determined in a manner similar to the one described above. At every angle, the same method was used to interpolate voxel intensities along a line in the midmodiolar cross-section. The line of interpolation ran parallel to the modiolar axis and was located exactly halfway between the outer and inner wall points. As with the outer and inner walls, the location of the bottom wall was determined in the resulting image profile by finding the minima and maxima and assuming the bottom wall was located there where the voxel intensity was halfway between the adjacent minimum and maximum values. The green circle in Figure 1b shows the location of the bottom wall determined by this method.

Radial distances and vertical trajectory

To describe cochlear morphology, radial distances from the modiolar axis to the outer and inner wall were measured per angular distance from the RW to a maximum of 720 degrees (representing the basal and second turn). The averaged distance for the complete population of 479 inner ears was used to determine the average size and standard deviation (SD) as a function of cochlear angle. By subtracting the inner wall radius from the outer wall radius, the diameter of the cochlear canal was calculated. In addition, the vertical trajectory was determined for each individual patient by determining the z-coordinates of the floor of the ST relative to the center of the RW.

Spiral fitting of cochlear walls

Cochlear shape was also described by applying a spiral fit through the radial distances of the inner and outer walls separately. From observations, an assumption was made that the outer and inner wall radial distances did not completely follow a logarithmic spiral function, but remained more or less constant from halfway through the second turn towards the apical region. Therefore, we introduced an offset value into the logarithmic spiral function that is commonly used to describe the cochlear curve^{5,7}. Subsequently, the curve that optimally represents the 720 radial distances of the outer and inner walls to the center of the modiolus was fitted by an individually adjusted exponential fitting formula based on the curve of a logarithmic spiral, both without (equation 1) and with (equation 2) an offset value.

$$r(\Theta) = ae^{b\Theta} \quad (1)$$

$$r(\Theta) = ae^{b\Theta} + c \quad (2)$$

where r represents the distance to the center of the modiolus, Θ the corresponding angular distance, a and b the coefficients, and c the offset value. These fitting formulas were applied to each inner ear individually, as well as over the median measurements per angle of the 479 inner ears. The fit of the radial distances of the inner and outer walls, indicated by the root mean square (RMS), was compared between the function with and without an offset value.

Manually versus automatically determined cochlear walls

In a previous study at our institution, the outer and inner walls of the basal turn of the cochlea were determined manually by scrolling through the pre-operative MPRs, to search their boundaries ⁵. Four outer wall radii, four inner wall radii, and four cochlear duct sizes were determined at 0, 90, 180, and 270 degrees in accordance with the consensus on cochlear coordinates (Verbist, 2010). This comparison could only be made for the basal turn because only the automatically measurements extend beyond the basal turn. The measurements of the inner and outer radii were compared to the output from the automatically traced values using a paired samples t-test.

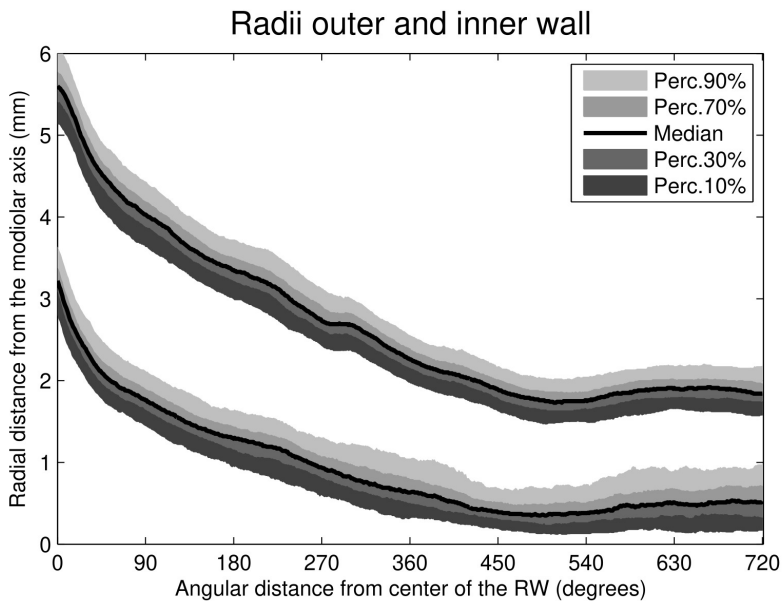


Figure 2: Automatically traced radial distances from the outer (upper lines) and inner (lower lines) walls to the modiolar axis from a cochlear angle of 0 to 720 degrees.

Data availability

The datasets generated in this study are available from the corresponding author on reasonable request.



Results

Method applicability

Tracing the complete two turns could be achieved in respectively all 479 for the outer wall and 192 cochleas for the inner wall. In the remaining 287 cochleas, the inner wall was traced up to 577 degrees on average (SD 161).

Radial distances and cochlear canal size

Figure 2 shows the median, 10th, 30th, 70th, and 90th percentile radii of the outer (upper lines) and inner (lower lines) walls, automatically traced from the center of the RW in the apical direction. The radii decreased gradually until 500 degrees for both the outer and inner walls. Between 500 and 720 degrees, the inner and outer walls do not further approximate the modiolus or each other; the radii slightly increase in size from there, the outer wall more so than the inner wall. The smallest median outer wall radius was measured at 516 degrees (1.74 mm). From this minimum in the apical direction, the largest outer wall radius was measured at 645 degrees (1.90 mm) ($p < 0.001$). For the inner wall, the shortest radius (0.39 mm) was measured at 492 degrees. More apical, the maximal radial distance of the inner wall to the modiolus was 0.53 mm at 619 degrees ($p < 0.001$). The limited decrease in the radial distances is also reflected in the size of the cochlear duct calculated from the median values for the outer and inner walls (Figure 3). At the basal portion, from 0 to 15 degrees, the median diameter of the cochlear duct gradually grows to a maximum of 2.6 mm. From 15 degrees, the lumen decreases gradually to a minimum of 1.5 mm at 500 degrees. Around 270 degrees, the radius of the outer wall remains more or less stable for approximately 30 degrees. This pattern is not present in the inner wall measurements. Thus, a slight decrease in the cochlear duct size is visible around that area. The smallest cochlear duct size was found around 500 degrees. From 555 degrees, the median cochlear duct size slightly expands to a maximum size of 1.7 mm at 662 degrees. The slightly irregular tapering of both the basal and second turn is clearly visible in Figures 2 and 3. Also, an increasing and uneven change in both radial distance and cochlear duct size from the basal end to the end of the second turn is evident. The median outer wall length for two complete cochlear turns was 35.1 mm (range 30.3–41.5 mm) in the entire population of 479 ears. The inner wall in 192 inner ears had a median length of 15.9 mm (range 10.6–24.8 mm).

Spiral fitting of cochlear walls

Figure 4 shows the median radial distances from the modiolar axis to the outer (red line) and inner (blue line) walls of the cochlea from 0 towards 720 angular degrees. The graph shows

an exponential reduction in the radial distance for the first approximately 500 degrees (1.4 turn), but beyond the length of the radii it remains almost constant. This suggests that an offset value needs to be added to the logarithmic spiral function in order to more veraciously model the course of the cochlear duct. Using logarithmic transformation and regression analysis, spiral fitting formula coefficients were determined for the radial lengths of the inner and outer walls for each individual inner ear, both with and without the implementation of an off-set value. With the implemented off-set value, the accuracy of the spiral function (R^2) to describe the radial distances increased from 0.90 (SD 0.05) to 0.96 (SD 0.04) for the outer wall ($p < 0.001$) and from 0.88 (SD 0.15) to 0.91 (SD 0.09) for the inner wall ($p < 0.001$). The median outer and inner wall radial distances (solid lines) in 479 inner ears and its logarithmic spiral function with off-set value (dashed lines) are shown in Figure 4.

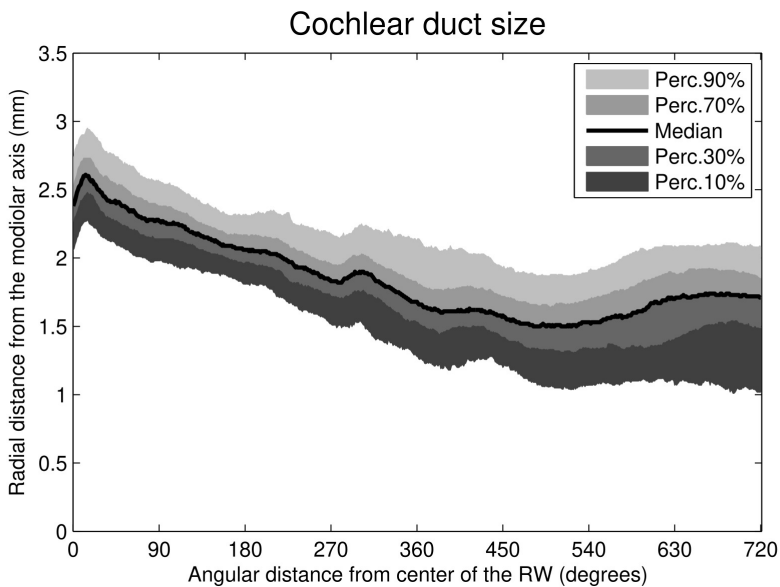


Figure 3: Diameter of the cochlear duct from 0 to 720 degrees.

Floor of the scala tympani

Figure 5 represents the median vertical trajectory of the floor of the ST, as well as the 10th, 30th, 70th, and 90th percentiles. The figure shows that, especially in the first 270 degrees, the vertical trajectory varies greatly. The least variation in the vertical trajectory is present at the confluence of the first and second turns. To illustrate the large variation, an overview of nine individual trajectories is presented in Figure 6. Roughly three different courses of the basal turn can be distinguished. Course 1 is a proximal rise and fall within the basal turn (Figure 6A-C). Course 2 is a late steep rising, with a preceding flat course (Figure 6D-F) or fall (Figure 6G) within the first 360 degrees. Course 3 has a more or less constant rising of the vertical slope (Figure 6H and I).

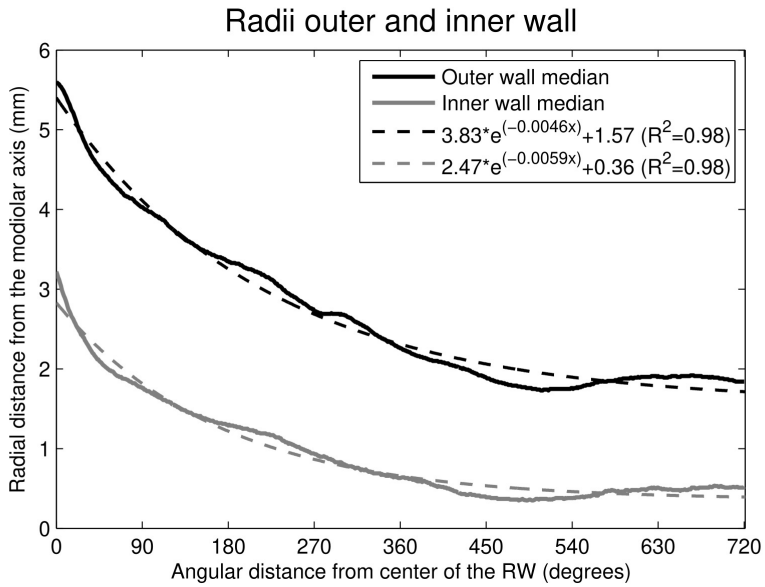


Figure 4: Median radial distances of the outer (red) and inner walls (blue) from the central axis of the modiolus. The dashed lines indicate the spiral functions.

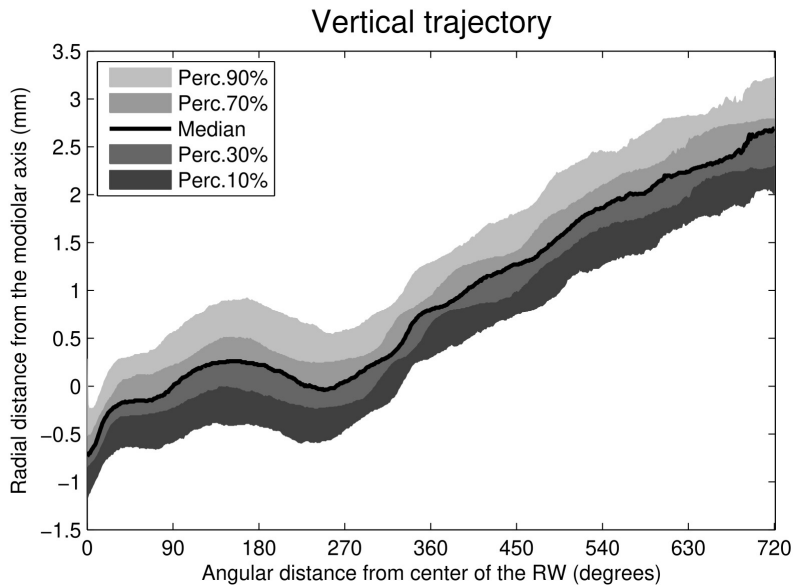


Figure 5: Automatically traced vertical trajectory of the floor of the scala tympani.

Vertical trajectories

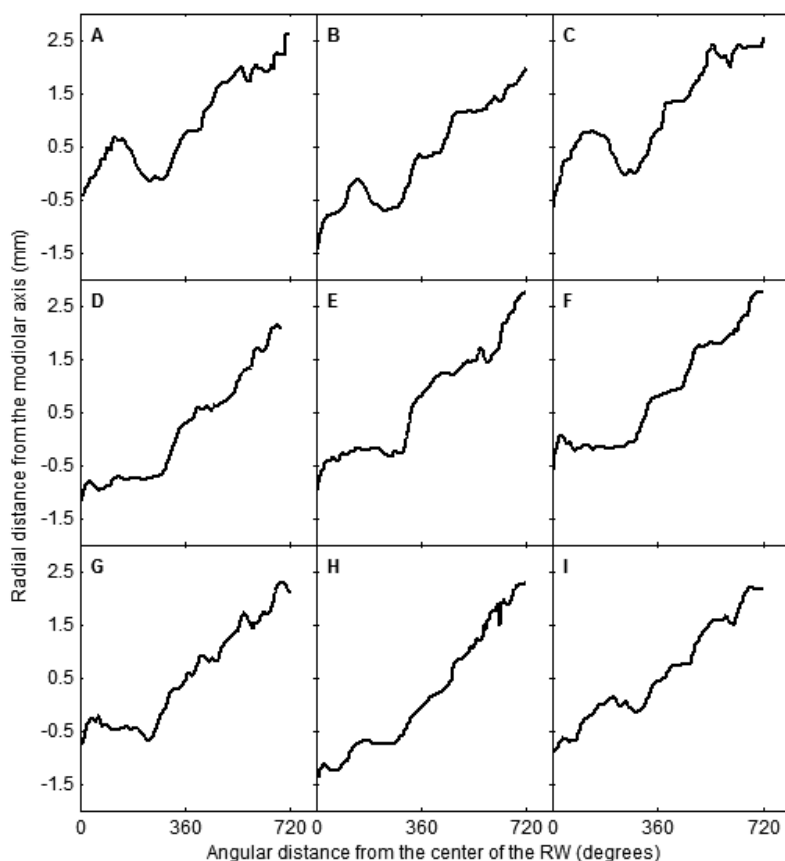


Figure 6: Examples of automatically traced vertical trajectories of the floor of the scala tympani showing a proximal rise and fall within the basal turn (A-C) and late steep rising, with a preceding fall or flat course (D-F) or preceding fall (G) within the first 360 degrees, or a more or less constant rising of the vertical slope (H-I).

Manually versus automatically determined cochlear walls

The outcomes of the manually and automatically determined radial distances are presented in Table 2. Significant differences between them were found for all measurements. For the outer wall at 0, 90, and 180 angular degrees from the RW, radial distances were larger when measured automatically. At 270 degrees, the automatic measurements obtained a smaller radial distance. A smaller radial distance was measured for the first three radii of the inner wall when measurements were performed automatically. The fourth inner wall radius, at 270 degrees, was larger when determined automatically. For both methods the mean paired difference and standard error of the mean increased along the cochlear duct toward the more apical measurements.

Table 2. Manually versus Automatically determined radial distances

Outer wall	Degrees	Manually	Automatically	Mean diff	Std. error mean	p-value	Effect size (Cohen's D)
		Mean (mm), <i>SD</i>	Mean (mm), <i>SD</i>				
1	0	5.60, 0.39	5.62, 0.40	-0.021	0.001	0.037	0.05
2	90	3.96, 0.31	4.01, 0.30	-0.042	0.012	<0.001	0.16
3	180	3.33, 0.29	3.35, 0.30	-0.014	0.012	0.032	0.07
4	270	2.81, 0.29	2.77, 0.27	0.064	0.013	<0.001	0.14
Inner wall							
1	0	3.41, 0.31	3.23, 0.33	0.177	0.009	<0.001	0.58
2	90	2.03, 0.28	1.76, 0.26	0.283	0.012	<0.001	0.96
3	180	1.45, 0.27	1.29, 0.28	0.309	0.014	<0.001	0.59
4	270	0.94, 0.23	0.95, 0.27	0.290	0.013	0.002	0.04



Discussion

This study is the first to measure cochlear morphology *in vivo* up to and including the second turn of the cochlea using an automatic tracing method based on voxel intensity. The greatest number of inner ear measurements is involved for describing the morphological characteristics of the human cochlea. This method allows *in vivo* evaluation of cochlear morphology, providing valuable insight into individual, patient-specific anatomical features and its variability on a large scale.

An important aspect of our study is the inclusion of the second turn of the cochlea to describe cochlear morphology *in vivo*. Although a few studies have reported on the variable dimensions of the second turn *ex vivo*, evaluation of the second turn in clinical practice has been very limited described^{2,3,10–12}. Würfel et al. introduced a methodology to determine individual cochlear length along the complete lateral wall from clinical Cone Beam CT scans, providing an indication of cochlear size. However, the inner walls were not determined in their study and therefore the ability to determine the diameter of the cochlear duct is lacking. Distinction of, particularly, the inner walls beyond the basal turn is challenging because of the increased noise caused by the modiolus. However, including the second turn in the preoperative evaluation may be valuable, as the majority of CI designs have a target insertion depth over 360 degrees. Van der Marel et al. demonstrated a surgical guidance model based on details of cochlear morphology derived from preoperative CT scans¹³. Optimal surgical insertion distance, indicated by the linear distance between the round window and most basal electrode contact, was studied in order to target a specific angular insertion depth. They tested two different methods; the spiral fit and the multiple regression method and found better results with the linear regression model including three input parameters.

The poorer prediction of the spiral fit model was explained by the fact that only the radial distances of the basal turn were available and implemented in the model to fit the spiral. This results in extrapolation from these known values, as the angular insertion depth is frequently located beyond the basal turn. This leads to less accurate estimation of the actual angular insertion depth. Our method allows inclusion of measurements of the second turn in order to hopefully achieve a better spiral fit and improvement of the spiral model for surgical guidance.

Theoretically, the algorithm we described could trace the complete cochlea, but this would likely introduce inaccuracies due to impaired depiction of the third turn. The diameter of the cochlear duct tapers substantially along its course towards the apical region where a mismatch with the diameter of the electrode array may occur ^{1,14-16}. The ability to measure the variability of the cochlear diameter up to 720 degrees on a large scale may be used to predict which cochleas are at risk for traumatic insertions. We showed that this narrowing pattern does not follow a gradual course along 720 degrees. Earlier studies already reported irregular narrowing of the cochlear canal in the first 360 degrees ⁵. A second valuable aspect of our study is the number of measurements used to determine cochlear size and shape. In previous studies, it was common to express the diameter of the cochlea in measurements along two, four, or eight radii ^{5,17,18}. Using 721 assessments, one per angular angle, the tapering course of the cochlear walls can be mapped more accurately.

An interesting outcome of our study was the stable radial distance between approximately 500 and 720 degrees, of both the outer and inner walls. This has not been described previously in the literature, though it was previously noted by Prof. A. Kral at the conference on Cochlear Implants and other Auditory Protheses (CIAP) in July 2015 ¹⁹. The shape of the cochlea is most often described on a logarithmic scale with exponentially decreasing radii ^{5,7}. However, in our study, adding an off-set value to the logarithmic function improved the fit of the cochlear shape to the logarithmic function.

The slope of the vertical trajectory is likely to influence the course of the electrode array and we predict a high risk of damaging the basilar membrane or osseous spiral lamina where the slope shows a steep in- or decrease. Such a decrease is generally present near the confluence of the first and second half of the basal turn, around 180 degrees ^{1,8}. Avci et al. demonstrated the considerable variability in the vertical slope of the cochlea and the impact of cochlear geometry on insertion forces^{1,20}. They studied micro-CT scans of temporal bones and applied a risk profile based on the presence of so-called dips, peaks, and vertical jumps, indicating significant changes in the vertical trajectory¹. Our measurements showed a change in steepness or direction of the slope at four specific locations in the basal turn (Figure 4). Taking the large variability shown in Figure 5 into account, our method allows in

vivo classification of slope characteristics and can be used to estimate the risk of insertion trauma.

Comparing manual and automatic measuring, the outer wall radii at 0, 90, and 180 degrees from the RW are smaller when determined manually, where the inner wall radii are larger at these three locations. Contrarily, the outer and inner wall radii at 270 degrees are smaller and larger, respectively, when manually determined. This finding can be explained by the difference in the voxel density of the aligning structures. Near the inner wall, the soft tissue within the modiolus hampers detection of the contours of the inner wall. The fact that the small differences reach significance for all eight outer and inner wall radii can presumably be explained by the large dataset. All automatically derived measurements are more consistent with micro-CT data from temporal bones ¹. In addition, two other studies, using plastic casts from unselected temporal bone specimen, reported measurements more consistent with our automatically derived measurements for all radii except the large diameter in 1 study^{2,4}. However, our results only demonstrate the differences between the manual and automatic measurement, without the ability to make a ruling which of the two methods approached reality the most. Ideally, a comparison must be made between our measurements, both manually and automatically, and measurements collected from histological preparations, but for obvious reasons this is not possible. However, we believe that the automatically measured ones are more accurate and less susceptible for observer variation because of the use of 180 measurements per cochlear turn instead of 4 and because an objective instead of subjective method is being used.

In this study, the dimensions of the cochlea were determined from automatically traced measurements of the outer and inner wall and the bottom of the ST. Within the cochlear duct, no distinction between ST and scala vestibuli (SV) was made. Previous studies demonstrated that the dimensions of both the ST and SV are not evenly distributed over the cochlear duct, and the shapes of both scalae change along the course ²¹⁻²⁴. Biedron et al. and Wysocki et al showed that the size of the ST is more prominent than the SV during the first half of the basal turn^{23,24}. The diameter of the cochlear duct has been shown to represent the diameter of the ST during this initial trajectory. Subsequently, the SV dominates the ST in size and is the size of the cochlear duct, not representative of the actual dimension of the ST ²⁵. A more distinctive depiction of the osseous spiral lamina is required to define scalar dimensions. Unfortunately, this is not achievable with current in vivo imaging techniques, particularly for the second turn, due to the limited spatial resolution of CT images. MRI may approximate the actual boundaries of the ST more accurately than CT. As CT shows the bony limit of the outer wall, MRI reveals the inner limit of the outer wall at the confluence of the perilymph in the ST to the outer wall. Using MRI may also overcome the challenges associated with measuring the inner wall. Nevertheless, this study was conducted using CT images because pre-operative evaluation of CI candidates is carried out using only CT in



most institutions. In the near future, a study will be conducted in the near future to compare CT and MRI using our method.

Conclusion

In conclusion, the automatic method we introduced here offers an objective way of determining the morphology of the basal and second turn of the cochlea. We demonstrated that the shape of the cochlear duct does not follow a pure logarithmic spiral function. An additional offset value to the function further approximates the true shape of the cochlear duct. The outcomes of our study can be used in a clinical setting as part of the pre-operative evaluation of CI candidates. Our results also provide valuable insight into the variability of individual human cochleas, especially the vertical trajectory and cochlear canal size.

References

1. Avci, E., Nauwelaers, T., Lenarz, T., Hamacher, V. & Kral, A. Variations in microanatomy of the human cochlea. *J. Comp. Neurol.* **522**, 3245–61 (2014).
2. Erixon, E., Högstorp, H., Wadin, K. & Rask-Andersen, H. Variational anatomy of the human cochlea: implications for cochlear implantation. *Otol. Neurotol.* **30**, 14–22 (2009).
3. Rask-Andersen, H. *et al.* Human cochlea: anatomical characteristics and their relevance for cochlear implantation. *Anat. Rec. (Hoboken)*. **295**, 1791–811 (2012).
4. Dimopoulos, P. & Muren, C. Anatomic variations of the cochlea and relations to other temporal bone structures. *Acta radiol.* **31**, 439–444 (1990).
5. van der Marel, K. S. *et al.* Diversity in Cochlear Morphology and Its Influence on Cochlear Implant Electrode Position. *Ear Hear.* 1–12 (2014). doi:10.1097/01.aud.0000436256.06395.63
6. Escudé, B. *et al.* The size of the cochlea and predictions of insertion depth angles for cochlear implant electrodes. *Audiol. Neurootol.* **11 Suppl 1**, 27–33 (2006).
7. Yoo, S. K., Wang, G., Rubinstein, J. T. & Vannier, M. W. Three-dimensional geometric modeling of the cochlea using helico-spiral approximation. *IEEE Trans. Biomed. Eng.* **47**, 1392–402 (2000).
8. Verbist, B. M. *et al.* Anatomic considerations of cochlear morphology and its implications for insertion trauma in cochlear implant surgery. *Otol. Neurotol.* **30**, 471–7 (2009).
9. Verbist, B. M., Finley, C. C., Roland, P. S. & Thomas, J. Consensus panel on a cochlear coordinate system applicable in histological, physiological and radiological studies of the human cochlea. *Otol neurotol* **31**, 722–730 (2011).
10. Bellos, C. *et al.* Reconstruction of cochlea based on micro-CT and histological images of the human inner ear. *Biomed Res. Int.* **2014**, 485783 (2014).
11. Braun, K., Böhnke, F. & Stark, T. Three-dimensional representation of the human cochlea using micro-computed tomography data: presenting an anatomical model for further numerical calculations. *Acta Otolaryngol.* **132**, 603–13 (2012).
12. Würfel, W., Lanfermann, H., Lenarz, T. & Majdani, O. Cochlear length determination using Cone Beam Computed Tomography in a clinical setting. *Hear. Res.* **316**, 65–72 (2014).
13. van der Marel, K. S., Briaire, J. J., Wolterbeek, R., Verbist, B. M. & Frijns, J. H. M. Development of insertion models predicting cochlear implant position (submitted). *Ear Hear.* (2015).
14. Aschendorff, A. *et al.* Main Articles Evaluation of the HiFocus[®] electrode array with positioner in human temporal bones. *J. Laryngol. en Neurotol.* **117**, 527–531 (2003).
15. Eshraghi, A. a, Yang, N. W. & Balkany, T. J. Comparative study of cochlear damage with three perimodiolar electrode designs. *Laryngoscope* **113**, 415–9 (2003).
16. Wardrop, P. *et al.* A temporal bone study of insertion trauma and intracochlear position of cochlear implant electrodes. I: Comparison of Nucleus banded and Nucleus Contour electrodes. *Hear. Res.* **203**, 54–67 (2005).
17. Escudé, B. *et al.* The size of the cochlea and predictions of insertion depth angles for cochlear implant electrodes. *Audiol. Neurootol.* **11 Suppl 1**, 27–33 (2006).



18. Pelliccia, P. *et al.* Cochlea size variability and implications in clinical practice. *Acta Otorhinolaryngol. Ital.* **34**, 42–49 (2014).
19. Kral, A. Towards individualized cochlear implants: variations of the cochlear microanatomy. in *Conference on Implantable Auditory Prostheses (CIAP)* (2015).
20. Avci, E., Nauwelaers, T., Hamacher, V. & Kral, A. Three-Dimensional Force Profile During Cochlear Implantation Depends on Individual Geometry and Insertion Trauma. 168–179 (2017).
21. Zrunek, M., Lischka, M., Hochmair-Desoyer, I. & Burian, K. Dimensions of the scala tympani in relation to the diameters of multichannel electrodes. *Arch. Otorhinolaryngol.* **229**, 159–65 (1980).
22. Rebscher, S. J. Considerations for design of future cochlear implant electrode arrays: Electrode array stiffness, size,. *J. Rehabil. Res. Dev.* **45**, 731–748 (2008).
23. Biedron, S., Prescher, A., Ilgner, J. & Westhofen, M. The internal dimensions of the cochlear scalae with special reference to cochlear electrode insertion trauma. *Otol. Neurotol.* **31**, 731–7 (2010).
24. Wysocki, J. Dimensions of the human vestibular and tympanic scalae. *Hear. Res.* **135**, 39–46 (1999).
25. Verbist, B. *Cochlear imaging in the era of cochlear implantation From silence to sound.* (2009).







Chapter 4

Comparison of the HiFocus
Mid-Scala and HiFocus 1J
electrode array; angular
insertion depths and
speech perception
outcomes

MA van der Jagt, JJ Briaire,
BM Verbist, JHM Frijns

Published in Audiology and Neurotology, 2016

Abstract

Recently the HiFocus Mid-Scala (MS) electrode array has been introduced onto the market. This pre-curved design with targeted mid-scalar intra-cochlear position pursues an atraumatic insertion and optimal distance for neural stimulation. In this study we prospectively examined the angular insertion depth achieved by and speech perception outcomes, till 6 months after implantation, resulting from the HiFocus MS electrode array and retrospectively compared these with the HiFocus 1J lateral wall electrode array. The mean angular insertion depth within the MS population ($n = 96$) was found at 470 degrees, 50 degrees shallower, but more consistent compared to the 1J electrode array ($n = 110$). Audiological evaluation within a subgroup including only post lingual, unilaterally implanted, adult CI recipients who were matched on preoperative speech perception scores and duration of deafness ($MS = 32$, $1J = 32$), showed no difference in speech perception outcomes between the MS and 1J population. Furthermore, speech perception outcome was not affected by angular insertion depth or frequency mismatch.

Introduction

The capability of cochlear implants has dramatically evolved through developments in speech processing strategies, surgical techniques and electrode designs. These advances have led to major improvements in cochlear implant (CI) recipients' performance, although a great variability in outcome still exists. Multiple patient, implant and surgery related factors are proposed as contributing to this variability. These include duration of deafness, insertion depth, distance from the electrode contacts to the modiolus, scalar location and intra-cochlear trauma following insertion [Finley, and Skinner, 2008; Hughes, and Abbas, 2006; Adunka, and Kiefer, 2006; Holden et al., 2013]. Driven by the goal to further improve speech intelligibility of cochlear implant recipients, atraumatic surgery became an important aim as injury to intra-cochlear structures during insertion provokes a range of changes, leading to fibrosis, ossification and neural tissue loss [Carlson et al., 2011; James et al., 2005]. These changes, in turn, may inhibit the signal transmission by the CI. In addition, the degree of trauma is found to be heavily associated with the loss of residual hearing and clinical outcome [Adunka, and Kiefer, 2006; Gstoettner et al., 1997; Choi, and Oghalai, 2005; Carlson et al., 2011]. Therefore, implant features committed to reduce intra-cochlear damage, are being developed continually and are translated into advanced electrode array designs.

Such translation is found in the recently launched HiFocus Mid-Scala (MS) electrode array (Advanced Bionics, Valencia, CA). This implant design offers the smallest pre-curved design targeting a mid-scalar position. These features, together with the possibility of a round window (RW) insertion aim to support atraumatic surgery by avoidance of forces against the cochlear walls during insertion. In addition, a more ideal distance between the electrode contacts and the auditory neurons is aimed for with the targeted mid-scalar position. Earlier research has shown lower auditory brainstem response (ABR) thresholds in the case of a closer position of the array to the modiolus [Wackym et al., 2004; Pasanisi et al., 2002; Shepherd et al., 1993]. This results in the need for less current and in a more focused stimulation. To approximate this position, pre-curved arrays and positioners were developed. However, when the array is positioned along the inner cochlear wall, as in perimodiolar designs, the occurrence of cross-turn stimulation via the modiolus at the level of the 2nd or 3rd turn was demonstrated by Frijns et al. [Frijns et al., 2001; Wanna, George BGifford et al., 2014]. This suggests that anatomical difference between the basal and more upper turns requires a different approach to electrical stimulation [Frijns et al., 2001]. Their model predicts that a more approximate position of the basal electrode contacts leads to reduced current thresholds while retaining a good dynamic range, the difference between threshold and comfortable levels, and spatial selectivity. This hypothesis is translated into the geometry of the MS electrode array. Besides different intra-scalar position, differences in geometry of electrode arrays might also influence insertion depth. Combined with array



length, this determines the range of stimulated frequencies. It is shown in earlier studies that deeply inserted electrode arrays results in increased intra-cochlear trauma and the loss in residual hearing[Adunka et al., 2006], limited stimulation of the basal frequencies[Finley, and Skinner, 2008] and confusion of the apical pitch due to neural interaction of the more densely located neural fibers in the apical regions in the cochlea[Gani et al., 2007]. On the other hand, other studies show that stimulation of the lower frequencies in the apical region of the cochlea are related to better speech perception outcomes[Hochmair et al., 2003; Yukawa et al., 2004], increased range of place pitches by stimulating a larger number of neural fibers[Landsberger, 2016], or reduced mismatch between the predicted and default frequencies by a further approximation of the normal frequency to place function of the cochlea[Landsberger et al., 2015]. Another study also showed that deeper inserted electrode arrays are not associated with scalar translocations[Wanna, George BGifford et al., 2014]. As a result of these divergent outcomes, and the use of different designs and sizes of electrode arrays in the discussed studies, the optimal insertion depth remains unclear.

Given the recent introduction of the HiFocus MS electrode array, studies reporting on speech perception outcome using this device are lacking. The aim of this present study was to report on the clinical outcomes of the new MS electrode array in terms of speech perception and angular insertion depth. To create a referential framework, these outcomes will be presented next to the outcomes of the HiFocus 1J electrode array.

Material and Methods

Patient population

For the evaluation angular insertion depth

Since the first implantation of the MS electrode array in June 2012, till October 2014, 96 patients with normal cochlear morphology were consecutively implanted with this CI electrode array design and were included to study angular insertion depth. For comparison, a similar-sized cohort of the last patients implanted with the 1J electrode was created by selecting all consecutively implanted 1J recipients from a partly overlapping period, viz. January 2010 till October 2014. This was considered to create groups with the least differences in selection criteria, surgical procedure, (experience of) surgeons and rehabilitation. This group counted 110 patients. Demographic characteristics of this patient population are described in table 1.

Table 1. Demographic characteristics

Total population (N = 206)		N = 96	N = 110	
Age at implantation	Mean, SD (years)	38.8, 29.2	47.4, 25.1	$p = 0.026$
Duration of deafness	Mean, SD (years)	16.0, 16.9	28.0, 20.5	$p = 0.001$
Preoperative phoneme scores*	Mean, SD (% correct)	48, 22	32, 23	$p < 0.001$
Population for speech perception analysis (N = 100)		N = 52	N = 48	
Age at implantation	Mean, SD (years)	61.6, 15.8	64.8, 11.9	<i>NS</i>
Duration of deafness	Mean, SD (years)	12.3, 12.3	24.8, 16.6	$p < 0.001$
Preoperative phoneme scores*	Mean, SD (% correct)	53.7, 19.6	40.7, 21.4	$P = 0.005$
Matched population for speech perception analysis (N = 64)		N = 32	N = 32	
Age at implantation	Mean, SD (years)	59.6, 17.4	64.9, 14.0	<i>NS</i>
Duration of deafness	Mean, SD (years)	13.9, 13.0	17.7, 13.8	<i>NS</i>
Preoperative phoneme scores*	Mean, SD (% correct)	52, 20	43, 20	<i>NS</i>

* Using a standard Dutch speech audiometric test of the Dutch Society of Audiology, consisting of phonetically balanced monosyllabic (CVC) phoneme lists.²²

For the evaluation of speech perception outcome

Evaluation of speech perception outcomes was performed within a subgroup including 100 post lingual, adult CI recipients whom were unilaterally implanted. Reimplanted patients were excluded from the analysis. As shown in Table 1, initially significant differences in preoperative speech perception and duration of deafness were present between the MS and 1J population. An explanation for these differences are the expanding implant criteria in our centre, evolved over the past few years, coinciding with a change of standard array for implantation from 1J to MS since 2013. To limit differences in demographic characteristics that might affect speech perception, the MS and 1J population were matched on duration of deafness, age at implantation and preoperative phoneme scores. This resulted in two groups of 32 patients. It should be noted that not all patients data at all follow-up measurements were available. Demographic characteristics of this subpopulation are specified in table 1. All patients participated in the standard intense rehabilitation procedure [van der Beek et al., 2005].

Electrode designs

The MS electrode array was launched in 2013 and includes a pre-curved array designed for mid-scalar position. It contains 16 electrode contacts arranged on a 0.9 mm pitch. The dimensions of each contact surface are 0.43 by 0.39 mm. The total length of the array from basal contact to the tip is 15.0 mm. The distance from tip to the proximal blue marker that indicates a full insertion is 18 mm. The cross-sectional diameter varies from approximately 0.5 mm at the most apical contact to approximately 0.7 mm at the most basal contact. In



this study, all MS insertions were performed using the insertion tool, which comes with the implant. Either a pure round window (RW, n = 30) or extended RW (n = 65) insertion was performed. In case of an extended round window approach the RW is enlarged in anterior-inferior direction. Information about the surgical approach is extracted from surgical procedure reports.

The 1J electrode array, introduced in 2003, is a less pre-curved array, designed for outer wall positioning. It contains 16 electrode contacts, spaced 1.1 mm apart, leading to a total length of the array from basal contact to the tip of 17 mm. There is an additional 3 mm length from the most basal contact to the marker contact, indicating a full insertion is 20 mm. The dimensions of each contact surface are 0.5 by 0.4 mm. The cross-sectional diameter of the array varies from approximately 0.4 mm at the most apical contact to approximately 0.8 mm at the most basal contact. All 1J electrode arrays were implanted through an extended RW approach, as the dimension of this design is not compatible with a pure RW approach. Electronic functionality is identical for both devices.

Radiological evaluation

All 206 patients underwent pre- and post-operative MSCT scans (Aquilion; Toshiba Medical Systems, Otowara, Japan) according the standard work-up for cochlear implant patients at our institution. Subsequently multiplanar reconstructions (MPRs) were made from these scans [Verbist et al., 2005]. To study angular insertion depths, MPRs from each patient were analysed by applying a three-dimensional coordinate system as described by Verbist et al. [Verbist et al., 2010]. Based on this coordinate system, the angular location of the RW was determined at the pre-operative CT scan and applied to the post-operative CT scan. Subsequently, the angle of the most apical electrode was defined as the angular insertion depth. The angular depth of all contacts in the array was used to calculate the frequency mismatch as described in detail in two earlier studies [van der Marel et al., 2015][Kalkman et al., 2014]. This mismatch indicates the difference between the frequency-to-place map as programmed in the implant system and the actual pitch associated with the electrode contact position, derived from the angular depth of each electrode contact, according to the tonotopical organization of the nerve fibers as described by Greenwood et al., combined with histological data from Stakhovskaya et al. [Greenwood, 1990][Stakhovskaya et al., 2007]. The overall frequency mismatch (ΔF) in each patient in semitones (equal to a twelfth of an octaves) was obtained by calculating the difference (Δf_i) between $f_{MF}(i)$ and $f_{SG}(\theta_i)$ in semitones with:

$$\Delta f_i = 12 \times {}^2\log f_{MF}(i) - 12 \times {}^2\log f_{SG}(\theta_i),$$

In this formula, $f_{MF}(i)$ represents the center frequencies obtained from the filter map assigned to the implant's channel by the manufacturer, for each contact number i (1 through 16). The predicted place pitch at the spiral ganglion for each electrode contact i , based on their angular position is indicated by $(f_{SG}(\theta_i))$. From this, the root mean square (RMS) is calculated with:

$$\Delta F = \sqrt{\frac{1}{N} \sum_{i=1}^N \Delta f_i^2}$$

These calculations were carried out by an in-house designed post-processing program written in Matlab (Mathworks, Novi, MI, USA). Also the number of electrode contacts that are active in the map are incorporated in the calculation of the degree of mismatch. The Matlab program was also used to assess the distance of each electrode contact to the inner wall, to the center of the modiolus, and to assess cochlear size. For this last purpose, the outer and inner wall distances to the center of the modiolus along 4 radial lines were measured. The accumulated radial distances at 0 and 180 degrees from the center of the RW indicate the largest cochlear diameter, named diameter A. The accumulated radial distances at 90 and 270 degrees from the RW indicate the smaller diameter, named diameter B [Escudé et al., 2006].

Evaluation of speech perception

Speech perception was assessed using the standard Dutch speech test of the Dutch Society of Audiology. Four lists of 11 monosyllabic (CVC) words were administered per speech level and the number of phonemes and words correct was determined. Patients were tested in quiet at speech levels of 65 and 75 dB SPL, over which the average score was calculated and used for analysis. When the average phoneme score in quiet was higher than 50%, patients were also tested in noise at a speech level of 65 dB. Speech scores in noise were assessed at a signal to noise ratio (SNR) of +10 dB and +5 dB. The assessments took place 1 week, 2 weeks, 1 month, 3 and 6 months after implantation. Speech scores in noise at 6 months after implantation are presented in our study. Table 2 shows the number of patients available per assessment.



Table 2. Number of patients available per follow-up measurement in quiet and both noise conditions.

	1 week	2 weeks	1 month	3 months	6 months
Phonemes MS					
Quiet	32	31	32	31	28
Noise +10 dB			27	27	27
Noise +5 dB			23	25	24
Phonemes 1J					
Quiet	32	32	31	30	25
Noise +10 dB			22	28	24
Noise +5 dB			20	24	21
Words MS					
Quiet	31	30	31	30	27
Noise +10 dB			26	26	26
Noise +5 dB			22	24	24
Words 1J					
Quiet	32	32	31	30	25
Noise +10 dB			22	28	24
Noise +5 dB			20	24	21

Statistical analysis

Statistical analyses were performed using SPSS (version 20, IBM, Armonk, New York). To study the difference in angular insertion depth between the MS and 1J population, an independent T-test was used. Subsequently, a linear mixed model analysis was used that incorporates the effect of cochlear size as possible factors of influence on the depth of insertion. The effect of surgical approach on angular insertion depth in the MS population was studied using an independent T-test. To study the difference in angular depth and distance to the inner wall of each individual electrode contact an independent T-test was used. For the analysis of speech perception at 5 (in silence) and 1 (in noise) phoneme and word measurements post implantation, the MS and 1J population were matched on duration of deafness and preoperative speech perception scores. The differences in phonemes and words, both in silence and in noise, were studied with an independent T-test. Eventually, a linear mixed model was used to study the individual and possibly combined effects of (1) implant design, (2) angular insertion depth, (3) frequency mismatch (4) age at implantation (5) preoperative speech perception scores and (6) duration of deafness on speech perception outcome within the matched population. A p-value < 0.05 was considered to indicate a statistically significant difference.

Results

Angular insertion depth

Figure 1 shows the distribution of the angular insertion depth in the two groups. The 96 MS patients showed a mean angular insertion depth of 422° with a standard deviation of 29°. The 110 1J patients showed a mean angular insertion depth of 478°, with a larger standard deviation of 66°. The 56° shallower angular insertion depth and 37° smaller standard deviation of the MS electrode array represent significant differences with the 1J population, both with a p-value < 0.001. The shallower insertion depth and narrower distribution of the pre-curved HiFocus MS array is clearly visible in Figure 1. The mean angular insertion depth within the matched population was 424° (SD 24°) for the MS and 469° (SD 69°) for the 1J recipients (p < 0.001).

Surgical approach, either a pure or extended round window approach, did not influence angular insertion depth of the MS population (p = NS). Cochlear size did have a significant effect on angular insertion depth in the 1J population only. An increase of 1 mm of diameter A, results in a shallower angular insertion depth of 44° (p = 0.010). Insertion depth in the MS population was not affected by cochlear size (p = NS).

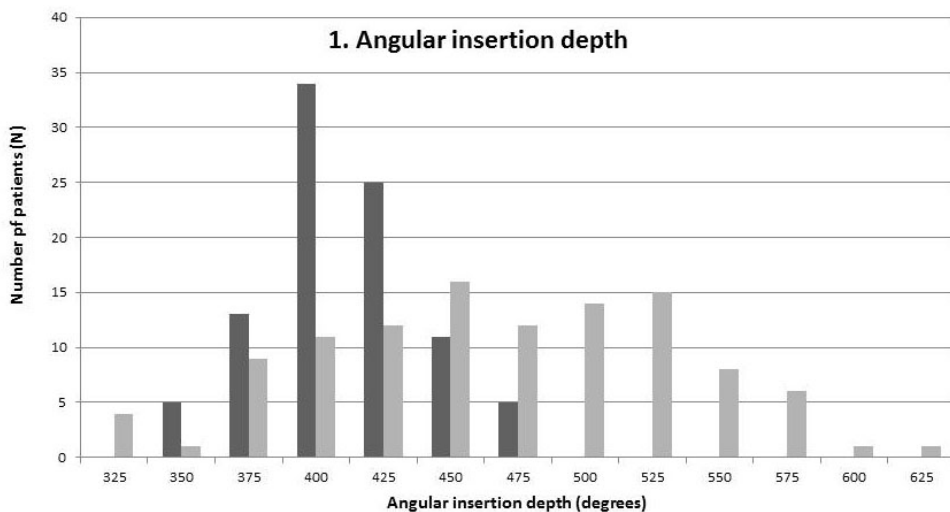


Figure 1. Angular insertion depth of the HiFocus MS (dark grey, n = 96) and HiFocus 1J (light grey, n = 110) and groups.

Intra-cochlear position

Figure 2A shows the mean angular depths of each individual electrode contact of the MS (dark grey) and 1J (light grey) electrode arrays. For each electrode contact the angular depth is significantly different between the MS and 1J electrode arrays (all p < 0.001). Figure 2B shows the mean distance from the electrode contacts to the inner wall for the MS (dark grey) and 1J (light grey) electrode array. The distance of electrode contact 8 and 7 were not

significant different from each other, the distances of all the other contacts were (p -value ranged from <0.001 till 0.008). Figure 2C is shown to illustrate the difference in intra-cochlear position in terms of angular depth and distance to the inner wall and center of the modiolus of each individual electrode contact. It is shown that the basal electrode contacts of the MS electrode array cover higher frequencies compared to the 1J electrode array and are positioned in close proximity with the inner wall at the basal region.

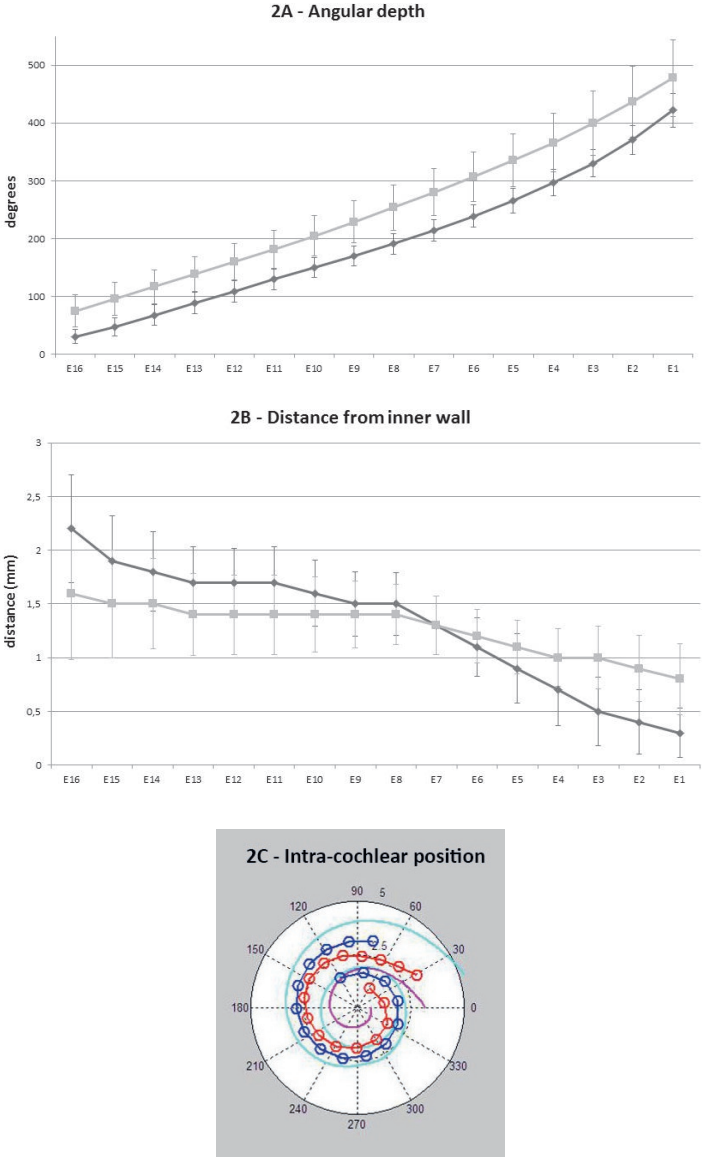


Figure 2A: Mean angular distance from each electrode contact (horizontal axis) for the HiFocus MS (dark grey) and HiFocus 1J (light grey) groups.

Figure 2B: Mean radial distance from each electrode contact (horizontal axis) to the inner wall for the HiFocus MS (dark grey) and HiFocus 1J (light grey) groups.

Figure 2C: The intra-cochlear position of the HiFocus MS (red) and HiFocus 1J (blue) electrode array, displayed within the outer (light blue) and inner (pink) wall of an average sized cochlea.

Frequency mismatch

Figure 3 shows the frequency mismatch in semitones plotted against the corresponding angular insertion depth of each individual patient. The mean frequency mismatch (ΔF) of the MS population of 10.3 semitones (SD 2.2) is significantly ($p < 0.001$) higher than in the 1J population which shows a frequency mismatch of 4.8 semitones (SD 3.0). It is clearly demonstrated that the higher frequency mismatch of the MS population is related to the shallower insertion observed with the MS electrode array. Within the matched population the mean frequency mismatch in the MS population is 9.58 semitones (SD 1.95). In the 1J population the mean frequency mismatch is 5.23 (SD 3.17) ($p < 0.001$).

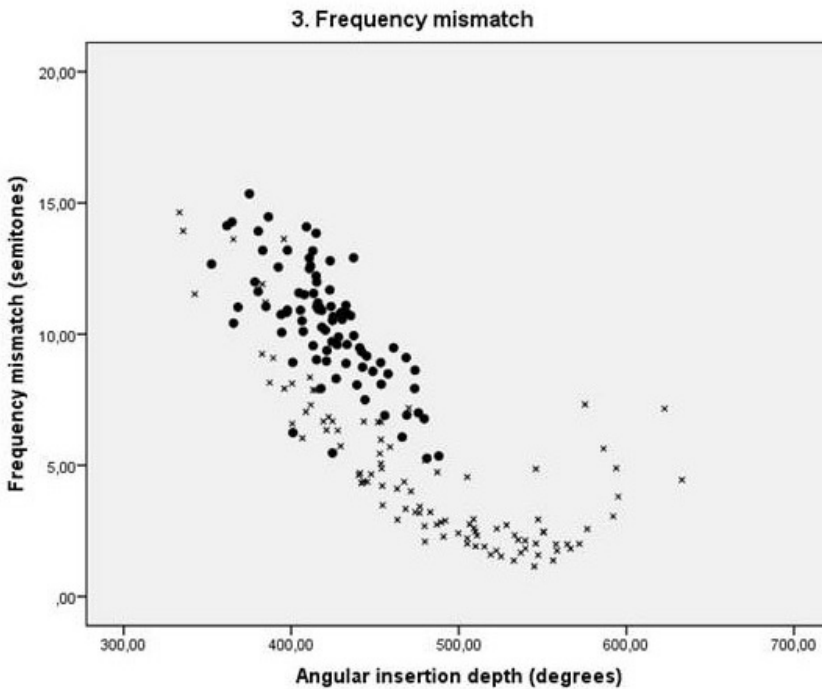


Figure 3. Frequency mismatch in semitones plotted against angular insertion depth of the HiFocus MS (dots) and HiFocus 1J (crosses) groups.

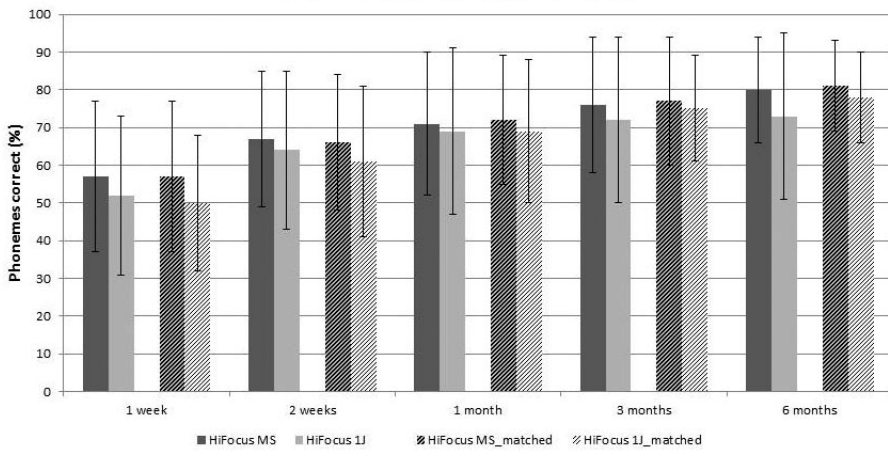
Speech perception scores

The results from the evaluation of speech perception at 5 intervals after implantation is showed in Figure 4. The bars in Figure 4A show the mean phoneme scores in quiet of both the unmatched (plain) and matched (shaded) MS and 1J population. In Figure 4B the mean

word scores in quiet are presented of both the unmatched (plain) and matched (shaded) population. The scores of the unmatched population are presented to show the results as clinically represented in our population of implanted patients. The scores of the matched group are used for statistical analysis. During the follow-up period, both groups show an increase in performance on the speech tests. Although there is a tendency for higher scores with the MS group, no significant difference in speech perception at all 10 measurements is present between the two groups. Figure 5 shows the phoneme and word scores after 6 months in quiet and in +10 and +5 dB SNR test conditions. No significant difference in phoneme or word scores at 6 months in quiet and at +10 dB and +5 dB SNR were found.

To evaluate the effect of implant design, angular insertion depth and frequency mismatch on speech perception in the matched groups, a linear mixed model analysis was performed. Additional factors that were included in the model are preoperative speech perception scores, age at implantation and duration of deafness. Implant design, angular insertion depth, frequency mismatch and age at implantation showed no significant effect on final speech perception outcomes. However, both preoperative speech perception score ($p = 0.002$) and duration of deafness ($p < 0.001$) did significantly affect speech perception outcome. For each increased percentage preoperative phoneme score, the speech perception outcome after implantation, corrected for all repeated measurements in both silence and noise, was increased by 0.16%. For each additional year in duration of deafness, the speech perception outcome score was 0.40% lower.

4.A Speech perception (phonemes)



4.B Speech perception (words)

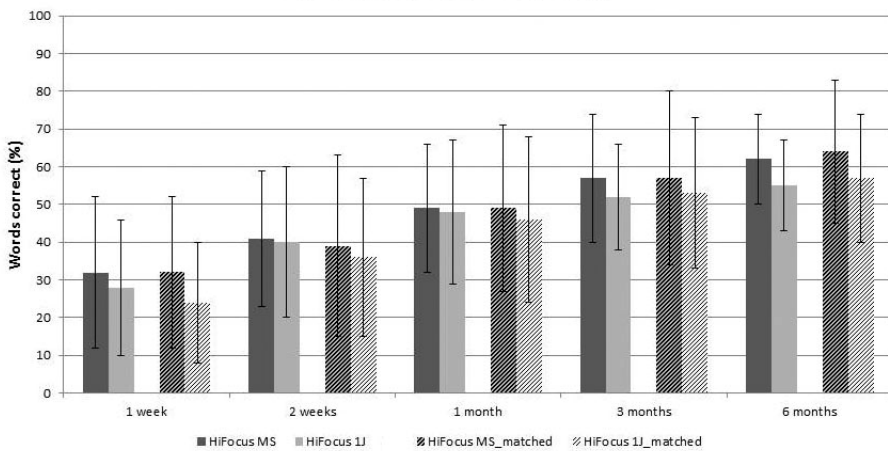


Figure 4A: Mean phoneme scores at 5 follow-up intervals after implantation for the HiFocus MS (dark grey) and HiFocus 1J (light grey). The scores of the unmatched group is presented as plain bars and the scores of the matched group is presented as shaded bars.

Figure 4B: Mean word scores at 5 follow-up intervals after implantation for the HiFocus MS (dark grey) and HiFocus 1J (light grey). The scores of the unmatched group is presented as plain bars and the scores of the matched group is presented as shaded bars.

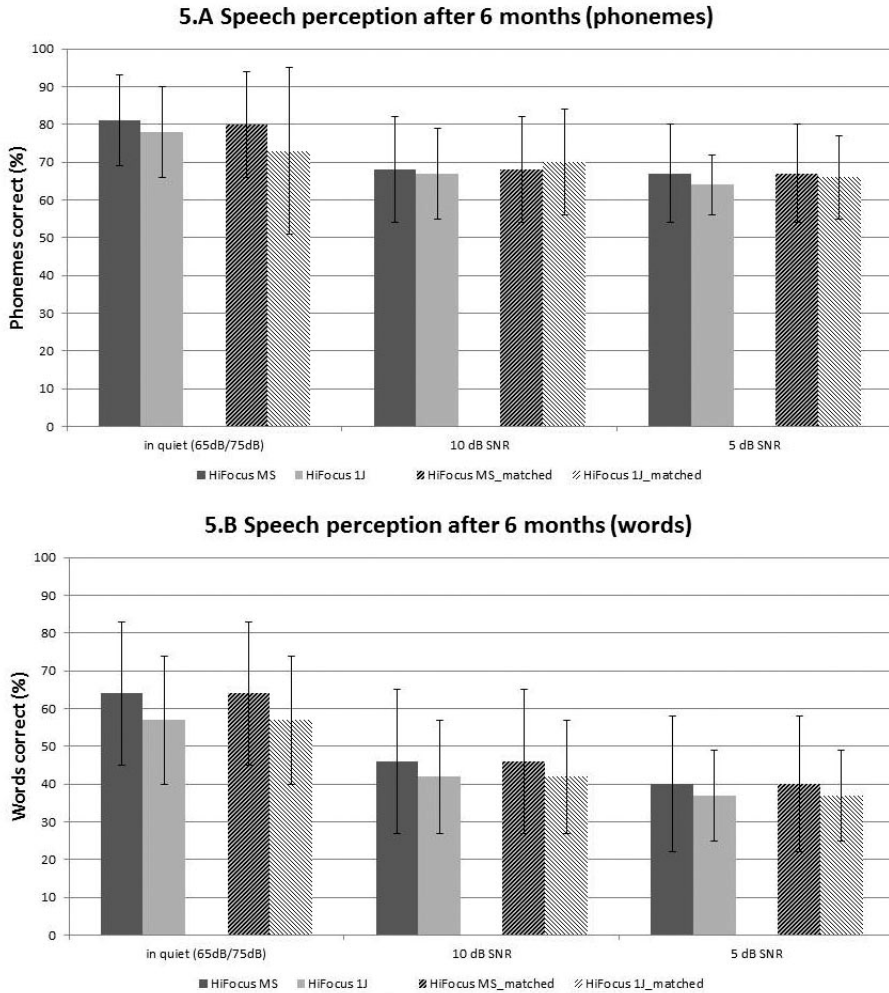


Figure 5A: Mean phoneme scores at 6 months after implantation in quiet, and at +10 dB SNR and +5 dB SNR noise conditions.

Figure 5B: Mean word scores at 6 months after implantation in quiet, and at +10 dB SNR and +5 dB SNR noise conditions.

Discussion

This study is the first to report on the clinical outcome of the new precurved HiFocus MS electrode array. Results regarding angular insertion depth and speech perception outcomes up until 6 months after implantation are reported and set against outcomes of the straight HiFocus 1J electrode array. Our study found a shallower but more consistent angular insertion depth for the MS implanted patients, resulting in a larger frequency mismatch. In addition, cochlear size and surgical approach did not affect angular insertion depth in the MS



population. Speech perception outcomes were studied in two groups matched on duration of deafness and preoperative speech perception scores. This analysis showed that up till 6 months after implantation, the population implanted with an MS electrode array performs similarly to the 1J population, however, there is a trend toward better performance within the MS population. Additionally, a linear mixed model analysis showed that neither angular insertion depth, frequency mismatch or electrode design affected speech performance outcome. The baseline parameters duration of deafness and preoperative phoneme scores turned both out to significantly affect speech perception outcomes, corroborating findings in previous research [Holden et al., 2013; Rubinstein et al., 1999; Blamey, and Arndt, 1996; Green et al., 2007].

Two earlier studies on the MS electrode array are published, showing similar angular insertion depths. One includes a temporal bone study by Hassepass et al., where they analyzed angular insertion depth and intra-cochlear trauma using rotational tomography for the MS electrode array in 20 temporal bones [Hassepass et al., 2014]. A mean angular insertion depth of 406° from the center of the RW was reported. Atraumatic insertion (Grade 0 trauma) was shown in 18 of 19 scala tympani (ST) inserted temporal bones: less trauma than reported in previous temporal bone studies [Rebscher et al., 2008; Wardrop et al., 2005]. A second temporal bone study by Frisch et al. investigated implant position and depth of insertion using micro-CT in 8 temporal bones [Frisch et al., 2015]. A mean angular insertion depth of 429.6° was reported, with 1 implant (12.5%) showing a translocation to the scala vestibuli. This last study distinguished between insertions through the RW or a cochleostomy, showing a deeper insertions with RW insertions. In our population, either a pure or extended RW approach was used. Between these two approaches, no significant difference in angular insertion depth was found.

Previous studies focusing on insertion depth alone and in relation to speech perception outcomes show conflicting results. Consistent with our results, no correlation between insertion depth and speech perception outcome was reported by Van der Marel et al. who studied the effect of multiple variables related to implant position in a group of 203 patients who received an AB cochlear implant [Marel et al., 2015]. In accordance with our finding of the lack of a correlation between angular insertion depth and speech perception outcomes, Finley et al. reported no correlation between the angular insertion depth of the apical electrode and speech perception in 14 AB CI-recipients. Nevertheless, they did find a correlation between angular insertion depth of the most basal electrode and speech perception. However, this was no longer significant after controlling for age, probably due to their limited population size [Finley, and Skinner, 2008]. Skinner et al. did find a correlation between insertion depth and word scores, but the average depth of insertion for that group of Nucleus-22 recipients was 333 degrees, significantly shallower compared to our population. [Skinner et al., 2002]. Their results show that very shallow insertions hinder

speech recognition, whereas, insertions in which all electrodes are inserted into the cochlea or insertions that are to the intended design depth of the array, benefit speech recognition. Furthermore, Holden et al. did not find correlation between speech perception and angular insertion depth of the most apical electrode in a group of 144 CI patients, of whom 19 received an Advanced Bionics CI system [Holden et al., 2013]. However, the angular depth of the most basal electrode was significantly correlated to performance in this study. They state that the most basal electrode position is the best descriptor of the degree of over insertion and is therefore more reliable to study the correlation between performance and angular insertion depth. Yukawa et al. used multiple regression analysis to investigate the effect of insertion depth on speech perception in 26 patients implanted with a Nucleus-22 or Nucleus-24 CI with a straight array and indicated insertion depth as a positive predictive value for speech perception [Yukawa et al., 2004]. They used Cohen's method on a modified Stenver's view radiograph [Cohen et al., 1996], and reported also shallower insertions compared to our population, with their mean angular depth being 357.7 (SD 63.2).

We demonstrated that the angular insertion depth of the MS electrode array is relatively constant and less susceptible to variations in cochlear dimensions. Perhaps also contributing to this increased stability is the use of the tool which increases the control over the basal electrode contacts. With the HiFocus 1J, almost 80% of angular insertion depth variance can be predicted by surgical insertion distance [van der Marel et al., 2015]. Due to the precurved design, electrode migration is also expected to be less likely to occur [van der Marel et al., 2012]. Nevertheless, one patient implanted with an MS electrode array was rescanned due to a drop in performance (from 93% to 71% phonemes correct) accompanied by increasing T-levels for the basal electrodes (average increase of 30 current units (CU)). The new scan showed a retraction of approximately 4 mm, corresponding to 50 angular degrees, slightly over 3 electrode contact distances. Despite this retraction, all active contacts were in an intra-cochlear position, and performance could partially be restored by reprogramming the device. This patient is the only one of approximately 130 patients implanted with an MS electrode array in our institution with this finding. A previous study carried out by Van der Marel et al. described a migration rate of 29% (10/35) in patients implanted with a HiFocus 1 or HiFocus 1J array, of whom 2 experienced a drop in speech perception [van der Marel et al., 2012]. A more recent study of Mittman et al., studying electrode migration of perimodiolar electrode arrays, showed a migration rate of 26% (7/27) [Mittmann et al., 2015]. This migrational behaviour might obscure the correlation analysis on insertion depth and speech perception outcome, as insertion depth at the moment of evaluating speech perception could potentially be more shallow than calculated from the postoperative CT-scan obtained 1 day after implantation.

In summary, this first report on the clinical outcome of the HiFocus Mid-Scala electrode array shows favourable speech perception outcomes comparable to patients implanted

with a 1J electrode array, despite significant differences in angular insertion depth and related increased frequency mismatch. We found that the angular insertion depth is more consistent with the MS electrode array and that insertion depth in the MS population was not affected by cochlear size, contrarily to the 1J population, or surgical approach. In other words, differences in electrode design and related intra-cochlear position did not have an effect on the performance of CI recipients. Perhaps, inherent limitations of electrical stimulation might restrict improving speech perception after cochlear implantation. Further improvements of technical capabilities, or different techniques such as injection of neural growths, might potentially push the ability of CI systems further towards optimal hearing rehabilitation.



References

1. Finley CC, Skinner MW: Role of electrode placement as a contributor to variability in cochlear implant outcomes. *Otol Neurotol* 2008;29:920–928.
2. Hughes ML, Abbas PJ: Electrophysiologic channel interaction, electrode pitch ranking, and behavioral threshold in straight versus perimodiolar cochlear implant electrode arrays. *J Acoust Soc Am* 2006;119:1538.
3. Adunka O, Kiefer J: Impact of electrode insertion depth on intracochlear trauma. *Otolaryngol Head Neck Surg* 2006 Sep;135:374–82.
4. Holden LK, Finley CC, Firszt JB, Holden T a, Brenner C, Potts LG, et al.: Factors affecting open-set word recognition in adults with cochlear implants. *Ear Hear* 2013;34:342–60.
5. Carlson ML, Driscoll CLW, Gifford RH, Service GJ, Tombers NM, Hughes-Borst BJ, et al.: Implications of minimizing trauma during conventional cochlear implantation. *Otol Neurotol* 2011 Aug;32:962–8.
6. James C, Albegger K, Battmer R, Burdo S, Deggouj N, Deguine O, et al.: Preservation of residual hearing with cochlear implantation: How and why. *Acta Otolaryngol* 2005 May;125:481–491.
7. Gstoettner W, Plenk H, Franz P, Hamzavi J, Baumgartner W, Czerny C, et al.: Cochlear implant deep electrode insertion: extent of insertional trauma. *Acta Otolaryngol* 1997 Mar;117:274–7.
8. Choi C-H, Oghalai JS: Predicting the effect of post-implant cochlear fibrosis on residual hearing. *Hear Res* 2005 Jul;205:193–200.
9. Wackym PA, Firszt JB, Gaggl W, Runge-samuelson CL, Reeder RM, Raulie JC: Electrophysiologic Effects of Placing Cochlear Implant Electrodes in a Perimodiolar Position in Young Children. *Laryngoscope* 2004;114:71–76.
10. Pasanisi E, Vincenti V, Bacciu A, Guida M, Bacciu S, Hypothesis O: The Nucleus Contour Electrode Array : An Electrophysiological Study. *Laryngoscope* 2002;1653–1656.
11. Shepherd RK, Hatsushika S, Clark GM: Electrical stimulation of the auditory nerve: the effect of electrode position on neural excitation. *Hear Res* 1993 Mar;66:108–20.
12. Frijns JH, Briaire JJ, Grote JJ: The importance of human cochlear anatomy for the results of modiolus-hugging multichannel cochlear implants. *Otol Neurotol* 2001 May;22:340–9.
13. Wanna, George BGifford H, Noble JH, Carlson ML, Dietrich MS, Haynes DS, Dawant BM, et al.: Impact of Electrode Design and Surgical Approach on Scalar Location and Cochlear Implant Outcomes. *Laryngoscope* 2014;124:1–7.
14. Adunka OF, Pillsbury HC, Kiefer J: Combining perimodiolar electrode placement and atraumatic insertion properties in cochlear implantation -- fact or fantasy? *Acta Otolaryngol* 2006 May;126:475–82.
15. Gani M, Valentini G, Sigrist A, Kós M-I, Boëx C: Implications of deep electrode insertion on cochlear implant fitting. *J Assoc Res Otolaryngol* 2007 Mar;8:69–83.
16. Hochmair I, Arnold W, Nopp P, Jolly C, Müller J, Roland P: Deep electrode insertion in cochlear implants: apical morphology, electrodes and speech perception results. [Internet]. . *Acta Otolaryngol* 2003 Jun;123:612–7.



17. Yukawa K, Cohen L, Blamey P, Pyman B, Tungvachirakul V, O'Leary S: Effects of insertion depth of cochlear implant electrodes upon speech perception. *Audiol Neurootol* 2004;9:163–72.
18. Landsberger DM: Perceptual changes in place of stimulation with long cochlear implant electrode arrays 2016;135:75–81.
19. Landsberger DM, Svrakic M, Roland JT, Svirsky M: The Relationship Between Insertion Angles , Default Frequency Allocations , and Spiral Ganglion Place Pitch in Cochlear Implants 2015;
20. Van der Beek FB, Boermans PPBM, Verbist BM, Briaire JJ, Frijns JHM: Clinical evaluation of the Clarion CII HiFocus 1 with and without positioner. *Ear Hear* 2005 Dec;26:577–92.
21. Verbist BM, Frijns JHM, Geleijns J, van Buchem M a: Multisection CT as a valuable tool in the postoperative assessment of cochlear implant patients. *AJNR Am J Neuroradiol* 2005 Feb;26:424–9.
22. Verbist BM, Joemai RMS, Briaire JJ, Teeuwisse WM, Veldkamp WJH, Frijns JHM: Cochlear coordinates in regard to cochlear implantation: a clinically individually applicable 3 dimensional CT-based method. *Otol Neurotol* 2010 Jul;31:738–44.
23. Van der Marel KS, Briaire JJ, Wolterbeek R, Verbist BM, Frijns JHM: Development of insertion models predicting cochlear implant position (accepted). *Ear Hear* 2015;
24. Kalkman RK, Briaire JJ, Dekker DMT, Frijns JHM: Place pitch versus electrode location in a realistic computational model of the implanted human cochlea. *Hear Res* 2014 Sep;315:10–24.
25. Greenwood DD: A cochlear frequency-position function for several species--29 years later. *J Acoust Soc Am* 1990 Jun;87:2592–605.
26. Stakhovskaya O, Sridhar D, Bonham BH, Leake P a: Frequency map for the human cochlear spiral ganglion: implications for cochlear implants. *J Assoc Res Otolaryngol* 2007 Jun;8:220–33.
27. Escudé B, James C, Deguine O, Cochard N, Eter E, Fraysse B: The size of the cochlea and predictions of insertion depth angles for cochlear implant electrodes. *Audiol Neurootol* 2006 Jan;11 Suppl 1:27–33.
28. Rubinstein JT, Parkinson WS, Tyler RS, Gantz BJ: Residual speech recognition and cochlear implant performance effects of implantation criteria. *Am J Otol* 1999;20:445–452.
29. Blamey P, Arndt P: Factors affecting auditory performance of postlinguistically deaf adults using cochlear implants. *Audiol Neurootol* 1996;1:293–306.
30. Green KMJ, Bhatt YM, Mawman DJ, O'Driscoll MP, Saeed SR, Ramsden RT: Predictors of audiological outcome following cochlear implantation in adults *. *Cochlear Implant* 2007;8:1–11.
31. Hasepass F, Bulla S, Maier W, Laszig R, Arndt S, Beck R, et al.: The New Mid-Scala Electrode Array: A Radiologic and Histologic Study in Human Temporal Bones. *Otol Neurotol* 2014 May 15;35:1454–1420.
32. Rebscher SJ, Hetherington A, Bonham B, Wardrop P, Leake PA: Considerations for the design of future cochlear implant electrode arrays: electrode array stiffness, size and depth of insertion 2008;45:731–748.
33. Wardrop P, Whinney D, Rebscher SJ, Roland JT, Luxford W, Leake P a: A temporal bone study of insertion trauma and intracochlear position of cochlear implant electrodes. I: Comparison of Nucleus banded and Nucleus Contour electrodes. *Hear Res* 2005 May;203:54–67.

34. Frisch CD, Carlson ML, Lane JI, Driscoll CLW: Evaluation of a new mid-scala cochlear implant electrode using microcomputed tomography. [Internet]. . Laryngoscope 2015 May 6 [cited 2015 May 28];1–6.
35. Marel KS Van Der, Briaire J, Verbist BM, Muurling J: The Influence of Cochlear Implant Electrode Position on Performance. *Audiol Neurotol* 2015;202–211.
36. Skinner MW, Ketten DR, Holden LK, Harding GW, Smith PG, Gates G a, et al.: CT-derived estimation of cochlear morphology and electrode array position in relation to word recognition in Nucleus-22 recipients. *J Assoc Res Otolaryngol* 2002 Sep;3:332–50.
37. Cohen LT, Xu J, Xu SA, Clark GM: Improved and simplified methods for specifying positions of the electrode bands of a cochlear implant array. *Am J Otol* 1996;17:859–865.
38. Van der Marel KS, Verbist BM, Briaire JJ, Joemai RMS, Frijns JHM: Electrode migration in cochlear implant patients: not an exception. *Audiol Neurotol* 2012 Jan;17:275–81.
39. Mittmann P, Rademacher G, Mutze S, Ernst A, Todt I: Electrode Migration in Patients with Perimodiolar Cochlear Implant Electrodes. *Audiol Neurotol* 2015;20:349–353.







Chapter 5

Improved cochlear implant
position detection with spatially
synchronized pre- and post-
operative midmodiolar
cross-section CT
and MR images

MA van der Jagt, JJ Briaire,
S Boehringer, BM Verbist, JHM Frijns

Under review

Abstract

Objectives: In vivo evaluation of intrascalar position of a cochlear implant electrode array provides surgical feedback but is challenging due to scattering effects of the electrode array. This study introduces and assesses an evaluation method using spatially synchronized pre- and post-operative midmodiolar cross-sections of CT and MR images.

Methods: Three observers scored the intra-scalar position of all electrode contacts of 15 HiFocus 1J and 15 HiFocus Mid-Scala electrode arrays using 3 different methods; on midmodiolar cross-sections in post-operative CT images only (1), supported with spatially synchronized pre-operative CT (2) or MR (3) images. The intra- and inter-observer coefficients were calculated and compared between the 3 methods.

Results: Using spatially synchronized pre-operative images increases inter-observer coefficients in the 1J population from 0.75 to 0.79 and 0.80 with the use of pre-operative CT and MRI, respectively. In the MS population an increase from 0.77 to 0.83 (CT and MR) was found. For the intra-observer correlation coefficients, increases from 0.72 to 0.81 (CT) and 0.82 (MR) in the 1J and from 0.72 to 0.86 (CT) and 0.84 (MR) in the MS population were seen. No difference between the use of CT and MR images was found. A significant effect of angular insertion depth on the inter- and intra-observer coefficients was found in the MS population only, with increased coefficients for the more apical electrode contacts. Additionally, the use of a pre-operative framework increased the degree of certainty in allocations.

Conclusion: Using a referential pre-operative CT or MR scan improves the detection of scalar position and translocation of cochlear implants electrode array position.

Introduction

Cochlear implantation carries the risk of damaging intra-cochlear structures when inserting the electrode array into the cochlea. This damage may result in degeneration of neural structures, which could inhibit electrical stimulus transmission to the auditory cortex. Translocation of the array from the scala tympani to vestibuli will also lead to an increased distance between a contact and the spiral ganglion cells, hereby further adding to suboptimal stimulation. Although not conclusively proven, it is postulated that preservation of the intra-cochlear architecture is crucial for optimal hearing outcomes and that intra-cochlear damage might contribute, at least in part, to inter-patient variability in word recognition and residual hearing.¹ Moreover, for long-term purposes, preventing trauma facilitates the re-implantation of new devices. Therefore, detection and limitation of insertion trauma plays a crucial role in optimizing both short- and long-term performance, following cochlear implantation.

Evaluation of cochlear implant position additionally provides feedback on surgical procedures and implant designs and it can support fitting procedures. By in vivo assessment of the CI electrode array position, correlations between the precise position and clinical outcome can be examined in a large cohort of patients. To evaluate their position, structures that indicate the partitioning of the cochlear duct, like the osseous interscalar septum and soft structured basilar and Reissner's membranes, play an important role. Micro-CT depicts fine intra-cochlear structures in high detail, due to the high spatial resolution and also histological examination provides accurate details on both osseous and soft tissue structures. However, both histological and micro-CT analyses are only applicable in cadaveric studies, which are typically carried out in small series.

In a clinical setting high resolution CT scans or Cone beam CT scans can be used for post-implantation evaluations. However, the accuracy of clinical CT scans for evaluation of cochlear trauma may be degraded by the metal blooming artefacts caused by the electrode array. This blooming effect obscures the scalar boundaries, which are crucial to determine the electrode array position. The use of midmodiolar cross-sectional CT images for the determination of cochlear implant electrode array positions was validated with anatomic microdissections, in a study by Lecerf et al.² To be more specific about the intra-scalar position, a linear 5-point grading scale was introduced by Helbig et al.³ and Connor et al.⁴ This approach offered a simple, but standardized method. Yet, the authors report that it became increasingly difficult to correctly determine the position of the electrode carrier beyond 360 degrees.

The aim of this present study was to evaluate and compare the clinical reliability of three methods for determining the position of a cochlear implant electrode array on post-operative



CT images, based on the principle of combining pre- and postoperative midmodiolar cross-sectional images. The following three methods were carried out; evaluation on midmodiolar cross-section post-operative CT images only (1), supported with spatially synchronized pre-operative CT (2) or MR (3) images.

Materials & Methods

Patient population and implant designs

To test the method in patients with both translocated and non-translocated electrode arrays, we conducted a prior screening assessment of post-operative CT scans from patients that received cochlear implants between 2012 and 2015. We selected 30 adult patients with normal inner ear anatomy, that underwent unilateral implantation of a pre-curved HiFocus Mid-Scala (MS; n=15) or a straight HiFocus 1J (1J; n=15) electrode array (Advanced Bionics, Valencia, CA). The MS electrode is a pre-curved array, designed to achieve a mid-scalar position. It contains 16 electrode contacts and total active length of the array from basal contact to the tip is 15 mm. The distance from tip to the proximal blue marker that indicates a full insertion is 18 mm. The cross-sectional diameter varies from approximately 0.5 mm at the most apical contact to approximately 0.7 mm at the most basal contact. The 1J electrode array is a less pre-curved array, designed for outer wall positioning. It also contains 16 electrode contacts, leading to a total length of the array from basal contact to the tip of 17 mm. There is an additional 3 mm length from the most basal contact to the marker contact, indicating that a full insertion is 20 mm. The cross-sectional diameter of the array varies from approximately 0.4 mm at the most apical contact to approximately 0.8 mm at the most basal contact. Patient demographics are described in Table 1.

Radiological evaluation

All 30 patients received 3T MRI (Philips Achieva or Ingenia; Philips Healthcare, Best, The Netherlands) and multi-slice CT (MSCT; Aquilion; Toshiba Medical Systems, Otoware, Japan) examinations prior to implantation. An MSCT examination was also performed 1 day post-implantation, according to the standard work-up for patients with cochlear implants at our medical institution. Subsequently, multiplanar reconstructions were created from all 3 scans. The multiplanar reconstructions were based on a plane that ran through the basal cochlear turn, which provided the commonly used cochlear view, and a perpendicular line that ran through the modiolar axis. Within these reconstructions, the 3-dimensional (3D) consensus coordinate system was applied, as described by Verbist et al.⁵ This framework included three consistent landmarks: the cochlear apex, the round window, and the most lateral part of the lateral semicircular canal. Thus, measurements could be directly compared between any original 3D datasets that included these landmarks; i.e., preoperative CT and MRI inner ear datasets. With this coordinate system, the location of the round window was defined

in the pre-operative CT image and applied to both the pre-operative MRI and the post-operative CT images. Subsequently, the centre of each electrode contact was determined manually.⁶ A custom algorithm was written using MATLAB and its image processing toolbox (version R2015a) to present the spatially synchronized midmodiolar images adjacently, based on the coordinates of each electrode contact that determined the angle of cross-section in both MPRs.

Evaluation of intra-scalar electrode contact positions

Three methods were compared to evaluate the individual positions of 16 electrode contacts (Figure 1). The first method required a single midmodiolar cross-sectional image of the post-operative CT (Figure 1A). In this method, the scalar position of the electrode contact was determined based solely on the information provided in the post-operative scan. The second method combined the pre-operative (Figure B) and post-operative (Figure A2) CT scans, acquired at the exact same angular position from the round window and presented side by side. Thus, the pre-operative scan served as a referential framework by depicting the osseous spiral lamina and interscalar septum, which are commonly less visible on the post-operative CT scan, due to the presence of the array and the blooming artefacts caused by its metallic components. However, Figure 1B shows that the cochlear boundaries beyond the first turn were more poorly depicted, because the smaller structures become less resolved with progression from the basal to apical ends. This may impede accurate determination of the position of the more apical electrode contacts. In an attempt to overcome this limitation, a third method was conceived. In this method, the pre-operative 3T MRI (C) was acquired at the same angular position from the round window as the post-operative CT scan (A3). When these images were presented adjacent to one another, they provided additional, more distinct information on the second and third cochlear turns.

Three observers with different levels of experience judged each individual electrode contact twice for each evaluation method. Observer A is an experienced radiologist specialized in head and neck radiology, observer B is an ENT-surgeon in training and PhD student with training and sustained practice in imaging of the temporal bone, observer C is a PhD student focussing on speech coding strategies in cochlear implantation, without experience in imaging of the temporal bone. Observer 3 was instructed to evaluate midmodiolar cross-sections of cochlear images by observer 2. A score between 0 and 5 was assigned that reflected the position of the electrode contact within the cochlear lumen.^{3,4} Scores 1 and 2 indicated a ST position; scores 4 and 5 indicated a SV position, with different degrees of certainty. Thus, a score of 1 reflected a certain and 2 reflected a likely ST position; a score of 5 reflected a certain and 4 reflected a likely SV position. A score of 3 could be chosen for an intermediate position, and a score of 0 was given when the observer was unable to assess the position. The observers could adjust the Houndsfield settings and use the zoom



tool to optimize evaluations of the cross-sectional images. The scans were presented in randomized order, and the observers were blinded to patient name and electrode design.

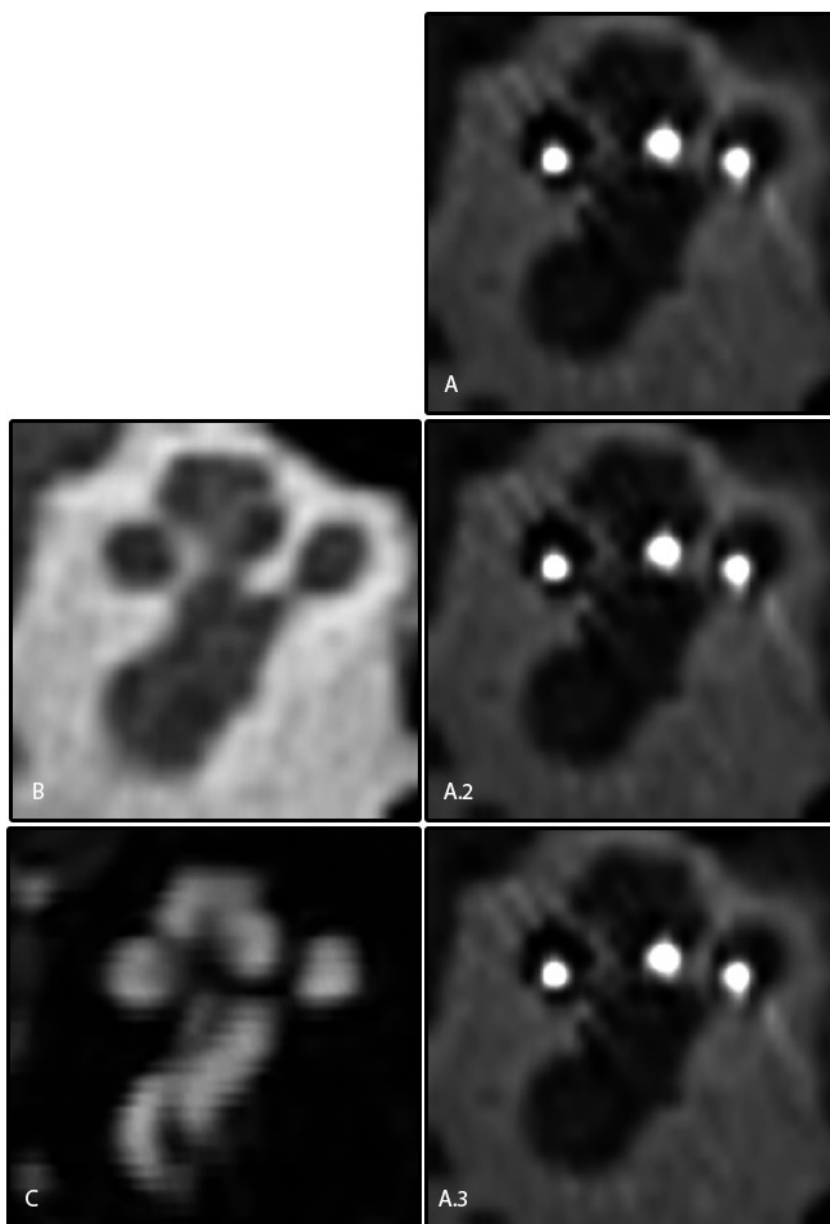


Figure 1: Midmodiolar cross-sectional postoperative CT-images (A), and spatially synchronized CT (B) and MR (C) images.

Statistical analysis

Statistical analyses were performed with SPSS (version 20; IBM, Armonk, New York). To evaluate demographic differences between patients that received the HiFocus MS and the HiFocus 1J implants, a student's T-test for continuous and a chi-square test for categorical outcomes was used. Student's T test was also used to determine differences between groups for the angular insertion depth (Table 1).

Table 1. Demographic characteristics of the studied population

	HiFocus 1J	HiFocus MS	
Patient characteristics			
Implant design (N)	15	15	NS
Age, years (mean ± SD)	58 ± 14	58±18	NS
Male: female	10:5	6:9	NS
Side (AS:AD)	7:8	5:10	NS
Surgical characteristics			
Angular insertion depth, degrees (mean ± SD)	447 ± 57	424±28	P = 0.039
Surgical approach			
Extended RW insertion	15	11	P < 0.000
RW insertion	0	4	

Abbreviations: MS: pre-curved HiFocus Mid-Scala; 1J: straight HiFocus 1J; AS: left ear; AD: right ear; RW: round window

Scores were evaluated on a continuous scale. This choice is justified by the fact that rater disagreement mostly occurs between adjacent score values for which a comparable scale can be assumed. The intra-class correlation (ICC) was calculated for both inter- and intra-observer agreements using the SPSS Reliability-analysis, with a two-way random-effect model. All samples were rated by all raters two times and intra-observer ICC reflects how consistent each rater repeatedly scored the same sample. The inter-observer ICC reflects how consistent the different raters scored the same sample. The ICC was calculated for each electrode contact separately, using the average of the two ratings per observer. These ICC values were used as outcomes in a linear mixed model to evaluate the effect of evaluation method, observer and angular insertion depth on rater agreement as measured by the ICC. From clinical perspective, we were interested in the effect of adding a referential framework based on pre-operative scans. Therefore, for prior analysis, the ICC outcomes for the methods with pre-operative CT and MR images were analysed as one group and compared with the outcomes based on the post-operative scans alone. All electrodes were included in this analysis and a random effect for electrode was used to reflect the correlation between ICCs of neighboring electrodes. This analysis was stratified per implant design.



Table 2. Distribution of scores

	Without	+ CT	+MRI
Score 5: certain SV	101	222	252
Score 4: likely SV	375	383	261
Score 3: intermediate	608	659	546
Score 2: likely ST	1164	731	658
Score 1: certain ST	626	879	1161
Score 0: not assessable	6	6	2
Total of scores	2880	2880	2880

Results

Table 1 demonstrates the comparison of the 1J and MS population. As expected based on the different designs, a significant difference in angular insertion depth exists between the two groups, with the 1J electrode array being on average 33 angular degrees more deeply inserted. Additionally, the average insertion depth of the HiFocus 1J population is on average 33 degrees shallower compared to previous reports from our 1J population^{6,7}. The HiFocus 1J is not compatible with a pure RW insertion, and all these electrode arrays were inserted through an extended window approach. Four HiFocus MS implants were inserted through a round window approach. All other characteristics did not differ significantly between the two groups. A total of 8640 scores were included in the analyses. Table 2 shows the distribution of all scores, per method of evaluation. The most notable differences between methods were reflected in scores 1 and 2.

Inter- and intra-observer agreement

The inter- and intra-observer ICCs were calculated for each individual electrode contact within the 1J and MS population separately. The average inter- and intra-observer ICCs per electrode contact for each method of evaluation are shown in Figure 2A and 2B, respectively. It is immediately noticeable that the ICCs show different patterns in the 1J and MS population, for both the inter- and intra-observer ICCs. In the MS population the ICC scores increase from basal to apical contact. The consistency of scores within and between observers for the 1J electrode array shows a more irregular pattern with the highest conformity at the basal contacts. Table 3 and 4 present an overview of the mean and standard deviations of the inter- and intra-observer ICC per method and implant design. Differences in inter-observer ICC's, were only significant between group 1 (only postop images) and group 3 (adding MR) in the 1J ($p = 0.048$) and MS ($p = 0.047$) population. For the mean intra-observer ICC in the 1J population, the ICC's are significantly different between using no pre-operative images and adding CT (1J: $p = 0.008$, MS: $p = 0.002$) or MRI (1J: $p = 0.044$, MS: $p = 0.026$).

Table 3. Inter-observer ICC

	Without	+ CT	+MRI
HiFocus MS (mean, SD)	0,767 (0.234)	0,830 (0.140)	0,829 (0.157)
HiFocus 1J (mean, SD)	0,727 (0.129)	0,781 (0.092)	0,785 (0.081)

A linear mixed model analysis for the inter-observer ICC in the 1J population showed a significant effect for method ($p = 0.015$), with a 0,047 lower ICC when no pre-operative support was used. We found no significant effect of angular insertion depth on the inter-observer ICC. In the MS population, the inter-observer ICC was 0,062 lower when no pre-operative support was used ($p = 0.025$). There was an effect of angular insertion depth on the inter-observer ICC found, with an increase of 0,012 ICC per angular degree.

For evaluation of the intra-observer ICC, also the variable ‘observer’ was included in the linear mixed model. This revealed a significant effect of method ($p < 0.001$) and observer ($p = 0.015$) for the 1J electrode arrays. Using no referential framework resulted in 0.091 lower ICC’s. Observer 3 scored a 0.0844 lower ICC compared to observer 1 ($p = 0.004$). No significant difference was found between observer pairs 3/2 and 1/2. In addition, no significant effect of angular insertion depth was found. For the MS implant design, a significant effect of method ($p < 0.001$), angular insertion depth ($p < 0.001$) and observer ($p = 0.008$) was found. Using no pre-operative support resulted in a 0,107 lower ICC. On average, a one angular degree deeper located electrode contact showed a 0,001 higher intra-observer ICC. Additionally, the model showed a 0,061 lower ICC for observer 3 compared to observer 1 ($p = 0.002$), and a 0,091 lower ICC compared to observer 2 ($p = 0.039$).

Table 4. Intra-observer ICC

HiFocus MS	Without	+ CT	+MRI
Observer 1 (mean, SD)	0,771 (0.214)	0,942 (0.059)	0,853 (0.260)
Observer 2 (mean, SD)	0,746 (0.249)	0,849 (0.162)	0,883 (0.181)
Observer 3 (mean, SD)	0,714 (0.265)	0,794 (0.129)	0,784 (0.221)
Average 3 observers (mean, SD)	0.744 (0.226)	0.861 (0.095)	0.840 (0.179)
HiFocus 1J	Without	+ CT	+MRI
Observer 1 (mean, SD)	0,764 (0.213)	0,854 (0.076)	0,853 (0.118)
Observer 2 (mean, SD)	0,717 (0.100)	0,802 (0.084)	0,845 (0.086)
Observer 3 (mean, SD)	0,687 (0.216)	0,774 (0.179)	0,756 (0.186)
Average 3 observers (mean, SD)	0.723 (0.122)	0.810 (0.081)	0.818 (0.091)

Abbreviations:

MS = mid-scalar, CI = cochlear implant, ST = scala tympani, SV = scala vestibuli,

ICC = intra- or interclass correlation coefficient, MPR = multiplanar reconstruction



Likelihood of allocated intra-scalar positions

To reflect the certainty of assessments, the percentage of certain versus likely allocations of ST and SV positions were compared. For the 1J electrode arrays, the percentage of certain ST allocations rose from 22.4% to 44.0%, when referential CT images, and to 56.0%, when referential MRI images were employed ($p < 0.001$). The percentage of certain SV allocations improved from 16.9% to 23.1%, when CT images, and to 35.3%, when MRI images were employed ($p = 0.007$). Within the MS population, the percentage of certain ST allocations increased from 44.2% to 61.2% and 70.0% with the use of referential CT and MR images, respectively ($p = 0.016$). The percentage of certain SV allocations changed from 24.5% to 50.8% and 59.0% with the use of pre-operative CT and MRI respectively ($p = 0.05$).

Discussion

In this study, we evaluated an easily applicable and reproducible method for determining the intra-scalar position of electrode arrays after cochlear implantation. This method uses spatially synchronized, pre- and post-operative midmodiolar cross-sectional images, presented adjacently, for identifying the scalar boundaries to support localization of cochlear implant electrode arrays. The addition of pre-operative CT or MR images used as reference for the post-operative images significantly improved the consistency of evaluations, demonstrated by increased inter- and intra-observer agreements. This method also increased the certainty of the observers in assessing implant positions. Subsequently, we found no additional, significant benefit of pre-operative MR images in comparison with pre-operative CT images, despite the increased intra- and inter ICC's in the 1J population, when MR images were added. Additionally, our data shows that the consistency and assuredness is highly dependent on angular insertion depth, implant design and its related intra-scalar position. The latter was evidently reflected by the difference in ICC's between the basal and apical contacts in the HiFocus MS population, which differ both in distance between electrode contact and modiolus and in intra-scalar position in superior-inferior direction. Additionally, level of experience also determines the reliability of the evaluation of the intra-scalar position of the electrode contact.

In our study, we demonstrated that angular insertion depth of an electrode contact has a significant effect on both intra- and inter-observer correlations, but only in the MS population. Against expectations, an increase in reliability was found for more deeply inserted electrode arrays and for the more apical contacts. The opposite was assumed because of the decreased size of the anatomical structures in the apical region, which makes it more difficult to distinguish the scalar boundaries. However, this finding might be explained by the in general shallower angular insertion depth of this implant design compared to the 1J electrode array, resulting in less difference between the size of the cochlear lumen at the

tip and the most basal electrode contact of the array. Additionally, we observed that the HiFocus MS electrode array is frequently positioned at the bottom of the scala tympani at the apical region because of the increase vertical stiffness, making it easier to determine its scalar location. This underlines the consequence of electrode design on the evaluation of the intra-scalar localization.

Midmodiolar cross-sectional images are commonly used to evaluate cochlear implant positions, in both ex- and in-vivo studies, and with different modalities.^{2,8-10} The latest generation CT scanners have achieved improvements in image resolution, facilitating the use of midmodiolar reconstructions of clinical CT scans as a valuable radiologic tool for predicting electrode array positions. In a clinical study from Lane et al.¹¹ multiplanar reconstructions of CT scans were used to localize cochlear implant electrode arrays, after validating this particular method with micro-CT.¹² They evaluated 23 electrode arrays on multiplanar reconstructions derived from CT images. With this method, they assessed the positions of 16 (70%) of the electrode arrays within the basal turn. The other 7 (30%) electrode arrays could not be localized, due to pathology that obscured the depiction of the scalar boundaries; i.e., retrofenestral otosclerosis, labyrinthitis ossificans, and incomplete partitioning. In our study, patients with pathological findings on pre-operative images were excluded from participation and 99,84% of the electrode contacts could be localized. Furthermore, in their study they only evaluated the electrode contacts within the basal cochlear turn, because localization of the electrode array beyond the basal turn was considered less reliable, due to the limited depiction of the spiral lamina more apical and the decreasing calibre of the cochlear lumen. In our study, we performed evaluations along the entire length of the electrode array, in order to assess translocations beyond 360 angular degrees.

Other scan modalities have been proposed as clinical tools for implant position evaluations. In a study by Aschendorff et al.⁸, rotational tomography offered superior quality over spiral CT. Compared to single- and multirow detector CT, the resolution of rotational tomography was superior, because it provided a more precise definition of the electrode and less metal artefacts. Nevertheless, this technique was rarely described in scientific studies after 2005. Fischer et al.¹³ used conebeam computed tomography (CBCT) to determine the scalar position of electrodes. The main advantages of the CBCT over the conventional CT are its lower sensitivity to metal disturbances and its high resolution. Although these two scan modalities were not included in our study, the method used here is also applicable to these scan modalities.

Skinner et al.¹⁰ and Finley et al.¹⁴ used rigid registration of clinical CTs and a high resolution atlas, based on micro-CT and orthogonal-plane fluorescence sectioning microscopy images, to determine in vivo electrode positions. However, from earlier studies, we have learned



that cochlear morphology is highly variable.^{6,15,16} This variability implies that the use of a single male donor would not suffice for all implanted patients, unless the atlas could be tailored to match patient-specific morphological characteristics by stretching, tilting, or rotating, as used in rigid registration techniques described by Cakir et al¹⁷. This limitation led to the method of using multiple atlases,¹⁸ and eventually, using the patient's own pre-operative CT scans as a reference for the anatomical structures of interest.¹⁹ In some institutions, pre-operative images are not acquired in the standard work-up of candidates for cochlear implants. In those cases, the morphological appearance of the contralateral inner ear on the post-operative scan can be used for alignment, because in most cases the ears are highly symmetric for the purposes of cochlear implants.²⁰ It is difficult to compare the previous methods with our method, in terms of accuracy. However, a primary advantage of our method was that it required no additional appliances, other than those used for routine clinical actions, in contrast to the above described registration methods.

Previous studies have not described the use of MRIs for evaluating the intra-scalar position of the CI electrode. Post-implantation, MRI use is restricted, due to the risk that the electrode array might shift or heat up due to the magnetic field of. Although the magnet of some implants are designed to withstand MRI examinations at 1.5 or even 3 Tesla, clinicians are reluctant to use MRI, because they obviously wish to avoid such adverse events. In our institution, both MRI and CT images are acquired as part of the standard pre-operative work-up for CI candidates. MRI allows the detection of nerve anomalies and can depict obliteration or incomplete partitioning of the cochlea. Midmodiolar cross-sectional MRIs show specific structures of interest, like the osseous spiral lamina and the interscalar septum, in higher detail compared to CT images. A recent study demonstrated that the 7 Tesla MRI provided further improved visualization of certain anatomical details of the inner ear, compared to 3 Tesla images.²¹ In the present study, however, we found no difference or additional value between CTs and MRIs in terms of consistency in scoring. This might be the result of image quality degradation following creating MPR's or otherwise because of the already high quality of the CT images. However, the use of 7 Tesla MRI could potentially offer more benefit, when implemented with our method for determining the intra-scalar position of electrode arrays.

Conclusion

This study evaluated the use of spatially synchronized multiplanar reconstructions based on CT and MR images acquired pre- and post-implantation. We demonstrated that this method was an easily applicable approach for determining the intra-scalar position of an electrode array, is more reliable than the use of postoperative images alone and provides

the observers more certainty in their assessment. This method can be used to examine insertion traumas in a clinical setting.



References

1. Hoskison E, Mitchell S, Coulson C. Systematic review: Radiological and histological evidence of cochlear implant insertion trauma in adult patients. *Cochlear Implants Int.* 2017;18(4):192-197. doi:10.1080/14670100.2017.1330735
2. Lecerf P, Bakhos D, Cottier J-P, Lescanne E, Trijolet JP, Robier A. Midmodiolar reconstruction as a valuable tool to determine the exact position of the cochlear implant electrode array. *Otol Neurotol.* 2011;32(7):1075-1081. doi:10.1097/MAO.0b013e318229d4dd
3. Helbig S, Mack M, Schell B, Bratzke H, Stöver T, Helbig M. Scalar localization by computed tomography of cochlear implant electrode carriers designed for deep insertion. *Otol Neurotol.* 2012;33(5):745-750. doi:10.1097/MAO.0b013e318259520c
4. Connor SEJ, Holland NJ, Agger A, et al. Round window electrode insertion potentiates retention in the scala tympani. *Acta Otolaryngol.* 2012;132(9):932-937. doi:10.3109/00016489.2012.680493
5. Verbist BM, Finley CC, Roland PS, Thomas J. Consensus panel on a cochlear coordinate system applicable in histological, physiological and radiological studies of the human cochlea. *Otol neurotol.* 2010;31:722-730.
6. van der Marel KS, Briaire JJ, Wolterbeek R, Snel-Bongers J, Verbist BM, Frijns JHM. Diversity in Cochlear Morphology and Its Influence on Cochlear Implant Electrode Position. *Ear Hear.* November 2013:1-12. doi:10.1097/01.aud.0000436256.06395.63
7. van der Jagt MA, Briaire JJ, Verbist BM, Frijns JHM. Comparison of the HiFocus Mid-Scala and HiFocus 1J Electrode Array: Angular Insertion Depths and Speech Perception Outcomes. *Audiol Neurotol.* 2016:316-325. doi:10.1159/000448581
8. Aschendorff A, Kubalek R, Turowski B, et al. Quality control after cochlear implant surgery by means of rotational tomography. *Otol Neurotol.* 2005;26(1):34-37. <http://www.ncbi.nlm.nih.gov/pubmed/15699717>.
9. Teymouri J, Hullar TE, Holden TA, Chole RA. Verification of Computed Tomographic Estimates of Cochlear Implant Array Position: A Micro-CT and Histological Analysis. *Otol Neurotol.* 2011;32(6):980-986. doi:10.1097/MAO.0b013e3182255915.Verification
10. Skinner MW, Holden T a., Whiting BR, et al. In Vivo Estimates of the Position of Advanced Bionics Electrode Arrays in the Human Cochlea. *Ann Otol Rhinol Laryngol.* 2007;116(4):2-24. doi:10.1177/000348940711600401
11. Lane JI, Witte RJ, Driscoll CLW, Shallop JK, Beatty CW, Primak AN. Scalar localization of the electrode array after cochlear implantation: clinical experience using 64-slice multidetector computed tomography. *Otol Neurotol.* 2007;28(5):658-662. doi:10.1097/MAO.0b013e3180686e26
12. Lane JI, Driscoll CLW, Witte RJ, Primak A, Lindell EP. Scalar localization of the electrode array after cochlear implantation: a cadaveric validation study comparing 64-slice multidetector computed tomography with microcomputed tomography. *Otol Neurotol.* 2007;28(2):191-194. doi:10.1097/01.mao.0000247817.31572.ed

13. Fischer N, Pinggera L, Weichbold V, Dejaco D, Schmutzhard J, Widmann G. Radiologic and Functional Evaluation of Electrode Dislocation from the Scala Tympani to the Scala Vestibuli in Patients with Cochlear Implants. *Am J neuroradiology*. 2015:1-6.
14. Finley CC, Skinner MW. Role of electrode placement as a contributor to variability in cochlear implant outcomes. *Otol Neurotol*. 2008;29(7):920-928.
15. Erixon E, Högstorp H, Wadin K, Rask-Andersen H. Variational anatomy of the human cochlea: implications for cochlear implantation. *Otol Neurotol*. 2009;30(1):14-22. doi:10.1097/MAO.0b013e31818a08e8
16. Jagt AMAV Der, Kalkman RK, Briaire JJ, Verbist BM, Frijns JHM. Variations in cochlear duct shape revealed on clinical CT images with an automatic tracing method. *Sci Rep*. 2017;7(1):1-9. doi:10.1038/s41598-017-16126-6
17. Cakir AA, Labadie RF, Zuniga MG, Dawant ABM, Noble AJH. Evaluation of Rigid Cochlear Models for Measuring Cochlear Implant Electrode Position. 2016:1560-1564. doi:10.1097/MAO.0000000000001245
18. Wanna GB, Noble JH, McRackan TR, et al. Assessment of electrode placement and audiological outcomes in bilateral cochlear implantation. *Otol Neurotol*. 2011;32(3):428-432. doi:10.1097/MAO.0b013e3182096dc2
19. Schuman T a, Noble JH, Wright CG, Wanna GB, Dawant B, Labadie RF. Anatomic verification of a novel method for precise intrascalar localization of cochlear implant electrodes in adult temporal bones using clinically available computed tomography. *Laryngoscope*. 2010;120(11):2277-2283. doi:10.1002/lary.21104
20. Reda F a, McRackan TR, Labadie RF, Dawant BM, Noble JH. Automatic segmentation of intra-cochlear anatomy in post-implantation CT of unilateral cochlear implant recipients. *Med Image Anal*. 2014;18(3):605-615. doi:10.1016/j.media.2014.02.001
21. van der Jagt M a, Brink WM, Versluis MJ, et al. Visualization of Human Inner Ear Anatomy with High-Resolution MR Imaging at 7T: Initial Clinical Assessment. *AJNR Am J Neuroradiol*. August 2014:1-6. doi:10.3174/ajnr.A4084







Chapter 6

Prolonged insertion time
reduces translocation rate of the
HiFocus Mid-Scala electrode
array in cochlear
implantation

MA van der Jagt, JJ Briaire,
S Boehringer, BM Verbist,
JHM Frijns

*Accepted for publication in Otolology &
Neurotology*

Abstract

Hypothesis: Insertion speed during cochlear implantation determines the risk of cochlear trauma. By slowing down insertion speed tactile feedback is improved. This is highly conducive to control the course of the electrode array along the cochlear contour and prevent translocation from the scala tympani to the scala vestibuli.

Background: Limiting insertion trauma is a dedicated goal in cochlear implantation in order to maintain the most favourable situation for electrical stimulation of the remaining stimuable neural components of the cochlea. Surgical technique is one of the potential influencers on translocation behaviour of the electrode array.

Methods: The intra-scalar position of 226 patients, all implanted with a HiFocus Mid-Scala electrode array was evaluated. One group (n = 113) represented implantation with an insertion time less than 25 seconds (fast insertion) and the other group (n = 113) was implanted in 25 or more seconds (slow insertion). A logistic regression analysis studied the effect of insertion speed on insertion trauma. Furthermore, the effect of translocation on speech performance was evaluated using a linear mixed model.

Results: The translocation rate within the fast and slow insertion groups were respectively 27 and 10% ($p < 0.001$). A logistic regression analysis showed that the odds of dislocation increases by 2.527 times with a fast insertion (95% CI = 1.135, 5.625). We failed to find a difference in speech recognition between patients with and without translocated electrode arrays.

Conclusion: Slowing down insertion speed till 25 seconds or longer reduces the incidence of translocations of the HiFocus MS electrode array.

Introduction

A dedicated goal with cochlear implants (CIs) is to limit intra-cochlear trauma during surgery. Atraumatic insertions preserve residual hearing, accommodate simultaneous electric and acoustic stimulation, and provide the best conditions for optimal stimulation of auditory neurons; thus, they should facilitate best speech perception outcomes^(1,2).

Although it remains largely unknown how translocation of a CI electrode array occurs, it is assumed that this is influenced by the surgical technique, cochlear morphology, and the physical qualities of the array (i.e., length, stiffness, and cross-sectional diameter). To reduce insertion trauma, several advances have been made in implant designs and surgical techniques, referred to as ‘soft surgery techniques’³. To minimize damage to the basilar membrane, arrays were designed with soft, thinner tips, reduced cross-sectional dimensions, and less vertical stiffness. Despite these improvements, insertion trauma rates remain high with all current devices (up to 32.6%)⁴.

In recent years, a CI with a pre-curved electrode array that was designed to maintain a mid-modiolar position within the scala tympani was introduced (HiFocus Mid-Scala (MS) electrode array; Advanced Bionics, Valencia, CA). Theoretically, this design retains an optimal distance between the electrode contacts and the modiolus, but avoids contact with both the modiolus and lateral wall. Moreover, the small size of the array allows a pure round window (RW) insertion, potentially causing less trauma during insertions. Three studies investigated the electrode position and angular insertion depth of this implant design when inserted into temporal bones of small cohorts. They reported translocation rates of 0-12.5%⁵⁻⁷. In previous clinical studies on several pre-curved designs, considerably higher translocation rates were reported (29-54%)⁴.

Currently, the favoured surgical approach technique is a pure round window (RW) insertion; indeed, some have considered it to be the least traumatic approach^{8,9}. With this approach, the implant is inserted directly into the RW without drilling a cochleostomy or drilling away part of the crista ante fenestram. However, this approach might impair visualization into the scala tympani, and thus, reduce control of the optimal direction of insertion, which could increase the risk of initial trauma at the base¹⁰. Furthermore, slowing down the insertion speed was reported to facilitate hearing preservation¹¹. It is postulated that slower insertion speeds can maintain the intracochlear fluid pressure, and thus, prevent basilar membrane rupture. A correlation between the insertion speed and intracochlear fluid pressure was previously shown by Todt et al.¹².



This study investigated the rate of translocations with the pre-curved HiFocus MS electrode array. We evaluated whether different insertion times, and cochlear approaches affected the translocation rate.

Materials & Methods

Patients

This study included data of 226 primarily implanted ears from 209 consecutive patients of all ages that received implantations with a HiFocus MS electrode array, between June 2012 and November 2017 at our institution. We excluded patients with characteristics that might influence the electrode array trajectory, such as severe malformations or cochlear ossifications. A subgroup of unilaterally implanted adult patients with postlingual deafness was selected for a speech perception analysis. Patients were grouped according to the insertion time (Table 1).

Table 1. Characteristics of the study population

Patients	N = 226
Insertion speed (fast : slow)	113 : 113
Age at implantation, years (mean \pm SD)	43 (\pm 29)
Male : Female	93:133
Side (AD : AS)	114:112
Cochlear size (mean, \pm SD)	60 (\pm 5)
Audiological characteristics	
Pre-operative phoneme scores (mean \pm SD)	50 (\pm 23)
Pre-operative word scores (mean \pm SD)	28(\pm 20)

*Fast insertions: electrode arrays inserted in 25 s or less, or implanted before January 2015. Slow insertions: electrode arrays inserted in 25 s or more. AD: right ear AS: left ear, RW: round window, SD = standard deviation.

Electrode designs and surgical approach

The pre-curved HiFocus MS electrode array was launched in 2013 and was designed to maintain a mid-scalar position. The array has a total active length of 15.0 mm, from the basal contact to the tip and contains 16 electrode contacts, arranged on a 0.9 mm pitch. Two blue markers, with a distance of 13.5 mm in-between, are included to ensure proper insertion, either with an insertion tool or free-hand, and to indicate full insertion of the active electrode array. The cross-sectional diameter is approximately 0.5 mm and 0.7 mm at the most apical and basal contact, respectively. In this study, all insertions were performed with the insertion tool provided with the implant. Insertion was performed either with a pure RW (n = 43) or an extended RW (n = 183) approach, based on the size and orientation

of the RW opening. RWs were measured with a 0.8 mm sizer during the surgical procedure. The insertion of the electrode array is performed as one steady, continuous progression.

In the context of evaluation of care, an uncontrolled interim analysis was performed in January 2015 to evaluate translocation between the two surgical approaches. A higher incidence of translocations was found with the pure RW insertions (30% versus 23%). This finding somewhat changed the procedure by making the surgeons more reluctant to use this approach in future implantations. Consequently, most pure RW insertions were performed before 2015 with faster implantations. This confounding factor was taken into account with the later analyses. All implantations were performed by 5 otorhinolaryngologists with different levels of experience in cochlear implantations (i.e., 1 to 20 years). The majority of the implantations (183/226) was performed by the 2 most experienced surgeons.



Radiological evaluation of electrode contact positions

All 226 patients were scanned with a multi-slice computed tomography scanner (Aquilion; Toshiba Medical Systems, Otowara, Japan), both before and 1 day after implantation, according to the standard work-up for CI candidates in our institution. Multiplanar reconstructions were created from these scans. A 3D coordinate system was applied, which is generally used for universal evaluation of the CI position¹³. The angular and radial positions of each individual electrode contact within the coordinate system were calculated with an in-house post-processing program, written in Matlab (Mathworks, Novi, MI, USA). This program generated spatially synchronized midmodiolar cross-sectional images, which allowed a side-by-side presentation of the pre- and postoperative CT scans acquired at the same angular distance from the RW. This method was validated in an earlier study¹⁴.

Intra-cochlear CI electrode array positions were evaluated with a 5-point scale. Evaluations were based on the superior-inferior position of the electrode contact within the cochlear lumen and the level of certainty, as follows: scores of 1 and 2 indicated a certain and probable scala tympani position, respectively; a score of 3 indicated an intermediate position; and scores of 4 and 5 indicated a probable and certain scala vestibuli position, respectively. When two or more electrode contacts were within the scala vestibuli (i.e., a score 4 or 5), the electrode array was considered translocated.

Evaluation of insertion time and insertion characteristics

To gain more insight into the effect of the insertion speed on the trauma incidence, the exact duration of the tool insertion was recorded, starting in January 2015. This insertion time was defined as the time between insertion of the apical and basal blue marker of the electrode array through the (extended) RW. From January 2015, surgeons were asked to pursue an insertion time of 25 s or more, corresponding with an insertion speed of 32 mm/min. This cut off of 25 s was chosen, in part, based on the results of Todt et al., who

reported an increase in intracochlear fluid pressure with rapid insertions¹². In contrast, insertions performed before 2015 were performed well within 25 s, probably even within 10 s; therefore, an objective comparison was feasible.

Group 1 included all patients that received implants before the change in January 2015 (n = 108) and all patients that received implants after this change with insertion times of 25 s or less (n = 5). Group 2 included all patients that received implants with insertion times longer than 25 s (n = 113).

We also extracted data from the surgical and radiological reports to assess the angular insertion depth, resistance, electrode array rotations, and incomplete insertions.

Factors that influence translocation

Potential factors that might influence the translocation behaviour of a CI electrode array were analysed with a multivariate logistic regression analysis. The following variables were included; a fast or slow insertion, the surgical approach, the angular insertion depth, and the surgeon. Because data regarding the absolute insertion time was only available of the patients implanted since January 2015, a sub analysis studying absolute insertion time on translocation rate was performed with an estimated time of insertion of 10 seconds in the fast inserted population.

Evaluation of speech performance

Speech performance was evaluated in a group of 133 adults with postlingual deafness; of these, 59 and 74 were in the fast and slow insertion groups, respectively. Speech perception was assessed with the standard Dutch speech test of the Dutch Society of Audiology¹⁵. Briefly, four lists of 11 monosyllabic words were administered, and we recorded the number of phonemes and words correctly recognized. These assessments were conducted at 1 week, 2 weeks, and at 1, 3, 6, and 12 months after hook-up of the implant.

Statistical analysis

Statistical analyses were performed with SPSS (version 20, IBM, Armonk, New York). The Chi-square test was used to compare translocation incidences between fast and slow insertion groups and between the pure and extended RW surgical approaches. A logistic regression analysis was performed to study the effects of the surgical approach, the insertion time, the surgical approach, the cochlear size and the angular insertion depth on the incidence of traumatic insertions. A linear mixed model analysis was performed to study the effect of translocation on speech performance. In the mixed models, a random intercept per patient and a random effect for time was used. These random effects measure the fluctuation of patient slopes and intercepts for speech performance around the overall regression line.

Covariance structure was chosen as unstructured. All tests were 2-tailed. P-values <0.05 were considered statistically significant.

Results

Translocations

In all 226 cases, a complete insertion was achieved. Translocations occurred in 41 cases (18%). Thirty translocations occurred following a fast insertion (27%), versus 11 after a slow insertion (10%). All translocations occurred in a relatively restricted area. The mean angular depth of the most basal translocated electrode contact was 167° (SD 20°). In all cases, the electrode array remained within the scala vestibuli after translocation.

Insertion characteristics

The mean angular insertion depth was significantly deeper in the fast insertion group (421°, SD 29) than in the slow insertion group (409°, SD 40; $p=0.009$). The mean angular insertion depth was 427° in translocated electrode arrays and 412° in full scala tympani insertions, respectively ($p=0.012$).

Overall, traumatic insertions occurred in 27/183 (15%) extended RW insertions and in 14/43 (33%) pure RW insertions ($p=0.008$). In the slow insertion group, the translocation rates were 1/7 (14%) and 10/106 (9%) with the pure and extended RW approaches, respectively ($p = 0,675$). In the fast insertions group, the translocation rates were 13/36 (36%) and 17/77 (22%) with the pure and extended RW approaches, respectively ($p = 0.115$).

In 7 out of 226 implantations, the electrode array had to be re-inserted due to twisting of the electrode array ($n=2$) in one of these cases also resistance was felt. Other reasons for re-insertion were; incomplete insertion ($n=2$), an unstable position of the lead ($n=2$) and in one case the opening of the extended window turned out to be too narrow.

After beginning to pursue slower insertion times (25 s or more), the insertion times were recorded in 113 cases. Among these, 5 cases failed to achieve the 25-s limit, because either the final array insertion was reached earlier than expected, or the slow insertion resulted in instability of the surgeon's hand. Among the remaining 108 cases, the mean insertion time was 45 s (range, 25-95 s).

With a multivariate logistic regression analysis we studied the effect of the variables fast/slow insertion, angular insertion depth, surgical approach, cochlear size and surgeon on the occurrence of translocation. To rule out an interaction between angular insertion depth and cochlear size, between angular insertion depth and fast/slow insertion, and between surgical



approach and fast/slow insertion, the possibilities of these interactions were included in the work-up of the model. No interaction was found between angular insertion depth and cochlear size ($p = 0,441$), angular insertion depth and fast/slow insertion ($p = 0,683$) and surgical approach and fast/slow insertion ($p = 0,722$). For the final analysis we tried to follow the ‘number of events / 10 rule’ to analyse a reliable model. This means a maximum of 4 variables were included, i.e. fast/slow insertion, angular insertion depth, surgical approach and cochlear size. The outcomes of the multivariate logistic regression analysis are shown in Table 2. With a fast insertion the odds for a translocation of the electrode array increases by 2.527 times (95% CI = 1.135 – 5.625), controlled for surgical approach, angular insertion depth and size of the implanted cochlea. The Hosmer Lemeshow test shows a good fit of the model (ChiSquare 5.773, 8 degrees of freedom, $p = 0.673$). Likely, there is also an association between angular insertion depth and translocation, although with a p-value of 0.050 this cannot be asserted with certainty. The sub analysis studying insertion time as a continuous variable, with the estimated insertion time of 10 seconds for all the fast implanted patients, did not show a significant association of the absolute insertion time with translocation ($p = 0.354$).

Table 2 . Surgical characteristics of the study population

Surgical characteristics	Fast insertion (n = 113)	Slow insertion (n = 113)
Translocation (N,%)	30, 23%	11, 10%
Angular insertion depth, degrees (mean \pm SD)	420 (\pm 29)	409 (\pm 40)
Duration of insertion, s (mean \pm SD)	N/A	44 (\pm 16)
Surgical approach		
Extended : Pure RW insertion	77:36	106:7

Fast insertions: electrode arrays inserted in 25 s or less, or implanted before January 2015. Slow insertions: electrode arrays inserted in 25 s or more.

RW: round window, SD = standard deviation

Speech performance

Among the 172 patients that received unilateral implants, 133 had postlingual deafness and were included in the sub-analysis for evaluating speech perception. Translocations were detected in 21 patients. Figure 2A, B shows the results of phoneme and word tests conducted after implantation. At all 6 time points, the groups showed no significant differences in speech perception. Table 3 shows the number of patients per number of follow-up measurements. Overall, 97/798 (12.2%) and 110/798 (13.4) of the phoneme and word scores, respectively, were missing. These percentages were deemed to be acceptable, especially because of the linear mixed model (missing at random). We constructed a linear mixed model, for the phonemes and word scores separately, while taking into account other

possible influencing factors; the pre-operative speech perception scores and the angular insertion depth. These two variables were analysed as fixed effects. A random intercept and random time model was fit for the 6 time intervals. The analyses show an effect of pre-operative speech perception scores on post-operative speech perception scores; for each added pre-operative phoneme score, the postoperative phoneme outcome increases with 0.264 ($p < 0.001$) and for each added pre-operative word score, the postoperative word outcome increases with 0.385 ($p < 0.001$). We failed to find a difference in speech recognition between patients with and without translocated electrode arrays. The random effects show large variances as compared to residual variance, indicating heterogeneity between patients. The details of the linear mixed model analyses are presented in Table 4 and 5.

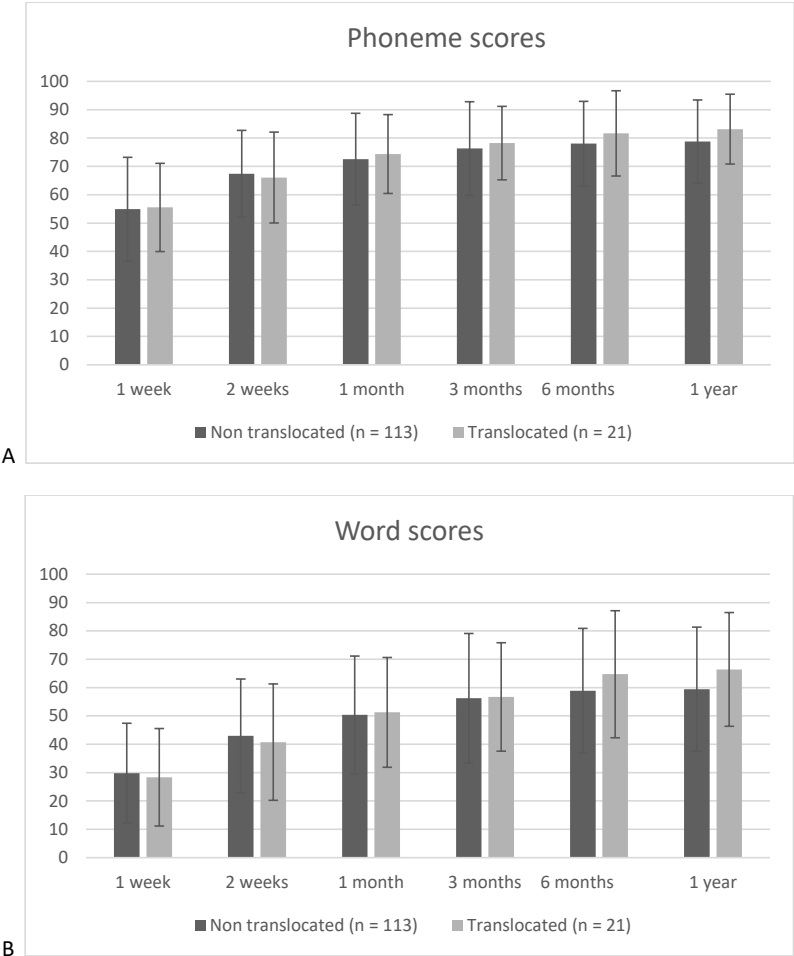


Figure 1: Mean phoneme (A) and word (B) recognition scores and standard deviations at 6 follow-up intervals of non-translocated (dark grey) and translocated (light grey) and HiFocus MS electrode arrays.

Table 3. Output Logistic Regression Analysis; effect parameters on translocation outcomes

Parameter	odds Ratio Estimate	p-value	Lower bound 95% CI interval	Upper bound 95% CI interval
Fast insertion speed	2.527	0.023	1.135	5.625
Pure round window insertion	1.817	0.154	0.799	4.132
Angular insertion depth	1.011	0.050	1.000	1.023
Size of the implanted cochlea	0.964	0.270	0.904	1.029

Table 4. Output Linear Mixed Model Analyses; effect parameters on speech perception outcomes (phonemes)

Parameter	Estimate	p-value	95% Confidence Interval	
			Lower Bound	Upper Bound
Estimates of Fixed Effects				
Intercept	44,757	0,005	14,051	75,463
Dislocation = yes	-3,010	0,342	-9,261	3,242
Angular insertion depth	0,025	0,460	-0,042	0,931
Preoperative phoneme score	0,252	<0,001	0,140	0,363
Estimates of Random Effects				
Time interval*	0,371	<0,001	0,315	0,427

* in weeks after first hook-up

Table 5. Output Linear Mixed Model Analyses; effect parameters on speech perception outcomes (words)

Parameter	Estimate	p-value	95% Confidence Interval	
			Lower Bound	Upper Bound
Estimates of Fixed Effects				
Intercept	10,778	0,613	-31,272	52,829
Dislocation = yes	-1,766	0,685	-10,377	6,845
Angular insertion depth	0,051	0,285	-0,043	0,145
Preoperative word score	0,393	<0,001	0,231	0,555
Estimates of Random Effects				
Time interval**	0,514	<0,001	0,443	0,585

** in weeks after first hook-up

Table 6. Number of patients per number of follow-up measurements

Number of follow-up measurements	Phonemes	Words
6 (complete follow-up)	62	58
5	53	54
4	12	12
3	5	6
2	0	0
1	1	0
0*	0	3
Total	133	133

* These patients were not included in the linear mixed model analysis



Discussion

We demonstrated that using a fast, versus a slow, insertion of the pre-curved MS electrode array, increases the odds of translocation by 2.527 times. The translocations of the CI array were found to occur in a relatively narrow region around 167° (SD 20°) from the RW. Approximately halfway the basal turn of the cochlea where its vertical trajectory usually shows a steep increase^{16,17}. Yet, speech recognition till 1 year after implantation was similar in patients with and without translocations. These findings should be considered in the future development and evaluation of CI electrode arrays and surgical techniques.

Implant designs

The ideal electrode array should combine trauma prevention features with an intra-cochlear position that provides optimal stimulation of the spiral ganglion cells; i.e. closely corresponds to the natural cochlear tonotopy, has a broad dynamic range, and provides high spatial discrimination. However, improvements in one domain often lead to compromises in other domains. Earlier studies that investigated insertion trauma rates with different electrode arrays have shown divergent outcomes. A recent systematic review of 653 implantations from 21 studies, including in vivo, ex vivo, radiological, and histological studies, reported that 115 cases (17.6%) showed evidence of trauma. The traumas varied from an elevated basilar membrane to scalar translocations¹⁸. Focusing on the studies comparable to ours, which included only the in vivo radiological studies that applied conventional, conebeam, or flat-plane CT images to evaluate trauma (5 studies), they found an average trauma incidence of 26% (range, 13 to 57%). This rate was substantially higher than our 10% incidence achieved with prolonged insertion times, but it was comparable to the 27% observed in our fast insertion group. Similarly, in the 12 histological examinations, the trauma incidence was 28%. However, it should be emphasized that, in those studies, in addition to translocations from the scala tympani to scala vestibuli, they included any evidence of basilar membrane

elevations or ruptures, which can only be investigated histologically. The latter types of trauma might also lead to impairments in residual hearing and fibrosis formation; thus, they could potentially negatively influence postoperative speech intelligibility. Consequently, an in vivo evaluation might underestimate the actual extent of trauma.

During insertion, pre-curved arrays are thought to behave differently from lateral-wall electrode arrays, due to differences in stiffness in the horizontal and vertical planes. Rebscher et al.¹⁹ reported that the size and shape of the array directly affected the trauma incidence. For example, arrays that are stiffer in the plane perpendicular to the cochlear spiral plane are less likely to cause severe trauma than arrays with similar stiffness in the vertical and horizontal planes. Less stiffness made it difficult to steer arrays and provided less tactile feedback during insertion. On the other hand, more stiffness could cause more damage when it contacted the basilar membrane or floor of the scala tympani, therefore pre-curved arrays carry a greater risk of translocation²⁰. Moreover, the variability in cochlear morphology, in particular the vertical trajectory¹⁶, presumably plays a role in the occurrence of translocation of the CI electrode array. This suggests a difference in compatibility with individual coiling geometries between electrode array designs. Further research is necessary to clarify this.

Because the HiFocus MS electrode array is a relatively new design on the CI market, few reports have focused on insertion traumas with this particular design. In three cadaveric studies, the HiFocus MS electrode array was inserted into 8, 16, and 20 temporal bones; they reported translocation rates of 12.5, 0, and 5.3%, respectively⁵⁻⁷. Two clinical studies reported divergent translocation rates of 57.1% (8/14) and 6.7% (2/30). Both included relatively small patient populations and none of them reported on insertion speed.

Surgical approach

Over time, new insights have led to changes in the definition of the ideal or least traumatic surgical approach. Early electrode arrays were introduced through a cochleostomy, simply because the arrays were relatively large. However, several later studies demonstrated that electrode arrays inserted through a cochleostomy carried a higher risk of basal trauma (48%) compared to insertions through the RW membrane.^{21,23} With the introduction of smaller CIs, a pure RW window approach was feasible; this approach avoided drilling-induced trauma and allowed preservation of the intra-cochlear architecture. However, it should be noted that the trajectory of the electrode array is highly influenced by the anatomical features of the RW. In addition, a slit RW insertion limits the view into the scala tympani, which risks damage to the modiolus or insertion into the vestibulum. With the extended RW approach, a good balance was found between avoiding the harm caused by drilling and increasing the visualization into the scala tympani by enlarging the RW opening, which facilitated

determinations of the ideal insertion vector. Although we initially found a higher incidence of traumatic insertions in the pure RW insertions in the uncontrolled analysis, this was not found in the final evaluation in a larger population. Because the outcomes of an uncontrolled interim analysis led to an alteration of procedure, i.e. being more reluctant with pure RW insertion, while at the same time insertion was prolonged, the question raised whether the lack of a significant effect of surgical approach on translocation was potentially biased by the almost predominantly use of an extended RW approach in the slow inserted population. However, the multivariate logistic regression analyses rejected this.

Insertion speed

Little is known about the relationship between insertion speed and trauma incidence. However, the role of insertion speed in preserving residual hearing was previously discussed.^{11,12,24} Those studies investigated the effects of insertion speed on intra-cochlear fluid pressure¹², insertion forces,²⁴ and inner ear function¹¹, which are all presumably related to intra-cochlear trauma. Todt et al. showed that rapid insertion speeds were associated with high intra-cochlear fluid pressures.¹² Increased pressure can damage the neuro-epithelium of the cochlea and the vestibular system²⁵. Kontoris et al. demonstrated that higher insertion speeds significantly increased insertion forces²⁴, which increased the risk of damaging intra-cochlear structures. Speeds of 10 to 200 mm/min led to average insertion forces of 0.09 to 0.185 N and maximum forces of 0.18 to 0.42 N. In human cochlear implantations, the average insertion speed was 96.5 mm/min, which corresponded to average forces of 0.138 – 0.155 N.²⁴ Another study showed that forces of 0.029 to 0.039 N could rupture the basilar membrane.²⁶ Rajan et al. compared implantations at the standard speed (60 mm/min) and implantations at a slower speed (15 mm/min). The slow insertions significantly reduced hearing loss (10.5 vs. 16 dB) and the incidence of impaired balance (0 vs. 22%)¹¹. Consistent with our results, these outcomes advocated a prolonged insertion time to preserve intracochlear structures and residual hearing. The mean insertion speed in the slow insertion groups corresponds to 18mm/min (45 seconds), comparable with the speed in the slow insertions described by Rajan et al. We also analysed insertion times as a continuous variable. However, this analysis did not show a significant effect. However, when we analysed the insertion time as a dichotomous variable with a cut-off of 25 s, corresponding to a speed of 32mm/min, the results favoured the slowly inserted array. This result suggested that our cut-off value was correctly chosen within a realistic clinical framework.

Translocation and hearing outcomes

Interest in soft surgery has arisen from the general belief that atraumatic insertions are beneficial for electrical stimulus transmissions and the preservation of residual hearing, and therefore, they should lead to optimized speech recognition. However, convincing studies are sparse, partly due to the limited number of in vivo determinations of the



cochlear implant position. Nevertheless, Holden et al. showed that monosyllabic word test scores were higher in patients with larger numbers of electrode contacts situated in the scala tympani.¹ More recently, O'Connell et al. studied a group of 137 patients at 12-16 months after implantation, and found that purely scala tympani insertions showed superior audiological results compared to translocated insertions²¹. Those results contrasted with our findings. This discrepancy might be explained by: (1) different method for evaluation of translocation, (2) different types of electrode arrays; they tested 9 different electrode arrays and we only tested the HiFocus Mid-Scala electrode array; or (3) different methods for measuring postoperative audiometric performance or (4) heterogeneity of the patient populations. They studied 14 HiFocus Mid-Scala electrode arrays and found 8 translocations (57%). Interestingly, they found that the mean angular electrode array insertion depths were shallower in the non-translocated group (385°) compared to the translocation group (438°). Additionally, they found that the electrode array angular insertion depth was an independent predictor of better speech perception; i.e., deep insertions showed better outcomes than shallow insertions. Again, that finding was not consistent with our findings, and the discrepancy might be explained by methodological differences between the two studies.

Conclusion and future remarks

This study showed that an extended insertion time could limit insertion trauma. These results can support future developments in atraumatic surgical procedures and electrode arrays. In the present study the surgeon received the feedback from imaging postoperatively. However, ideally, surgeons should receive real-time feedback during surgery to adjust the insertion of an electrode array if desired. Such feedback can be provided with intracochlear electrocochleography. However, preliminary results with this method are still ambiguous^{27,28}.

References

1. Holden LK, Finley CC, Firszt JB, et al. Factors affecting open-set word recognition in adults with cochlear implants. *Ear Hear*. 2013;34(3):342-360.
2. Kamakura T, Nadol JB. Correlation between word recognition score and intracochlear new bone and fibrous tissue after cochlear implantation in the human. *Hear Res*. 2016;339:132-141. doi:10.1016/j.heares.2016.06.015
3. Friedland DR, Runge-Samuelsen C. Soft cochlear implantation: rationale for the surgical approach. *Trends Amplif*. 2009;13(2):124-138. doi:10.1177/1084713809336422
4. Hoskison E, Mitchell S, Coulson C. Systematic review: Radiological and histological evidence of cochlear implant insertion trauma in adult patients. *Cochlear Implants Int*. 2017;18(4):192-197. doi:10.1080/14670100.2017.1330735
5. Hassepass F, Bulla S, Maier W, et al. The New Mid-Scala Electrode Array: A Radiologic and Histologic Study in Human Temporal Bones. *Otol Neurotol*. 2014;35(8):1454-1420.
6. Frisch CD, Carlson ML, Lane JI, Driscoll CLW. Evaluation of a new mid-scala cochlear implant electrode using microcomputed tomography. *Laryngoscope*. May 2015:1-6. <http://www.ncbi.nlm.nih.gov/pubmed/25946683>. Accessed May 28, 2015.
7. Dietz A, Gazibegovic D, Tervaniemi J, Vartiainen VM, Löppönen H. Insertion characteristics and placement of the Mid-Scala electrode array in human temporal bones using detailed cone beam computed tomography. *Eur Arch Oto-Rhino-Laryngology*. 2016;273(12):4135-4143. doi:10.1007/s00405-016-4099-x
8. Briggs RJS, Tykocinski M, Xu J, et al. Comparison of round window and cochleostomy approaches with a prototype hearing preservation electrode. *Audiol Neurotol*. 2006;11 Suppl 1(suppl 1):42-48. doi:10.1159/000095613
9. Roland PS, Wright CG, Isaacson B. Cochlear implant electrode insertion: the round window revisited. *Laryngoscope*. 2007;117(8):1397-1402. doi:10.1097/MLG.0b013e318064e891
10. Richard C, Fayad JN, Doherty J, Linthicum Jr. FH. Round window versus Cochleostomy Technique in Cochlear Implantation: Histological Findings. *Otology*. 2013;33(7):1181-1187. doi:10.1097/MAO.0b013e318263d56d.Round
11. Rajan GP, Kontorinis G, Kuthubutheen J. The effects of insertion speed on inner ear function during cochlear implantation: A comparison study. *Audiol Neurotol*. 2012;18(1):17-22. doi:10.1159/000342821
12. Todt I, Mittmann P, Ernst a. Intracochlear Fluid Pressure Changes Related to the Insertional Speed of a CI Electrode. *Biomed Res Int*. 2014;2014:507241. doi:10.1155/2014/507241
13. Verbist BM, Finley CC, Roland PS, Thomas J. Consensus panel on a cochlear coordinate system applicable in histological, physiological and radiological studies of the human cochlea. *Otol neurotol*. 2010;31:722-730.
14. van der Jagt AMA., Briare J.J, Boehringer S., Verbist B.M Frijns JHM. Improved cochlear implant position detection with spatially synchronized pre- and post-operative midmodiolar cross-section CT and MR images. *submitted*.



15. Bosman A, Smoorenburg G. Intelligibility of Dutch CVC syllables and sentences for listeners with normal hearing and with three types of hearing impairment. *Audiology*. 1995;34:260-284.
16. van der Jagt AMA, Kalkman RK, Briaire JJ, Verbist BM, Frijns JHM. Variations in cochlear duct shape revealed on clinical CT images with an automatic tracing method. *Sci Rep*. 2017;7(1):1-9. doi:10.1038/s41598-017-16126-6
17. Verbist BM, Ferrarini L, Briaire JJ, et al. Anatomic considerations of cochlear morphology and its implications for insertion trauma in cochlear implant surgery. *Otol Neurotol*. 2009;30(4):471-477. doi:10.1097/MAO.0b013e3181a32c0d
18. Hoskison E, Mitchell S, Coulson C, Hoskison E, Mitchell S, Coulson C. Systematic review : Radiological and histological evidence of cochlear implant insertion trauma in adult patients Systematic review : Radiological and histological evidence of cochlear implant insertion trauma in adult patients. 2017;0100(June). doi:10.1080/14670100.2017.1330735
19. Rebscher SJ. Considerations for design of future cochlear implant electrode arrays: Electrode array stiffness, size. *J Rehabil Res Dev*. 2008;45(5):731-748. doi:10.1682/JRRD.2007.08.0119
20. Wanna, George BGifford H, Noble JH, Carlson ML, et al. Impact of Electrode Design and Surgical Approach on Scalar Location and Cochlear Implant Outcomes. *Laryngoscope*. 2014;124(November):1-7. doi:10.1002/lary.24728
21. O'Connell BP, Kahir A, Hunter JB, et al. Electrode Location and Angular Insertion Depth Are Predictors of Audiologic Outcomes in Cochlear Implantation. In: *Otology and Neurotology*. ; 2016. doi:10.1097/MAO.0000000000001125
22. Zelener F, Majdani O, Römer A, et al. Relations between Scalar Shift and Insertion Depth in Human Cochlear Implantation. *Otol Neurotol*. 2019;98(17):14-16. doi:10.1097/MAO.0000000000002460
23. Adunka OF, Dillon MT, Adunka MC, King ER, Pillsbury HC, Buchman C a. Cochleostomy versus round window insertions: influence on functional outcomes in electric-acoustic stimulation of the auditory system. *Otol Neurotol*. 2014;35(4):613-618. doi:10.1097/MAO.0000000000000269
24. Kontorinis G, Lenarz T, Stöver T, Paasche G. Impact of the insertion speed of cochlear implant electrodes on the insertion forces. *Otol Neurotol*. 2011;32(4):565-570. doi:10.1097/MAO.0b013e318219f6ac
25. Roland JT. A model for cochlear implant electrode insertion and force evaluation: results with a new electrode design and insertion technique. *Laryngoscope*. 2005;115(8):1325-1339. doi:10.1097/01.mlg.0000167993.05007.35
26. Ishii T, Takayama M, Takahashi Y. Mechanical properties of human round window, basilar and Reissner's membranes. *Acta Otolaryngol Suppl*. 1995;519:78-82. doi:10.3109/00016489509121875
27. Riggs WJ, Dwyer RT, Holder JT, et al. Intracochlear Electrocochleography: Influence of Scalar Position of the Cochlear Implant Electrode on Postinsertion Results. *Otol Neurotol*. 2019;40(5):e503-e510. doi:10.1097/MAO.0000000000002202
28. Koka K, Riggs WJ, Dwyer R, et al. Intra-Cochlear Electrocochleography During Cochlear Implant Electrode Insertion Is Predictive of Final Scalar Location. *Otol Neurotol*. 2018;39(8):e654-e659. doi:10.1097/MAO.0000000000001906







Chapter 7

Discussion

Discussion and implications for future developments

The goal of this thesis was to gain insight into cochlear morphology and the intra-cochlear position of cochlear implant electrode arrays and, in this way, contribute to the overall aim of cochlear implantation: to improve speech perception in recipients of cochlear implants.

Imaging techniques and applications

Since the first cochlear implantations were performed in the 1960's, the quality of both CTs and MRIs has improved enormously. Currently, CTs and MRIs are considered valuable assets for detecting the most clinically relevant pathologies and anatomical deviations prior to implantation and for evaluating the intra-cochlear position of the electrode array after implantation. Nevertheless, improving image quality to reveal more anatomical details is an important motivation for the ongoing development of imaging techniques and applications.

In the field of cochlear implantation, growing interest exists in improving assessments of cochlear shape, cochlear patency, and inner ear neural structures of candidates for cochlear implants. In Chapter 2, we explored the potential of ultra-high 7T MRI for improving the visualization of inner ear structures. Currently, MRI scanners with a magnetic field strength of 1.5T or 3T are routinely used in clinical practice. These images provide a clear depiction of the fluid-filled cochlea and labyrinth within the dense otic capsule. Additionally, the inner ear canal, with its facial, cochlear, and vestibular nerves, can be evaluated thoroughly with either 1.5T or 3T MRI. Nevertheless, visualizations of the membranous structures in the cochlea and the finer structures of the neural pathways remain challenging in inner ear imaging. In our study (described in Chapter 2), the increased SNR provided by 7T MRI enhanced the representation of most of the small-sized, delicate anatomic structures, compared to 3T MRI. Specifically, Reissner's membrane, which delineates the scala media, could be distinguished in 7 out of 52 evaluations of 7T images, compared to none of the evaluations of 3T images. Nevertheless, this benefit was modest; thus, further effort is required to improve scan quality and resolution. Furthermore, the clinical relevance of depicting this anatomic region has not been determined, although it is a region of interest, because it houses the Organ of Corti. In addition to more careful evaluations of individual anatomic features, improving the visualization of anatomic structures can generate normative data on, for instance, cochlear size and shape. These data would be particularly interesting for cochlear implantations, because they could potentially influence the intra-cochlear positioning of the electrode array¹.

Several known difficulties related to an ultra-high magnetic field were encountered in our study. These difficulties presumably attribute to the fact that, currently, ultra-high 7T MRI is not widely clinically available. The inhomogeneity of the static (B_0) and radiofrequency (B_1) fields resulted in signal loss in the inner ear region. The high-permittivity dielectric pads

containing a suspension of barium titanate were indispensable for optimizing the signal in the inner ear region and made it suitable for clinical evaluation². This method is also applicable to other regions of interest, but each region requires a different pad configuration. For inner ear scanning, two geometric designs were developed, based on patient sex. The pads were placed in the head coil, in close proximity to the targeted inner ear.

Although dielectric pads were easy to apply and they optimized the homogeneity in the inner ear region, their clinical applicability is somewhat questionable, because they interfere with the workflow, and most researchers and clinicians lack experience with dielectric pads. Moreover, the usage of the pads prolonged the scan duration, although to a limited extent, and they are susceptible to misplacement or movements, which could lead to non-diagnostic images. Because different anatomic regions require different pad configurations, it takes time to design unique pads for each individual application. Consequently, the extra time, the lack of experience, and the lack of software and resources limit the use of this method by the entire MRI community. To improve accessibility, van Gemert et al. developed an easy-to-use software tool for designing application-specific pads.³ Hopefully, this software will stimulate clinical implementations of dielectric pads and create more awareness of this method in all fields of MRI, including inner ear imaging. Furthermore, the specific type of scanner operating in our institution and the dielectric pads require CE marking (to declare conformity with European health and safety requirements) and reimbursement. This support is essential for applying our results to a clinical cohort of patients.

Another issue related to ultra-high magnetic field MRI, is the limited tolerance in patients. Dizziness and nausea are the most commonly described side effects associated with 7T scanning^{4,5}. In our study, patients did not experience excessive discomfort. However, it is generally expected that, when the magnetic field strength is increased beyond a certain level, patient tolerance will be exceeded, and safety might be compromised. To date, studies have described in vivo human neuroimaging at a maximum of 9.4T for research purposes^{6,7}. Once the maximum magnet strength is reached, the quality of images acquired with ultra-high MRI field strength might be further improved with software and hardware developments.

A 3T vs. 7T MRI comparative study of the inner ear is ongoing, and it has included patients with Menière's disease. Although the latter patient population does not specifically represent the population of individuals that require cochlear implants, unravelling the characteristics related to the underlying causes of hearing loss is extremely relevant to the entire population of patients with hearing loss. In future studies, the increased SNR provided with 7T MRI might benefit investigations of other features of inner ear anatomy, such as the auditory nerve volume. This approach could lead to evaluations of potential correlations between anatomy and speech perception outcomes following cochlear implantations. This



information could facilitate patient counselling. Another structure that might benefit from 7T imaging is the cochlear nucleus, located at the dorso-lateral side of the brainstem. This structure is the target area for an auditory brainstem implant, but it is extremely difficult to characterize with routine MRI. Recently, a study showed that 7T diffusion tensor imaging could successfully visualize the location of the cochlear nucleus by evaluating the different orientations of fibres in the different neural pathways⁸. This technique might be used to facilitate the challenging surgical placement of an auditory brainstem implant.

CT image quality has improved over the years. Developments in several aspects of CT imaging, such as detector elements and image reconstruction algorithms, have led to an increased SNR, and images can be acquired within a limited time and radiation dose⁹. The radiation exposure time needs to be limited, due to the risks of cellular damage and cancer development¹⁰. Therefore, clinical scan protocols seek to apply the least radiation possible without compromising the image quality required for clinical evaluations. The image qualities achieved with current CT imaging techniques were essential for performing the automatic tracing technique we introduced in Chapter 3.

We found that the shape of the basal and second turns of the cochlea could be revealed with an automatic tracing method. This tracing method identified the cochlear boundaries based on differences in voxel density. The results provided insight into the irregularity of the diameter of the cochlear duct and the vertical trajectory of the scala tympani, up to and including the second turn. Beyond the second turn, the delicacy of the cochlear structures increased, and one voxel was too large to capture subtle differentiations. Consequently, the third turn could not be evaluated with this technique. Nevertheless, this tracing method can facilitate the study of individual cochleae, in high detail, before implantation. Thus, special attention can be given to features that might influence the trajectory of the electrode array and features that might increase the risk of electrode array translocation. Additionally, this method could be used to evaluate a large cohort of patients to establish a range of 'normal' cochlear dimensions.

In the future, if CT imaging accuracy can be increased with smaller voxels and better SNRs, our automatic tracing technique might be applicable to evaluations of the third turn. Although most existing electrode arrays are not designed to target the most apical areas of the cochlea, this targeting might become possible in the future. In the tracing method described here (Chapter 3), we determined 3 datapoints per cross-sectional mid-modiolus image: one on the innermost wall, one on the outermost wall, and one at the bottom of the scala tympani. In an ongoing study in our institution, Siebrecht et al. are further developing the automatic tracing algorithm. By determining the boundaries of the complete circumference of the cochlear duct, they could generate a 3D volume of the complete cochlear duct. This approach could provide valuable information about the vertical slope and tilting pattern of

the scala tympani in individuals, which is relevant for identifying areas at risk of electrode array translocation during insertion. Secondly, evaluation of a large number of patients gains insight in the variability of cochlear duct volumes. Additionally, an accurate representation of the osseous spiral lamina is subject of their ongoing research and could permit an accurate distinction between the scala tympani and the scala vestibuli. Combining these details with the (automatically) determined locations of individual electrode contacts could enable a postoperative evaluation of the intra-cochlear, and potentially translocated, position of the cochlear implant electrode array. Moreover, the algorithm we used can also be applied to MRI datasets. Indeed, the enhanced SNR of the 7T MRI could further improve the accuracy of the tracing technique.

Visualizing the implanted cochlea is challenging, due to the presence of metallic artefacts. Blooming artefacts deteriorate the surrounding anatomical details, which makes it difficult to determine the precise intra-cochlear position of the electrode array. The method we described in Chapter 5 was developed to overcome this problem. By placing the corresponding preoperative image adjacent to the image of the implant in situ, we could determine the intra-cochlear position of individual electrode contacts more accurately. An advantage of this method was that we could avoid using complex, and sometimes time-consuming, co-registration software. The good image quality provided with the latest generation of scanner was a fundamental factor in this method. Surprisingly, although our evaluation of the electrode array location had improved, compared to using only the postoperative scan, we found no difference between using a preoperative CT or a preoperative MRI scan. In fact, we expected that the MRI would provide an advantage, based on its high resolution. A potential explanation for the similarity in CT and MRI results might be that the image quality deteriorated after retrieving, processing, and storing the images on multiple computer systems and after applying multiple programs to create multiplanar reconstructions (MPRs) for 3D image processing. Additionally, part of the explanation could be that some of the observers were more familiar with CT images than with MRIs. Nevertheless, at this point, this method is highly eligible for clinical evaluation, due to its feasibility and its independence from any additional software. Future evolution of techniques involving image quality are likely to improve the abilities of both CT and MRI to visualize the anatomic structures depicted in mid-modiolus cross-sectional images.

Several other methods have been described for thoroughly evaluating the intra-cochlear position of cochlear implant electrode arrays. Among those methods, some have incorporated image segmentation techniques¹¹. This image processing technique uses computer algorithms to partition a digital image into multiple segments. For example, Huetink et al.¹² described an automatic segmentation method, based on a deep learning framework, developed with an extensive clinical dataset of ultra-high resolution CT images. Following segmentation, the obtained image volumes were used for comprehensive



measurements; however, they could also be used for co-registration or image fusion techniques. Image fusion techniques provide a means to combine details from two different scans. In the context of cochlear implantation, it is interesting to combine scans acquired before and after implantation. With this approach, it is possible to avoid the deterioration of intra-cochlear anatomic details, due to metallic artefacts caused by the electrode array. With co-registration techniques, it is possible to align scans from different modalities, like MRI and CT, where each scan shows different anatomic details. Previous studies have described various applications of co-registration in the field of cochlear implantation; for example, co-registration was used to align a clinical postoperative scan with a preoperative CT scan of the same patient; with the contralateral ear of the postoperative scan; or with a model, based on micro-CT data¹³⁻¹⁵. Because cochlear morphology is highly variable among patients (see Chapter 3), one must be aware that, when a general model is used, these variations may cause inaccurate alignments.

The development of functional imaging techniques is beyond of the scope of this thesis, but these techniques are potentially relevant for future implications. Functional imaging techniques rely on activity, rather than anatomic detail. Increasingly, the potential of these techniques for visualizing the auditory pathway has been explored, and they may be applicable to cochlear implant patients and candidates. The regularly used imaging modalities do not portray the fine neural structures of the auditory nerve, the hair cells of the Organ of Corti, the spiral ganglion neurons, or their connecting neural pathways, from the inner ear to the auditory cortex. Information about the condition of these neural structures, indicated by their functioning, might be correlated to the underlying cause of hearing loss, and the probability or prognosis of partially restoring hearing.

Intra-cochlear position of the cochlear implant electrode array

Improvements in imaging techniques and applications have made it possible to assess the intra-cochlear position of a cochlear implant electrode array more carefully. In fact, the intra-cochlear positions of several cochlear implant electrode array designs can be evaluated to determine whether they achieve the position they were specifically designed to target. Frequently, studies assess three features of the intra-cochlear position of cochlear implant electrode arrays that are thought to influence speech perception outcomes: the angular insertion depth, the proximity of the electrode to the modiolus, and more recently, the scalar location.

In Chapter 4, we compared the intra-cochlear positions of the straight HiFocus 1J electrode array and the pre-curved HiFocus MS electrode array. Compared to the HiFocus MS electrode array, on average, the angular insertion depth of the HiFocus 1J electrode array was 50 degrees deeper, with a mean depth of 478°. However, its angular insertion depth was less consistent, with a 37 degrees larger standard deviation, than those observed with

the HiFocus MS array. However, in two groups of patients that had been matched, based on the preoperative speech perception scores, the duration of deafness, and the age at implantation, we found similar speech perception outcomes; moreover, the outcomes were not influenced by the angular insertion depth or frequency mismatch.

The angular insertion depth depends on the length of the electrode array, surgical insertion depth, the intrascalar position of the electrode array and the size of the cochlea. Hypothetically, an electrode array that covers a larger part of the cochlea should result in better speech recognition. However, convincing support for this hypothesis is lacking¹⁶, due to conflicting outcomes from studies that evaluated different electrode designs and their related angular insertion depths¹⁶. Contributing to this ambiguity, it is debated which part of the neural pathway is stimulated, or should ideally be stimulated, by the cochlear implant electrode contacts. It remains unclear what role is played by the peripheral processes between the Organ of Corti and the bodies of the spiral ganglion cells in Rosenthal's canal. If they contribute substantially to hearing, then stimulating the more apical regions of the cochlea might improve speech perception outcomes. However, the curvy alignment of the central axons in the more apical regions are likely to result in broader, overlapping excitation regions; thus, stimulating the lower frequencies might provide limited benefit¹⁷. Furthermore, the potential advantage of deeply inserted cochlear implant electrode arrays might be offset by the increased risk of insertion trauma and the subsequent formation of fibrosis, or in cases of extensive trauma, damage to neural structures. Additionally, the cochlear blood flow toward the apical neural structures might be pinched, when the diameter of the cochlear implant electrode array is not matched to the diameter of the cochlear duct.

Another issue of debate is the optimal proximity of the electrode contacts to the modiolus. Cochlear implant electrode arrays that hug the modiolus can achieve a more focussed stimulation, and they have a longer battery life, due to less power consumption. However, this type of cochlear implant electrode array also increases the risk of insertion trauma, due to its increased stiffness. In addition, a potential mismatch between the curve of the array and the individual coiling pattern of the cochlea can cause the electrode array to be positioned too close or too far away from the inner wall, which can result in less effective electric current focussing. To date, there is no convincing evidence that either modiolus-hugging or lateral wall proximity results in superior speech perception outcomes. Consequently, this issue remains a subject of ongoing research.

Over time, it became clear that in a certain number of cases the CI electrode array inadvertently translocates from the targeted scala tympani into the scala vestibuli during insertion. Indeed, some studies have reported a 100% incidence of translocation¹⁸. Due to the expansion of patient inclusion criteria, interest has focussed on preventing insertion



trauma to retain residual hearing. It is generally believed that retaining the intra-cochlear architecture as much as possible will provide the most favourable situation for electrically stimulating the neural components. Nevertheless, previous studies that focused on the effects of electrode array translocation on speech perception outcomes have reported ambiguous findings^{19–23}. For example, in the study we described in Chapter 6, we did not find a difference in speech perception outcomes between patients with translocated electrode arrays and patients with electrode arrays located completely in the scala tympani, despite corrections for factors known to influence speech perception outcomes. Zelener et al. found a perfect intelligibility score of 100% in a patient with a translocated HiFocus MS electrode array²², which further illustrated the uncertain relationship between traumatic insertions and speech perception outcomes. Perhaps the electrical stimulus bypasses the damaged parts of the cochlea and predominantly stimulates the central axons of the auditory nerve located within the modiolus. Nevertheless, despite the lack of unambiguous proof that insertion trauma is strongly correlated with hearing outcomes, an atraumatic insertion remains the goal, to preserve residual hearing, allow EAS, and prevent fibrosis and ossification. Preventing fibrosis and ossification is important, in case a future re-implantation is necessary, which is particularly common among children with cochlear implants. Therefore, identifying risk factors related to insertion trauma remains an important goal.

The most frequently studied potential risk factors for insertion trauma are the surgical approach and the implant design. Previous studies showed that pre-curved electrode arrays and insertions through a cochleostomy were the most harmful insertion methods²⁴. In Chapter 6, we investigated the effects of the surgical approach and the time of insertion on the risk of translocation. An insertion time of 25 s or longer was associated with less frequent translocations of the cochlear implant electrode array. A determination of whether the electrode array has translocated constitutes important feedback for the surgeon. With this information, the surgeon can study the relationship between translocations and the characteristics of the surgical procedure, such as the directional vector of insertion, the experience of resistance during insertion, or problems with twisting or buckling of the electrode array. A prolonged insertion time is applicable to all implant designs, and it is potentially most relevant in cochleae with a steep increase in the vertical trajectory, which can be measured with the method we introduced in Chapter 3. However, implant designs are highly variable in the relevant mechanical properties. Therefore, the optimal surgical approach and insertion time must be evaluated for each electrode design. In addition, the surgical approach also depends on round window accessibility, because the angulation of the round window and the route of the facial nerve are potential limitations²⁵.

Future research should investigate other ways, beyond the topics of this thesis, to gain insight into the course of the electrode array during insertion, by obtaining direct, real-time feedback during surgery. It has been proposed that this feedback could be achieved

with electrocochleography (ECoChG). With ECoChG, cochlear function can be determined by measuring reflective hair cell activation, a process called cochlear microphonics. Hypothetically, when insertion trauma occurs, the hair cells are damaged, and cochlear microphonics can no longer be detected. Adunka et al. studied cochlear responses after different, consecutive surgical steps²⁶. Cochlear microphonics remained intact during the first surgical steps, which included drilling a cochleostomy and opening the round window membrane. After the electrode array was inserted, the cochlear microphonic amplitudes dropped, but they remained detectable, which implied persistent cochlear function. However, in many cases, no residual hearing could be detected after implantation. That finding suggested that drilling and a drop in perilymph pressure after opening the scala tympani did not stress the hair cells sufficiently to cause damage, but introducing the electrode array into the cochlear canal probably caused damage, either due to the steep increase in fluid pressure²⁷ or due to direct mechanical stress. Another interpretation of these results might be that the damage did not occur during surgery, but developed later, due to the molecular and cellular responses to the foreign object²⁸. This mechanism might also explain the change in residual hearing over time; indeed, in some cases, hearing is partially restored a long time after surgery. This 'dynamic' factor makes it difficult to correlate ECoChG measurements with cochlear implant outcomes. Other investigators who have studied ECoChG patterns during insertions to predict the scalar also showed largely variable changes of the ECoChG patterns during insertion among different patients and with different cochlear implant designs^{29,30}. Consequently, ECoChG has not been accepted as a completely reliable method for scalar localization.

Other methods proposed for real-time feedback during surgery include the detection of evoked compound action potentials and impedances^{31,32}. Furthermore, it has been suggested that intraoperative imaging, with conventional X-ray, CT, or fluoroscopy, could provide feedback during the insertion of the cochlear implant electrode array³³. However, that method has major drawbacks, including radiation exposure, prolonged surgical and anaesthesia times, and the associated increase in cost. Therefore, many institutions have reserved intraoperative imaging for cases with difficult anatomy that is expected to impede electrode placement.

Methods are also being explored for (partially) restoring or limiting intra-cochlear damage, for situations when insertion trauma is unavoidable. Corticosteroids, applied either locally or intravenously, have been tested prior to, during, or following implantation, to reduce stress reactions and the activation of ototoxic cytokines. Some studies have reported that residual hearing was improved with steroid treatments, and a recent meta-analysis indicated that intraoperative topical and postoperative oral steroids were beneficial³⁴. Hypothermia is another method that was proposed for reducing damage during or after insertion^{35,36}.



However, the limited evidence from available studies did not convincingly support this proposal.

Towards patient-tailored implantation

The key to improving speech perception outcomes with cochlear implants might be patient-tailored cochlear implantations. Currently, several prototypes of cochlear implant designs are available on the market, but the choice of design generally depends less on patient characteristics, than on the experience of the surgeon and the availability of a design in a given cochlear implant centre. An exception is the dual electrode array design, which can be used in a partially ossified cochlea, which may occur after meningitis. Moreover, some studies have described deliberate partial insertions. This approach specifically focuses on impairments in the high frequencies; partial insertions aim to stimulate only the neural components located at the basal part of the cochlea, without affecting residual hearing in the lower frequency areas; thus, making EAS feasible. Then, when lower frequency hearing deteriorates, for example, due to aging, the same electrode array can be advanced deeper into the cochlea³⁷.

The large variability in cochlear dimensions described in Chapter 4, has emphasized the need to step away from the 'one size fits all' concept of cochlear implant electrode arrays. By studying the morphology of the cochlea in high detail, prior to implantation, areas at risk of translocation can be predicted, and the surgeon can adjust the surgical technique accordingly. For instance, a specific surgical approach might be indicated, or the surgeon might simply slow down the insertion, when approaching high-risk areas. Moreover, the type or length of the electrode array can be chosen, based on morphological or even genetic characteristics. Of course, this requires a different, and presumably more time-consuming approach in the pre-operative work-up. However, appropriate work-ups may eventually lead to improved speech understanding in recipients of cochlear implants.

References

1. van der Marel KS, Briaire JJ, Wolterbeek R, Snel-Bongers J, Verbist BM, Frijns JHM. Diversity in Cochlear Morphology and Its Influence on Cochlear Implant Electrode Position. *Ear Hear*. November 2013;1-12. doi:10.1097/01.aud.0000436256.06395.63
2. Teeuwisse WM, Brink WM, Webb AG. Quantitative assessment of the effects of high-permittivity pads in 7 Tesla MRI of the brain. *Magn Reson Med*. 2012;67(5):1285-1293. doi:10.1002/mrm.23108
3. van Gemert J, Brink W, Webb A, Remis R. High-permittivity pad design tool for 7T neuroimaging and 3T body imaging. *Magn Reson Med*. 2019;81(5):3370-3378. doi:10.1002/mrm.27629
4. Versluis MJ, Teeuwisse WM, Kan HE, van Buchem M a, Webb AG, van Osch MJ. Subject tolerance of 7 T MRI examinations. *J Magn Reson Imaging*. 2013;38:722-725. doi:10.1002/jmri.23904
5. Heilmaier C, Theysohn JM, Maderwald S, Kraff O, Ladd ME, Ladd SC. A large-scale study on subjective perception of discomfort during 7 and 1.5 T MRI examinations. *Bioelectromagnetics*. 2011;32:610-619. doi:10.1002/bem.20680
6. Thulborn KR, Ma C, Sun C, et al. SERIAL transmit – parallel receive (STxPRx) MR imaging produces acceptable proton image uniformity without compromising field of view or SAR guidelines for human neuroimaging at 9.4 Tesla. *J Magn Reson*. 2018;293:145-153. doi:10.1016/j.jmr.2018.05.009
7. Atkinson IC, Claiborne TC, Thulborn KR. Feasibility of 39-potassium MR imaging of a human brain at 9.4 Tesla. *Magn Reson Med*. 2014;71(5):1819-1825. doi:10.1002/mrm.24821
8. Epprecht L, Qureshi A, Kozin ED, et al. Human Cochlear Nucleus on 7 Tesla Diffusion Tensor Imaging: Insights Into Micro-anatomy and Function for Auditory Brainstem Implant Surgery. *Otol Neurotol*. 2020;41(4):e484-e493. doi:10.1097/MAO.0000000000002565
9. Willemink MJ, Noël PB. The evolution of image reconstruction for CT—from filtered back projection to artificial intelligence. *Eur Radiol*. 2019;29(5):2185-2195. doi:10.1007/s00330-018-5810-7
10. Brenner DJ, Doll R, Goodhead DT, et al. Cancer risks attributable to low doses of ionizing radiation: assessing what we really know. *Proc Natl Acad Sci U S A*. 2003;100(24):13761-13766. doi:10.1073/pnas.2235592100
11. Kaur D, Kaur Y. Various Image Segmentation Techniques: A Review. *Int J Comput Sci Mob Comput*. 2014;3(5):809-814, date accessed: 18/05/2016.
12. Heutink F, Koch V, Verbist B, et al. Multi-Scale deep learning framework for cochlea localization, segmentation and analysis on clinical ultra-high-resolution CT images. *Comput Methods Programs Biomed*. 2020;191:105387. doi:10.1016/j.cmpb.2020.105387
13. Finley CC, Skinner MW. Role of electrode placement as a contributor to variability in cochlear implant outcomes. *Otol Neurotol*. 2008;29(7):920-928.
14. Skinner MW, Holden T a., Whiting BR, et al. In Vivo Estimates of the Position of Advanced Bionics Electrode Arrays in the Human Cochlea. *Ann Otol Rhinol Laryngol*. 2007;116(4):2-24. doi:10.1177/000348940711600401



15. Schuman T a, Noble JH, Wright CG, Wanna GB, Dawant B, Labadie RF. Anatomic verification of a novel method for precise intrascalar localization of cochlear implant electrodes in adult temporal bones using clinically available computed tomography. *Laryngoscope*. 2010;120(11):2277-2283. doi:10.1002/lary.21104
16. Heutink F, De Rijk SR, Verbist BM, Huinck WJ, Mylanus EAM. Angular Electrode Insertion Depth and Speech Perception in Adults with a Cochlear Implant: A Systematic Review. *Otol Neurotol*. 2019;40(7):900-910. doi:10.1097/MAO.0000000000002298
17. Kalkman RK, Briaire JJ, Frijns JHM. Current focussing in cochlear implants : An analysis of neural recruitment in a computational model. *Hear Res*. 2015;322:89-98. doi:10.1016/j.heares.2014.12.004
18. Hoskison E, Mitchell S, Coulson C. Systematic review: Radiological and histological evidence of cochlear implant insertion trauma in adult patients. *Cochlear Implants Int*. 2017;18(4):192-197. doi:10.1080/14670100.2017.1330735
19. Holden LK, Finley CC, Firszt JB, et al. Factors affecting open-set word recognition in adults with cochlear implants. *Ear Hear*. 2013;34(3):342-360.
20. Chakravorti S, Noble JH, Gifford RH, et al. Further Evidence of the Relationship Between Cochlear Implant Electrode Positioning and Hearing Outcomes. *Otol Neurotol*. 2019;40(5):617-624. doi:10.1097/MAO.0000000000002204
21. O'Connell BP, Cakir A, Hunter JB, et al. Electrode Location and Angular Insertion Depth Are Predictors of Audiologic Outcomes in Cochlear Implantation. *Otol Neurotol*. 2016;37(8):1016-1023. doi:10.1097/MAO.0000000000001125
22. Zelener F, Majdani O, Römer A, et al. Relations between Scalar Shift and Insertion Depth in Human Cochlear Implantation. *Otol Neurotol*. 2019;98(17):14-16. doi:10.1097/MAO.0000000000002460
23. Trudel M, Côté M, Philippon D, Simonyan D, Villemure-Poliquin N, Bussièrès R. Comparative Impacts of Scala Vestibuli Versus Scala Tympani Cochlear Implantation on Auditory Performances and Programming Parameters in Partially Ossified Cochleae. *Otol Neurotol*. 2018;39(6):700-706. doi:10.1097/MAO.0000000000001816
24. Hoskison E, Mitchell S, Coulson C, Hoskison E, Mitchell S, Coulson C. Systematic review : Radiological and histological evidence of cochlear implant insertion trauma in adult patients Systematic review : Radiological and histological evidence of cochlear implant insertion trauma in adult patients. 2017;0100(June). doi:10.1080/14670100.2017.1330735
25. Jain S, Deshmukh PT, Lakhotia P, Kalambe S, Chandravanshi D, Khatri M. Anatomical study of the facial recess with implications in round window visibility for cochlear implantation: Personal observations and review of the literature. *Int Arch Otorhinolaryngol*. 2019;23(3):E281-E291. doi:10.1055/s-0038-1676100
26. Giardina CK, Brown KD, Adunka OF, et al. Intracochlear electrocochleography: Response patterns during cochlear implantation and hearing preservation. *Ear Hear*. 2019;40(4):833-848. doi:10.1097/AUD.0000000000000659

27. Mittmann M, Ernst A, Mittmann P, Todt I. Insertional depth-dependent intracochlear pressure changes in a model of cochlear implantation. *Acta Otolaryngol.* 2017;137(2):113-118. doi:10.1080/00016489.2016.1219918
28. Jia H, Wang J, Francois F, Uziel A, Puel JL, Venail F. Molecular and cellular mechanisms of loss of residual hearing after cochlear implantation. *Ann Otol Rhinol Laryngol.* 2013;122(1):33-39. doi:10.1177/000348941312200107
29. Giardina CK, Brown KD, Adunka OF, et al. Intracochlear electrocochleography: Response patterns during cochlear implantation and hearing preservation. *Ear Hear.* 2019;40(4). doi:10.1097/AUD.0000000000000659
30. Koka K, Riggs WJ, Dwyer R, et al. Intra-Cochlear Electrocochleography During Cochlear Implant Electrode Insertion Is Predictive of Final Scalar Location. *Otol Neurotol.* 2018;39(8):e654-e659. doi:10.1097/MAO.0000000000001906
31. Adunka O, Roush P, Grose J, Macpherson C, Buchman CA. Monitoring of cochlear function during cochlear implantation. *Laryngoscope.* 2006;116(6):1017-1020. doi:10.1097/01.mlg.0000217224.94804.bb
32. Dong, Yu; Briaire, JJ; Siebrecht, M; Stronks, HC, Frijns J. Detection of Translocation of Cochlear Implant Electrode Arrays by Intracochlear Impedance Measurements. *Ear Hear.*
33. Appachi S, Schwartz S, Ishman S, Anne S. Utility of intraoperative imaging in cochlear implantation: A systematic review. *Laryngoscope.* 2018;128(8):1914-1921. doi:10.1002/lary.26973
34. Snels C, Int'Hout J, Mylanus E, Huinck W, Dhooge I. Hearing Preservation in Cochlear Implant Surgery: A Meta-Analysis. *Otol Neurotol.* 2019;40(2):145-153. doi:10.1097/MAO.0000000000002083
35. Tamames I, King C, Bas E, Dietrich WD, Telischi F, Rajguru SM. A cool approach to reducing electrode-induced trauma: Localized therapeutic hypothermia conserves residual hearing in cochlear implantation. *Hear Res.* 2016;339:32-39. doi:10.1016/j.heares.2016.05.015
36. Tamames I, King C, Huang CY, Telischi FF, Hoffer ME, Rajguru SM. Theoretical evaluation and experimental validation of localized therapeutic hypothermia application to preserve residual hearing after cochlear implantation. *Ear Hear.* 2018;39(4):712-719. doi:10.1097/AUD.0000000000000529
37. Lenarz T, Timm ME, Salcher R, Büchner A. Individual Hearing Preservation Cochlear Implantation Using the Concept of Partial Insertion. *Otol Neurotol.* 2019;40(3):E326-E335. doi:10.1097/MAO.0000000000002127







Chapter 8

Nederlandse Samenvatting

Cochleaire implantatie is een wereldwijd toegepaste behandeling voor patiënten met invaliderend perceptief gehoorverlies waarbij het dragen van conventionele hoortoestellen tot onvoldoende herstel van het gehoor leidt. Bij cochleaire implantatie worden de vezels van de gehoorzenuw elektrisch gestimuleerd door een in het slakkenhuis geïmplanteerde elektrode array. Sinds de introductie van het eerste cochleair implantaat in de jaren '60 is de capaciteit van een cochleair implantaat enorm verbeterd door ontwikkelingen van elektrode designs, soft- en hardware technieken. Het merendeel van de CI patiënten bereikt een spraakverstaanscore van 80% of meer na implantatie. Beeldvorming speelt een belangrijke rol bij verschillende facetten van cochleaire implantatie, zowel klinisch als wetenschappelijk. Voorafgaand aan implantatie geeft het inzicht in de anatomie en pathologie die potentieel ten grondslag ligt aan het gehoorverlies, of anatomische variaties waar rekening mee gehouden moet worden tijdens de operatie. Na implantatie geeft het de intra-cochleaire positie weer van de elektrode arrays en maakt het onder andere mogelijk om te onderzoeken of de intra-cochleaire positie van invloed is op de spraakverstaan resultaten. Met de ontwikkelingen van verschillende beeldvormende technieken en applicaties is het mogelijk geworden om de anatomie van het binnenoer steeds gedetailleerder af te beelden. Hierdoor kan de variatie van de cochleaire morfologie en de potentiële relatie met chirurgische en spraakverstaanuitkomsten na cochleaire implantatie op grote schaal worden onderzocht. Dit genereert belangrijke informatie voor onder andere de ontwikkelaars van verschillende soorten elektroden arrays. Ook de individuele variatie is van belang en kan in sommige gevallen de operateur ondersteunen in de keus voor een specifiek elektrode design of chirurgische benadering. Dit proefschrift beschrijft de klinische implicaties van geavanceerde beeldvormingstechnieken en – toepassingen voor de evaluatie van de cochleaire morfologie en geïmplanteerde binnenoren.

De inleiding van dit proefschrift, beschreven in Hoofdstuk 1, geeft een kort overzicht van de achtergrond van gehoorverlies en cochleaire implantatie. De klinische toepassing van beeldvormende technieken wordt toegelicht, alsmede de uitdagingen hiervan. Verder wordt er in gegaan op de evaluatie van de intra-cochleaire positie van elektrode arrays, in het bijzonder de detectie en implicatie van gedislokeerde elektrode arrays.

In hoofdstuk 2 wordt de eerste klinische toepassing van het scannen van binnenoren van CI kandidaten met de hoge resolutie 7 Tesla MRI scanner beschreven. Scannen met een hoog magnetisch veld heeft de potentie om de signal-to-noise ratio te verhogen waardoor anatomische structuren in meer detail kunnen worden weergegeven. Echter brengt dit hoge magnetische veld ook uitdagingen met zich mee. Zo ontstaat er een inhomogeen signaal ter plaatse van het os temporale door de vorm van de schedel. Het gebruik van dielectrische pads met bariumtitanaat, beschreven door Wyger et al. corrigeert dit signaal waardoor de kwaliteit van de MRI beelden geoptimaliseerd wordt. Op deze manier kon een groot aantal

anatomische structuren van het binnenoor duidelijker worden afgebeeld ten opzicht van op MR beelden vervaardigd met 3 Tesla scanners.

In hoofdstuk 3 introduceren we een automatische tracing methode gebaseerd op het verschil in voxel intensiteit van CT scans om de cochleaire binnen- en buitenwand en de bodem van de scala tympani te bepalen van de eerste en tweede cochleaire winding. Een grote groep van 479 binnenoren werd geëvalueerd en toonde aan dat zowel de diameter van de cochlea als het verticale beloop van de scala tympani een onregelmatig patroon heeft. Specifieke dalingen en stijgingen, of veranderingen hiervan, in het verticale beloop, vormen potentieel een verhoogd risico op insertietrauma. Deze inzichten kunnen worden toegepast voor individuele preoperatieve planning en in grote cohorten voor de evaluatie en ontwikkeling van nieuwe elektrode designs en implantatie technieken.

In hoofdstuk 4 wordt de intra-cochleaire positie en de spraakverstaanuitkomsten van 2 verschillende elektrode arrays met elkaar vergeleken. De HiFocus Mid-Scala elektrode array is een voorgevormde array met een beoogde ' zwevende ' positie tussen de modiolus en de laterale wand van de scala tympani. De oudere HiFocus 1J elektrode array is een rechte array die tegen de laterale wand van de scala tympani gelokaliseerd is. In dit hoofdstuk wordt het verschil in afstand tussen de elektrode contacten en de modiolus tussen de 2 typen elektrode arrays geïllustreerd, en een ondiepere insertiediepte van de HiFocus MS elektrode array beschreven. Echter werd er geen verschil in spraakverstaanuitkomst gemeten tussen de 2 groepen tot 6 maanden na implantatie ondanks het verschil in intra-cochleaire positie.

In hoofdstuk 5 wordt een methode geïntroduceerd om de intra-cochleaire positie van individuele elektrode contacten te beoordelen op gesynchroniseerde doorsnedes door de modiolus van de cochlea. Door gebruik te maken van identieke doorsnedes van pre- en postoperatieve CT en MR beelden, wordt het verstoorde signaal op de postoperatieve CT beelden, veroorzaakt door het metaal in de elektrode contacten, omzeild. Door de weergegeven begrenzingen van de scala tympani, media en vestibuli op de pre-implantatie beelden, kan een valide inschatting gemaakt worden van de intra-cochleaire positie van de elektroden door deze begrenzingen in te schatten op de postoperatieve beelden.

In hoofdstuk 6 wordt de incidentie van traumatische inserties, en het effect van insertiesnelheid hier op, in een groep van 226 patiënten geïmplantieerd met een HiFocus MS elektrode array, beschreven. Naar aanleiding van ex-vivo studies waarin de exponentiële intra-cochleaire druk toename werd beschreven bij snelle inserties, met mogelijke schade aan het neuro-epitheel, werd besloten de insertiesnelheid te vertragen. Door het vertragen van de insertie tot minimaal 25 seconden daalde het percentage traumatische inserties van 27 naar 10% in deze populatie. Met een model analyse, waarin gecorrigeerd werd voor andere factoren die mogelijk van invloed zijn op het al dan niet dislokeren van een elektrode



array, zoals de grootte van de cochlea en de chirurgische benadering, werd de kans op een traumatische insertie 2.5 keer groter met een snelle insertie. Echter, bleek dit niet te resulteren in slechtere spraakverstaan scores.

De bevindingen van hoofdstuk 2 t/m 6 worden bediscussieerd in Hoofdstuk 7. Tevens worden potentiële toepassingen van beeldvormende technieken en applicaties voor CI patiënten in de toekomst aangehaald. Ook wordt er aandacht besteed aan de variatie van cochleaire morfologie, intra-cochleaire positie van elektrode arrays en het aandeel hiervan aan de variatie in spraakverstaanuitkomsten. Het evalueren van deze potentiële correlaties draagt bij aan het begrijpen en uiteindelijk verbeteren van de potentie van een cochleair implantaat.







Appendices

Abbreviations

List of Publications

Acknowledgements

Curriculum Vitae

Abbreviations

3T	3 Tesla
7T	7 Tesla
AB	Advanced Bionics
BM	basilar membrane
CA	cochlear aqueduct
CDL	cochlear duct length
CI	cochlear implant or cochlear implantation
CPA	cerebellopontine angle
CSF	cerebrospinal fluid
CT	computed tomography
CVC	consonant-vowel-consonant
dB	decibel
EAS	electro-acoustic stimulation
ECochg	electrocochleography
FDA	food and drug administration
FOV	field of view
IAC	internal auditory canal
ICC	intra-class of inter-class correlation coefficient
LMM	linear mixed model
MATLAB	matrix laboratory
MPRs	multiplanar reconstructions
MRI	magnetic resonance imaging
MS	mid-scalar
MSCT	multi-slice computed tomography
NS	not significant
OSL	osseous spiral lamina
RW	round window
SD	standard deviation
SM	scala media
SNHL	sensorineural hearing loss
SNR	signal-to-noise ratio
ST	scala tympani
SV	scala vestibuli
TBs	temporal bones
VA	vestibular aqueduct
WHO	world health organization

List of publications

van der Jagt, M.A., Muirhead, J., Seymour, J.F., Bradstock, K.F., Paul, E., Wei, A. (2012). Risk factors for early death after high-dose cytosine arabinoside (HiDac)-based chemotherapy for adult AML. *Leukemia: Official Journal of the Leukemia Society of America, Leukemia Research Fund, U.K*, 26(2), 362-365.

Brink, W.M., **van der Jagt, M.A.**, Versluis, M.J., Verbist, B.M., Webb, A.G. (2014). High Permittivity Dielectric Pads Improve High Spatial Resolution Magnetic Resonance Imaging of the Inner Ear at 7 T. *Investigative Radiology*, 49, 471-477.

van der Jagt, M.A., Brink, W.M., Versluis, J.M., Steens, S.C.A., Briaire, J.J., Webb, A.G., Frijns, J.H.M. (2014). Visualization of Human Inner Ear Anatomy with High-Resolution MR Imaging at 7T: Initial Clinical Assessment. *American Journal of Neuroradiology*, 437-445.

van der Jagt, M.A., Webb, A.G., Frijns, J.H.M., Verbist, B.M. (2014). Reply letter Visualization of Human Inner Ear Anatomy with High-Resolution MR Imaging at 7T. *American Journal of Neuroradiology*, 35 (12).

van der Jagt, M.A., Briaire, J.J., Verbist, B.M., Frijns, J.H.M. (2016). Comparison of the HiFocus Mid-Scala and HiFocus 1J Electrode Array: Angular Insertion Depths and Speech Perception Outcomes. *Audiology & Neurotology*, 316-325.

van der Jagt, M.A., Kalkman, R.K., Briaire, J.J., Verbist, B.M., Frijns, J.H.M. (2017). Variations in cochlear duct shape revealed on clinical CT images with an automatic tracing method. *Nature Scientific Reports*, 7(1) 1-9.

van Beers, M.A., **van der Jagt, M.A.**, Meinesz, S.F. (2018). Een patiënt met amyloïdose en plots perceptief gehoorverlies; gerelateerd of toeval? *Nederlands Tijdschrift voor Keel-, Neus- en Oorheekunde*, 4, 130-133.

van der Jagt, M.A., Boehringer, S., Briaire, J.J., Verbist, B.M., Frijns, J.H.M. Improved cochlear implant position detection with spatially synchronized pre- and post-operative midmodiolar cross-section CT and MR images. *Under review*.

van der Jagt, M.A., Boehringer, S., Briaire, J.J., Verbist, B.M., Frijns, J.H.M. Prolonged insertion time reduces translocation rate of the HiFocus Mid-Scala electrode array in cochlear implantation. Accepted for publication in *Otology & Neurotology*.

van der Jagt, M.A., Verbist, B.M., Rotteveel, L.J.C., Frijns, J.H.M., Hensen, E.H. Cochlear implantation after intralabyrinthine haemorrhage. *Under review.*

Dankwoord

“It always seems impossible until it is done.”

Nelson Mandela, 2001

Voor het tot stand komen van dit proefschrift hebben velen een bijdrage geleverd. Zonder jullie had ik dit niet gekund en daar ben ik jullie voor altijd dankbaar voor. Een bijzonder woord van dank gaat uit naar:

Prof. dr. Ir. J.H.M. Frijns, beste Johan, bedankt voor de kans die je me gegeven hebt en het geduld wat je met me hebt gehad. Met jouw schat aan wetenschappelijke inzichten en ervaring werd ieder manuscript weer naar een hoger level getild.

Dr. ir. J.J. Briaire, beste Jeroen, bedankt voor het sparren, het laagdrempelige overleg en de memorabele momenten tijdens congressen.

Dr. B.M. Verbist, beste Berit, heel veel dank voor je begeleiding, je kritische blik en soms ‘vertalende’ rol. Jouw toewijding en kunde is inspirerend en maakt je onmisbaar voor ons vakgebied.

Beste Prof. Böhringer, heel veel dank voor de ondersteuning van de statische vraagstukken. Beste Randy, bedank voor je onuitputtelijke hulp bij het gebruik van Matlab, niets was jou te veel. Beste Michael en Danny, bedankt voor de samenwerking en de voortzetting van de evaluatie van insertietrauma. Beste Prof. Webb, Wieger en Maarten, bedankt voor de fijne samenwerking op het 7T Tesla binnenoor project. Beste Dr. Steens, bedankt voor de uren werk die je hebt verricht om de binnenoor structuren te scoren op de 3T en 7T beelden. Lieve collega onderzoekers, bedankt voor de vele inhoudelijke en minder inhoudelijke discussies in J2-55. Wat een mooie tijd was dat.

Beste stafartsen en collega’s van de afdeling KNO-heelkunde van het LUMC, HMC en Alrijne. Bedankt voor alles wat jullie me geleerd hebben en de fijne samenwerking.

Collega AIOS, wat een geluk om zo’n fijne groep collega’s om me heen te hebben. Bedankt voor alle gezelligheid en de support.

Marjolein, Kim, Inge, Esther, Laura, Sara, Katja, Stephanie, Faye, Jessie, Gijs en Jeroen en (schoon)familie. Bedankt voor alle avonturen en momenten van ontspanning samen, daar is nu gelukkig weer meer tijd voor.

Anouk en Kim, lieve paranimfen, vanaf de studie geneeskunde al dikke vriendinnetjes. Heel veel dank dat jullie mij op deze bijzondere dag willen bij staan.

IJsbrand, broer en maatje, onze band is speciaal en betekent heel veel voor mij. Dit proefschrift is ook een beetje voor jou.

Lieve pa en ma, bedankt voor de basis die jullie me hebben meegegeven en jullie onvoorwaardelijke liefde en steun voor alles wat ik doe. Zonder jullie was dit niet gelukt.

Lieve Lucas, mijn tegenpool en maatje, jouw niet medische kijk op medische zaken is soms heel verfrissend. Bedankt voor je liefde, humor en het vermaken van de kinderen als ik weer eens naar het LUMC afreisde.

Lieve Karel en Anouk, jullie toveren een lach op mijn gezicht (en wallen onder mijn ogen), wat heb ik zin in alles wat nog komen gaat met jullie.

Curriculum Vitae

Maria Anna (Annerie) van der Jagt was born on November 23th, in Leiden, The Netherlands. In 2004 she completed the secondary school (VWO) at the Andreas College location Pieter Groen in Katwijk. Subsequently started her medical study at the Leiden University Medical Center in the same year. During her study, she worked as a clinical assistant and data manager at the Centre for Human Drug Research. After her third year, she paused her study to full time participate in the Board of the Medical Faculty of Leiden Students. At the final part of her study, she followed a scientific internship at the Hematology Department at The Alfred Hospital in Melbourne, Australia. After completing her medical school in 2011, she started as a resident (not in training) at the General Surgery Department at the BovenIJ hospital in Amsterdam. In October 2012 she started a PhD trajectory at the Department of Otorhinolaryngology and Head & Neck Surgery at the Leiden University Medical Center. In October 2015 she started as a clinical resident in training at the same department, including a one year internship at the Haaglanden Medical Center (HMC) in 2015/2016 and the Alrijne hospital in 2018/2019. During her residency, she completed her research, resulting in this thesis.

